NASA Contractor Report 3152

Determination of Subcritical Frequency and Damping From B-1 Flight Flutter Test Data

S. K. Dobbs and C. H. Hodson

NASA

NASA Contractor Report 3152

Determination of Subcritical Frequency and Damping From B-1 Flight Flutter Test Data

S. K. Dobbs and C. H. Hodson
Rockwell International Corporation
Los Angeles, California

NASA

National Aeronautics
and Space Administration

**Scientific and Technical
Information Branch**

1979

SUMMARY

The application of the time-lag products correlation/
frequency analysis procedure to determine subcritical
frequency and damping from structural response measurements
made during flight flutter test of the B-1 prototype air-
plane is described. A detailed description of the analysis
procedure is presented, and the test airplane and flight
test procedures are described. Summary frequency and
damping results are presented for six transonic flight
conditions. Illustrative results obtained by applying
various options and variations of the analysis method are
presented for one flight condition.

INTRODUCTION

This study is one of several technology programs which
use B-1 flight test data and are being conducted in coopera-
tion among the United States Air Force, Rockwell
International, and NASA. Several features of the B-1 flight
flutter test program have enabled it to yield experimental
data well suited for the evaluation of subcritical flutter
response data analysis techniques. These features include
extensive aircraft instrumentation, an onboard flutter
excitation system, real-time telemetry monitoring, a data
acquisition system, transonic/low-altitude flight capability,
and a structural design based on flutter optimization
analyses and flutter model tests.

The purposes of this report are (1) to describe the
important features of the flight flutter and data analysis
programs, (2) to illustrate the application of the data
analyses methods to B-1 subcritical response data, and
(3) to show that the combination of the elements of the B-1
flight flutter test program resulted in the generation of
reliable subcritical frequency and damping information
which allowed efficient and safe flight envelope expansion.

Demonstration of the flutter stability of a high-performance aircraft to flight envelope limits is a critical development milestone. Because of the limits on accuracy of flutter analyses and flutter model tests, and the weight penalty involved if large margins of safety in design are used, flight flutter test demonstrations must be carried out on an actual prototype of all new high-performance aircraft.

The flight flutter test must provide evidence of the existence of a flutter margin of safety above the maximum operating speeds, including over-speed increments. However, the risk of catastrophic failure is too great to allow flight near the predicted flutter point. Therefore, the flutter clearance of the flight envelope is accomplished by measuring the frequency and damping of the structural vibration response at subcritical speeds, starting with low speeds and gradually increasing speed up to a maximum speed which allows for the required margin on the predicted flutter boundary. At a given test condition, these frequency and damping characteristics are extrapolated to the next higher speed or dynamic pressure condition to predict flutter stability for safe flight envelope expansion.

This approach to demonstrating the flutter margin of safety makes the safety of the flutter clearance program heavily dependent on the determination of the response frequency and damping from the subcritical response measured. Consequently, the continued improvement of the methods used to determine frequency and damping from flight test response data is of great interest to all organizations connected with aircraft design and development.

The basic intent of this study is to evaluate the basic elements required to obtain subcritical damping and frequency information. These basic elements include a method of exciting the structure in flight, instrumentation, test procedures, and analysis of the flight test subcritical response data. These evaluations will add to the technology base for future aircraft development.

LIST OF SYMBOLS

A	amplitude
ACCLRM	accelerometer
AMP	amplifier
COMP	computing
C_{xy}	cospectra of response and force
C_{yx}	cospectra of force and response
EMUX	electrical multiplex system
freq	frequency in cycles/seconds
F	Fourier transform
FLEX	flutter excitation system

g	structural damping = $2 \cdot$ (viscous damping)
$G(j\omega)$	gain or transfer function
h	frequency index number
j	$\sqrt{-1}$
k	10^3
L	entire time interval of a time history
LVDT	position transducer
m	correlation lag number
m	meters
M	maximum number of time lags
n	number of cycles
N	number of digitized data points or samples
N	Newton's metric force unit
pwr	power
q	dynamic pressure in kN/m^2
Qxy	quadrature spectra of response and force
Qyx	quadrature spectra of force and response
resol	resolution
R_{xx}	autocorrelation function of response
R_{yy}	autocorrelation function of input force
R_{xy}	cross-correlation function of response and force
R_{yx}	cross-correlation function of force and response
$R^2(\omega)$	coherence function
S_{xx}	power spectral density of response
S_{yy}	power spectral density of force
S_{xy}	cross spectra of response and force
S_{yx}	cross spectra of force and response
SR	sample rate
spect	spectral
T	sampling period in seconds per sample = 1/SR
t	time
x(t)	time history of response
y(t)	time history of input force
σ	mean deviation $= \sum_{j=1}^{n} \frac{|V_j - \bar{V}|}{n}$ where V is variable of interest, $\bar{V}$ is the average of n variables
τ	time length of correlation functions, seconds
ϕ	phase angle
Φ	power spectral density, $(units)^2 / \frac{RAD}{SEC}$
ω	frequency in radians/second

FLIGHT TEST PROGRAM

The B-1 Flutter Test Aircraft

General description. - The B-1 aircraft, shown in figure 1, is a prototype, long-range supersonic bomber with the capability of transonic and supersonic flight at high dynamic pressures. The aircraft utilizes a blended wing-body concept with variable-sweep wings, a single vertical stabilizer with a three-section (upper, intermediate, and lower) rudder, and horizontal stabilizers which provide both pitch and roll control. The variable-sweep (15 to 67.5 degrees) wing, as shown in figure 2, is equipped with slats, spoilers (which also function as speed brakes), and flaps which provide the aircraft with a highly versatile operating envelope. Canted vanes, mounted on each side of the forward fuselage, are part of the structural mode control system which reduces structural bending oscillations in the vertical and lateral axes. For flight flutter tests, a flutter excitation system (FLEX) was added to A/C-1.

The aircraft is powered by four YF101-GE-100 dual-rotor augmented turbo-fan engines in the 30,000-pound-thrust class. The engines are mounted in twin nacelles below the wing and aft of the wing pivot points. For supersonic speeds, an air induction control system varies the internal geometry of the nacelle inlet ducts to maintain the required airflow to the engines for all flight conditions.

Fuel is carried in integral tanks in the fuselage, wing carry-through, and wing outer panels. The fuel system is pressurized and inerted by nitrogen. Fuel transfer sequencing is automatic and provides center-of-gravity control. The aircraft has both in-flight and ground single-point refueling capabilities.

Instrumentation. - Figure 3 shows the 43 accelerometers and strain gages located throughout the airframe to sense the response of the airframe and FLEX exciters. The outputs of all of these transducers are recorded in analog form on an onboard tape. The outputs of 21 selected transducers are telemetered for presentation on three strip charts at the ground station at Edwards Air Force Base for real-time monitoring of flight safety and for evaluating the adequacy of frequency sweeps as they are completed.

The primary response accelerometers used for data analysis are on the wing, horizontal tail, and vertical tail tips. Both left and right wings and horizontal stabilizers are instrumented to allow determination of the symmetry or antisymmetry of the response. The left wing, left horizontal tail, and vertical fin have response accelerometers near the leading and trailing edges of the tip chords to aid in identifying bending or torsion responses. Control surfaces such as flaps, spoilers, and rudders are also instrumented. Other secondary components instrumented are the movable overwing fairing,

5

nacelle movable inlet ramp, structural mode control vanes, aft nacelle, and various fuselage locations. This array of instrumentation locations allows sufficient coverage of the vehicle to determine the subcritical response of the important components.

The flutter excitation system. - The B-1 flutter excitation system consists of five hydraulically driven, electronically controlled oscillating mass (or wand) inertial force exciters, mounted at the wing, horizontal tail, and vertical tail tips, as shown in figure 4, a. A photograph of an exciter mounted to a test stand is shown in figure 4, b. This inertial type of exciter offers certain advantageous characteristics, such as allowing the excitation forces to be independent of flight speed and wing sweep angle, and causing minimal aerodynamic interference on the surface.

The FLEX control loop is shown in figure 5. Its major components include the copilot's control panel, the oscillator control, an overresponse safety trip system, the pilot's emergency off switch, the hydraulic actuators and servo, a reference accelerometer mounted on the surface structure, and an accelerometer mounted on the wand. The wing and horizontal tail exciters are synchronized to operate either in phase for symmetrical excitation or out of phase for antisymmetric excitation.

The copilot's FLEX control panel, shown in figure 6, contains switches and controls for selecting wing, horizontal tail, or vertical tail, setting inertial force levels, selecting symmetric or antisymmetric, setting the excitation frequency at a discrete value for dwells, performing automatic frequency sweeps, and manual system shutdown. In the automatic frequency sweep mode, the excitation frequency is swept at a logarithmic rate from 1 to 65 Hz in approximately 55 seconds, as shown in figure 7. Reverse or down sweeps also can be made. The FLEX wand frequency is controlled by the oscillator signal. Due to the finite reaction time of the hydraulics to the sweep frequency command and a time lag introduced by the feedback rectifier, a frequency-dependent phase lag exists between the FLEX wand and the oscillator, as shown in figure 8.

The response safety trip system continuously monitors the amplitude of 13 accelerometers simultaneously. It provides automatic FLEX shutdown in the event that any one accelerometer indicates that wing, horizontal tail, or vertical tail is responding in excess of predetermined response limits. Automatic FLEX shutdown will also occur if the shaker forces should exceed predetermined limits. The cutoff response and force levels are chosen to be well below the amplitudes that could cause any structural or FLEX damage. In the event of failure of the hydraulic supply, the exciter wand is hydraulically locked to prevent the wand from responding to airframe motion.

The hydraulic actuator consists of two pistons operating in parallel, to directly drive the wand. Movement of the wand also drives a position indicator

(LVDT) which controls operation of the mass assembly about zero. An electrically operated hydraulic servo valve ports oil pressure to either side of the piston when commanded to move plus or minus by the electronics controller as a function of frequency.

Oscillation of the wand relative to the structure is sensed by the difference in output from two accelerometers. One accelerometer is on the wand, and the other is a reference accelerometer on the aircraft structure, immediately adjacent to the wand. The wand accelerometer and the reference accelerometer are at the same chordwise location on the aircraft surface. The chordwise location selected is the unique location at which the wand excitation force acts on the structure. At this location there is an inertia force, but no moment, due to relative motion between the wand and the aircraft structure. The inertia force and moment of the oscillating wand are reacted at the wand pivot point by a force and a moment. However, this combination of force and moment can be considered to be replaced by an inertia force alone acting at a location which gives the same moment about the wand pivot point. The location of this inertia force is calculated from the force and moment reactions at the wand pivot. Figure 9, a, represents the wand with a small rotation, β, relative to the aircraft structure. The vertical force at the wand center of gravity is:

$$F_{cg} = m\ddot{\beta}X_{cg}$$

where

X_{cg} = distance from wand pivot to wand c.g.

m = mass of wand

The vertical reaction at the wand pivot is:

$$F_{Pivot} = F_{cg}$$

The moment about the wand pivot is:

$$M_{Pivot} = I_{\beta}\ddot{\beta}$$

where

I_{β} = wand inertia about pivot

7

The location at which the reaction force and moment on the structure can be replaced by a vertical force alone is determined by dividing the wand inertial moment by the inertial force to yield

$$\chi_e = \frac{I_\beta}{m\chi_{cg}}$$

where

χ_e = distance from pivot to effective force location

An effective mass m_e at χ_e can be defined such that its inertia force will equal the wand inertia force and its moment about the wand pivot will equal the inertia moment of the wand. Equating the moments about the pivot due to the wand and due to the effective mass results in

$$m_e \chi_e^2 \ddot{\beta} = I_\beta \ddot{\beta}$$

so that

$$m_e = \frac{I_\beta}{\chi_e^2}$$

Substituting the preceding expression for χ_e and $S_\beta = m\chi_{cg}$, the effective mass given is

$$m_e = \frac{S_\beta^2}{I_\beta}$$

The wand inertia force then is given by

$$F_{FLEX} = m_e \Delta a$$

8

where Δa is the difference between the wand accelerometer and the reference accelerometer output. Any overall motion of the aircraft does not affect Δa since the wand and reference accelerometers are very close together. Any relative motion between the wand and the structure causes a nonzero Δa.

Lightweight wands weighing 137 newtons (31 pounds) with an equivalent point mass of 79.5 newton (18 pounds) were used for early flight flutter tests. The response obtained with the light wands sometimes was not large enough to provide consistent damping and frequency data when the aircraft was subjected to turbulence and buffet. Heavier wands were installed for later flight flutter tests to obtain larger responses relative to the responses to turbulence and buffet. The heavier wands weigh 184 newtons (41.3 pounds) and have an equivalent point mass of 123.8 newtons (27.8 pounds). Figure 10 shows the input force as a function of frequency for the wings, horizontal tails, and vertical tail for the lightweight and heavyweight wands. Ideally, the force should be constant at all frequencies; however, figure 10 shows that the force amplitude was a function of frequency. The FLEX force increased with frequency from zero to about 10 Hz due to displacement limitations of the wand travel. From about 10 to about 35 Hz, the force level was fairly constant. Above 35 Hz, the force decreased due to the increasing phase lag of the wand relative to the oscillator command. This latter rolloff is more pronounced with the heavyweight wands. The vertical tail wand had the lightweight version for all flights. The higher force level for the vertical tail on flight 1-50 compared to flight 1-13 is due to a higher amplitude setting on the copilot's FLEX control box.

Flight Tests

Test conditions. - Figure 11 shows the six flight-test conditions selected for analysis in this report. The test conditions consist of three altitudes at mach 0.90 and three altitudes at mach 0.95. The test points are arranged so that subcritical frequency and damping trends at constant mach number, constant dynamic pressure, and constant altitude can be determined by appropriate plots of the test data. Test dynamic pressure increments between points at constant mach number were chosen to be small enough so that decreases in damping with increasing dynamic pressure should be safely detectable. FLEX frequency sweeps were performed, and 5 minutes of random excitation response data were recorded at each flight condition. The maximum buffet response of the flight envelope was encountered at these two mach numbers and increased in amplitude with decreasing altitude.

Test procedures. - The flutter tests were performed with the wings at a 65-degree sweep angle. The aircraft was trimmed at the proper mach number and altitude for the chosen test condition. Five frequency sweeps were performed for each test configuration. All data presented in this report are for the stability and control augmentation system and the structural mode control system deactivated. The frequency sweeps performed were:

(1) Wing symmetric

(2) Wing antisymmetric

(3) Horizontal tail symmetric

(4) Horizontal tail antisymmetric

(5) Vertical tail

The sweeps covered a frequency range of 1 to 65 Hz and were about 55 seconds in duration. The resulting data were analyzed in three different time frames, as shown in figure 12. Real-time monitoring of the response and force data involved observation of analog strip charts in the Mission Control Center at Edwards Air Force Base. The strip chart monitor determines the successful completion of a FLEX sweep by observing such characteristics as adequate signal-to-noise ratios, response amplitudes not causing automatic FLEX shutdown, visual judgment of adequate damping in all modes, atmospheric turbulence not being excessive, and proper functioning of the accelerometers. If the monitor observes any potentially dangerous response, he can immediately inform the pilot by direct radio communication to deccelerate. Near real-time analysis uses a minicomputer in the Mission Control Center to digitize the data as a sweep is performed for subsequent data analysis. The data are analyzed using a time-lag products correlation/frequency analysis method described later. The frequency and damping of the modes contained in one chosen frequency range are calculated from the gain or transfer function, usually within 20 minutes after the completion of the sweep. Postflight data analysis either uses the minicomputer to complete the analysis of all modes analyzed during the flight, or employs the onboard tape recording of the sweep data for offsite time-lag products correlation/frequency analysis using a large storage IBM computer to calculate modal frequency and damping.

SUBCRITICAL RESPONSE ANALYSIS

Time-lag Products Correlation/Frequency Analysis Procedure

The primary procedure used to obtain the subcritical response from B-1 flight test data involves the time-lag products correlation/frequency analysis method. This method derives the time domain autocorrelation and cross-correlation functions for one pair of time history records, and estimates spectral density and transfer functions from these calculations using digitized data. Modal frequency and damping values are calculated from the various spectral density and correlation functions. Coherence estimates are also calculated. The procedure also includes an optional smoothing technique to improve the spectral estimates by the use of a "Hanning window," and an optional technique to calculate modal frequency and damping from the transfer function which uses an iterative, optimal, least squares complex curve fit.

The analysis procedure first plots the digitized data in the form of time histories of the chosen response channel and the corresponding FLEX force channel, or the oscillator signal (which controls the FLEX frequency). The time histories are plotted without and then with the mean amplitudes removed. The procedure then generates five types of data representations from which the modal frequency and/or dampings may be manually calculated.

The first type of data representation is the correlation functions. The autocorrelation function tends to identify a sinusoidal or periodic function buried in a single noisy time history, while the cross-correlation function identifies periodic functions which have common frequencies in two different time histories. Autocorrelation and cross-correlation functions are obtained by multiplying two time histories point by point and summing these products. Then, one of the waveforms is shifted or lagged by some time increment, and the sum of the point-by-point multiplication of the two wave forms is again calculated. For responses with stable damping, the greater the second time history is time shifted, the smaller the sum. The correlation function of the two time histories is obtained by plotting the sums of the time-lag products against the time shift or lag number. The autocorrelation multiplies a single time history and its identical time history, while the cross-correlation multiplies two different time histories. The autocorrelation and cross-correlation functions are calculated by the classical Backman and Tukey (ref. 1) time-lag products correlation method. If the input (force) time series is called $y(t)$, the corresponding autocorrelation function is denoted by $R_{yy}(mT)$ and is given by

$$R_{yy}(mT) = \frac{1}{N-m} \sum_{K=1}^{N-m} y_K \cdot y_{K+m}, \quad m = 0, 1, 2 \ldots M$$

11

where

N = total number of digitized data points

m = correlation "lag number"

M = maximum number of time lags (= 500 for this report)

T = sampling period in seconds = 1/(sample rate)

This calculation is performed for positive lag numbers only because R_{yy} is an even function; i.e.,

$$R_{yy}(mT) = R_{yy}(-mT)$$

The output time series (response of the structure) is denoted by $x(t)$. Its corresponding autocorrelation is denoted by $R_{xx}(mT)$ and is given by

$$R_{xx}(mT) = \frac{1}{N-m} \sum_{K=1}^{N-m} x_K \cdot x_{K+m}, \quad m = 0, 1, 2, \ldots M$$

R_{xx} is also an even function. R_{xx} and R_{yy} are plotted as a function of lag number. This may be converted to time by knowing the time shift per lag

$$\frac{\Delta t}{lag} = \frac{1}{SR} = T$$

where SR is the sample rate of digitization in samples per second and Δt is the time shift of each lag. For a sample rate of 360 samples per second, each lag would be

$$\Delta t = \frac{lag}{SR} = \frac{1}{360} \text{ seconds}$$

or 360 lags = 1 second.

The cross-correlation functions are then calculated and plotted in the same form as the autocorrelation functions. The cross-correlation function is denoted $R_{xy}(mt)$ and is given by

$$R_{xy}(mT) = \frac{1}{N-m} \sum_{K=1}^{N-m} x_K \cdot y_{K+m}, \quad m = 0, 1, 2,\ldots M$$

and the cross-correlation function $R_{yx}(mT)$ between input $y(t)$ and output $x(t)$ by

$$R_{yx}(mT) = \frac{1}{N-m} \sum_{K=1}^{N-m} y_K \cdot x_{K+m}, \quad m = 0, 1, 2,\ldots M$$

These functions are neither odd nor even but satisfy the relation

$$R_{xy}(mT) = R_{yx}(-mT)$$

This property is used for calculating the cross-spectral functions later.

The plots of the autocorrelation function of the response and the cross-correlation functions may be used directly to estimate the modal frequency and structural damping, g, for a single-degree-of-freedom system by treating the functions as a free-vibration decay with an initial displacement, as mentioned in ref. 2. Thus, the frequency is determined by counting the number of cycles occurring in 1 second, and the structural damping is calculated as the log decrement (figure 13, a) or

$$g \cong \frac{1}{n\pi} \ln \frac{A_o}{A_n}, \quad \text{for } g \le 0.30$$

where

n = number of cycles

A_o = amplitude of initial peak

A_n = amplitude on the nth peak

13

However, for analysis of a time history containing more than one mode, deriving the frequency and damping of a single mode would be very difficult, if not impractical, because the correlation function would contain information from all of the modes. Elimination of the unwanted mode may be accomplished for a swept-frequency, forced response by time windowing; i.e., by simply analyzing only that portion of the time history containing the mode of interest. However, this has limitations due to minimum time requirements for accurate data analysis. A problem with using the autocorrelation of the response for a direct frequency and damping determination is that any noise response in the time history (such as caused by turbulence or aircraft buffet) that contains frequencies in the realm of the mode frequency of interest will distort the function. However, this effect is minimized when using the cross-correlation function because the process of cross-correlation emphasizes response data which have a common frequency as the force. In general, correlation functions were not usually used to directly determine modal characteristics due to the reasons already mentioned. However, they are used to generate power spectral (frequency domain) density and transfer functions where the modal frequency and dampings can be determined.

The next step in the analysis procedure is to calculate the numerical or finite, discrete Fourier transform of the autocorrelation functions to derive the power spectral densities. The Fourier transform of the response is denoted as $S_{xx}(j\omega_h) = R_e[F\{R_{xx}(mT)\}]$. Because the correlation functions are of finite-time duration, truncation errors in the Fourier transform may be introduced if the amplitudes of the functions at the end points are not small. This effect may be partially compensated for by introducing a two-point correction (ref. 3) for the end points with equal weights of one-half. Applying the end-point corrections, the Fourier transform of $R_{xx}(mT)$ becomes

$$S_{xx}(j\omega_h) = T\left[R_{xx}(0) + 2\sum_{m=1}^{M-1} R_{xx}(mT)\cos m\omega_h T + R_{xx}(mT)\cos M\omega_h T\right]$$

The power spectral density of the response is then plotted from which frequencies and dampings of modes may be manually calculated by the half-power point method shown in figure 13, b. This type of data display does not take into account any variation in force amplitude as the swept frequency changes nor does it minimize response caused by turbulence or buffet noise inputs.

14

Likewise, the autospectral density of the input force is

$$S_{yy}(j\omega_h) = T\left[R_{yy}(0) + 2\sum_{m=1}^{M-1} R_{yy}(mT) \cos m\omega_h T + R_{yy}(MT) \cos M\omega_h T\right]$$

The cospectral and quadrature spectral functions are also used to calculate response frequencies and dampings. The cospectra is the component of the total response vector which is in-phase with the force vector, and the quadrature spectra is the out-of-phase component. The modal peak frequency is most accurately determined from the cospectra, and the damping calculation is made using the quadrature spectra, as shown in figure 13, c.

The cospectra, denoted as C_{xy}, and the quadrature spectra, denoted as Q_{xy}, are given as

$$C_{xy}(j\omega_h) = R_e[F\{\rho_c(mT)\}]$$

$$Q_{xy}(j\omega_h) = R_e[F\{\rho_q(mT)\}], \quad h = 1, 2\ldots,M$$

where

$$\rho_c(mT) = 1/2[R_{xy}(mT) + R_{yx}(mT)]$$

$$\rho_q(mT) = 1/2[R_{yx}(mT) - R_{xy}(mT)]$$

The Fourier transform with end-point correction factors gives

$$C_{xy}(j\omega_h) = \frac{T}{2}\left[\rho_c(0) + 2\sum_{m=1}^{M-1} \rho_c(mT) \cos m\omega_h T + \rho_c(MT) \cos M\omega_h T\right]$$

(an even function)

$$Q_{xy}(j\omega_h) = \frac{T}{2}\left[\rho_q(0)^0 + 2\sum_{m=1}^{M-1} \rho_q(mT) \sin m\omega_h T + \rho_q(MT) \sin M\omega_h T\right]$$

(an odd function)

15

The coherence function of the response and the force is also calculated. Coherence is a measure of the degree to which two time series $x(t)$ and $y(t)$ are related by a linear model, as shown in figure 14. In this case, $y(t)$ is the FLEX force input, $X^*(t)$ is the airframe response from the FLEX only, and $N(t)$ is extraneous noise inputs such as turbulence and buffet which are uncorrelated with $y(t)$. $\chi(t)$ is the total response of the airframe, and $G(j\omega)$ is the linear model or the transfer function. Coherence values range between zero and 1.0. A high coherence (say, greater than 0.5) means that the response and the force at a given frequency are related. The coherence function, denoted by $R^2(\omega)$, is given by

$$R^2(\omega) = \frac{C_{xy}^2(j\omega) + Q_{xy}^2(j\omega)}{S_{xx}(j\omega)S_{yy}(j\omega)}$$

and is plotted against ω. The function is used to help interpret the validity of a spectral peak; i.e., if a peak frequency has a corresponding high coherence, then it is assumed that the mode was predominantly excited by the FLEX force rather than by buffet or turbulence noise; therefore, the peak has minimum distortion and should yield valid damping and frequency values.

The frequency spectra of the noise may be obtained by knowing the spectra of the total response and the coherence function for the frequency range of interest. The noise spectra, denoted as $S_{nn}(j\omega)$, is given by

$$S_{nn}(j\omega) = S_{xx}(j\omega)[1 - R^2(\omega)]$$

The gain or transfer function is then calculated. This may be regarded as the frequency response function relating the input $y(t)$ to the output $x(t)$. The gain is denoted by $|G(j\omega)|$ and is given as

$$|G(j\omega)| = \sqrt{\frac{C_{xy}^2(j\omega) + Q_{xy}^2(j\omega)}{S_{yy}(j\omega)}}$$

The gain frequency spectra are then plotted from which the modal frequency and damping are manually calculated, as shown in figure 13, d.

16

The phase angle of the transfer function (or the phase between the FLEX force and response) is calculated and plotted. The phase is denoted by $\phi(j\omega)$ and is given by

$$\phi(j\omega) = \tan^{-1}\left(\frac{-Q_{xy}}{C_{xy}}\right)$$

The modal damping is calculated by using the slope of the phase curve, as is shown in figure 13, e.

The Hanning filter or window is an option which may be applied to smooth spectral estimates. This filter is described in ref. 1 and 4. This program uses weighting coefficients of one-fourth, one-half, and one-fourth as the Hanning filter weights and the coefficients are applied for S_{xx}, C_{xy}, and Q_{xy}, respectively.

Another option that may be applied is a least squares curve fit which tries to match the gain and phase frequency responses. This method fits a mathematical transfer function to autospectral and cross-spectral density estimates of data by an iterative process. The analyst must specify the order of the numerator and denominator of the mathematical transfer function. From the mathematical transfer function fit, the modal frequency and damping are derived.

Subcritical Response Analysis Variables

Accurate data analysis requires careful selection of the numerical values for the analysis variables. Improper combinations of sample rate, the time length of the data sample, number of time lags, and frequency resolution can yield frequency and damping values with errors.

Sample rate. - The minimum sample rate must be at least twice the highest frequency of interest to prevent aliasing. (A sample rate of five to six times the highest frequency is usually desirable.) The maximum sample rate which was used for the data analysis in this report was 360 samples per second with a low pass filter of 62.5 Hz. The highest frequency of interest was 60 Hz. This allowed a maximum-sample-rate-to-maximum-frequency ratio of 6. However, lower sample rates for analysis of low-frequency, lowly damped modes were required to prevent truncation of the correlation function, as discussed later.

This is accomplished by decimating the original data; i.e., using only every other digital point of the original 360 samples per second or an integer divisor thereof. Sample rates as low as 90 samples per second were used for the low-frequency ranges.

Time length of data sample. - For swept sine response data, the time length of the data sample required for analysis is largely determined by how much of the time history contains the frequency range of interest. However, the time length of the data sample affects the accuracy of the correlation and spectral density calculations. Truncation of the swept sine time history must be at the points where the frequencies of interest are not present and which allow sufficient time history duration; otherwise, truncation errors may be introduced into the correlation and spectral functions.

The total number of data points or samples N is the product of the time length of the data sample L times the sample rate (SR) or

$$N = L(SR) = L/T$$

To allow a minimum of two degrees of freedom to exist for a chi-squared distribution of the spectral estimates, the ratio of the number of data points (N) and the total number of time lags (M) should be

$$\frac{N}{M} \geq 2$$

A ratio of approximately 20 is usually preferred. The data analysis in this report used sample lengths of from 12.5 to 25 seconds, yielding a maximum of 18 chi-squared degrees of freedom for 500 lags.

Number of time lags. - Five hundred time lags were used for data analysis in this report. The number of time lags and the sample rate determine the time length of the correlation functions. If a given frequency contained in a response or cross-correlation function has not fully decayed at the last lag, truncation errors are introduced into the frequency spectra, and the peak frequency and damping will contain errors. The end-point corrections previously discussed partially correct for this. This truncation may further be minimized by increasing the time length of the correlation functions by increasing the number of time lags and/or decreasing the sample rate. The time length of the correlation functions is given by

$$\tau = \frac{M}{(\text{sample rate})} = MT$$

18

Suitable M and T variations are made until the decay amplitude of the desired frequency contained in the correlation function is small enough at τ so that the effects of truncation are negligible. Care must be taken that the sample rate does not become so slow that aliasing could occur, or that the M becomes too high compared to N.

An estimate can be made of the correlation time required for the function to decay to a small amplitude at the truncation time. To provide initial choices of M and T, τ is estimated by

$$\tau = MT = \frac{1}{fg\pi} \ln \frac{A_o}{A_\tau}$$

where

f = estimated frequency

g = estimated damping

A_o = maximum correlation function amplitude

A_τ = correlation function amplitude at τ

For example, for an estimated $f = 10$ Hz, $g \approx 0.06$, and $A_o/A_\tau = \frac{10}{1}$, the minimum correlation time would be

$$\tau = \frac{1}{(10)(0.06)\pi} \ln 10$$

$$= 1.126 \text{ seconds}$$

For a chosen sample rate of 360 samples/second, the required minimum number of lags would be

$$M \geq \frac{\tau}{T}$$

$$M \geq \frac{1.216}{T}$$

$$M \geq \frac{1.46}{(1/360)} \geq 438 \text{ lags}$$

19

If the analysis results prove to be inadequate, a higher M and/or a lower sample rate may be chosen and the analysis repeated.

Corrections for damping errors introduced by truncation are discussed in ref. 5 for a boxcar window, and in ref. 4 for a Hanning window.

Frequency resolution. - The incremental frequency chosen for calculating the spectral functions was

$$DF \geq \frac{1}{NT} \text{ (Hz)}, \quad N < 10,000$$

For NT = 25 seconds, DF = 0.04 Hz. To minimize any spectral errors caused by spectral window smearing, the desired minimum number of lags for a given DF is

$$M = \frac{1}{2 \ DF \ T} \quad , \qquad M \leq 500$$

This condition cannot always be met due to storage limitations of the computer for a chosen DF and T. The incremental frequency for the data analysis in this report varied from 0.04 to 0.08 Hz.

SUBCRITICAL FREQUENCY AND DAMPING RESULTS

Summary Results

The variations of the predicted subcritical frequencies and dampings with dynamic pressure for the six flight conditions listed in figure 11 are presented in figures 15 and 16. These results were obtained using FLEX excitation and are values averaged from several calculations using different options and variations of the time-lag products procedure.

Illustrative Analysis Results and Interpretation Techniques

Results from FLEX and random excitation (buffet and turbulence) obtained by using different options and variations of the analysis procedure are presented in tables I through V, and in figures 17 through 24 for a Mach number of 0.95 and an altitude of 1,794 meters (5,890 feet). This flight condition was chosen because the highest level of airplane buffet and turbulence response occurred here, thus providing response data that could be used to test the ability of the analysis method to separate modal responses excited by the FLEX system from responses induced by random excitation, and also to evaluate the capability of the analysis method to derive accurate modal

response from purely random excitation. Five modal responses were studied-- wing symmetric second bending, the horizontal tail symmetric second bending, and three vertical tail/empennage modes. These modes were identified by comparing the frequencies of the peak responses with the flutter analysis results. Each mode presents a different type of analysis problem, as shown in figures 17 and 18. Figure 17a, shows the transfer functions (gain) generated by the FLEX frequency sweeps, and figure 17, b, shows the power spectra of the response from random excitation only. The wing response is an example of a generally "clean," well-separated mode with a moderately high FLEX response to random response ratio. The horizontal tail response is an example of a noisy mode with a relatively low-level of response amplitude. The vertical tail/empennage responses are examples of three modes which are closely spaced together in frequency and are affected by buffet forces. These choices were also influenced by the fact that the complete aircraft flutter analysis predicted that the wing, horizontal tail, and two of the vertical tail/empennage modes are important to the flutter characteristics of the air- plane. The portions of the time histories containing the frequency ranges of interest of the forced response, FLEX force, oscillator signal, and response to random excitation are shown for each mode in figure 18, a through c.

Figure 19, a through g, shows the data analysis results for the wing mode excited by the FLEX system, which is considered a clean, well-separated response. Figure 19, a, shows the cross-correlation function decay calculated for 500 lags using a 25-second time history length sampled at 360 samples per second. The ideal function should appear as a log decrement decay with a constant frequency; however, the cross-correlation function is at best a rough decay with more than one frequency. This is due to the fact that a 25-second time segment of the frequency sweep was used which contains three other wing modes which are all present in the correlation function. Therefore, this correlation function does not lend itself for a direct calculation of the log decrement damping without further windowing.

Figure 19, b, shows the power spectra of the response (PSD) derived from the autocorrelation function for a frequency range of 36 to 66 radians per second (5.7 to 10.5 Hz). Since this calculation does not account for the relationship between the force and the response, it is most affected by buffet and turbulence noise inputs. A comparison of this function and the transfer function of figure 19, f, shows that the two minor peaks at 47.5 and 55.75 radians per second on the sides of the peak at 51.5 radians per second are more pronounced on the PSD than the transfer function, which indicates

they are largely caused by noise inputs. This means that the PSD peak generated from the autocorrelation function is distorted more by noise than is the transfer function peak calculated from the cross-correlation function. This is demonstrated by the fact that the PSD required a much greater extrapolation of the sides of the peak (figure 19, b) to the half-power point than the cross-correlation peak required. (Extrapolation of the sides of the peak as shown in the figure was a standard procedure when the peak was judged to contain distortions). However, the half-power point PSD damping was g = 0.126 and the peak frequency was 8.08 Hz, which is still in good agreement with the results of the other data displays which follow.

Figure 19, c, shows the same wing data displayed in the form of the cospectra (the in-phase component of the total response) which gives the most accurate determination of the peak frequency, which was 8.2 Hz.

Figure 19, d, displays the same wing data as the quadrature (out-of-phase component of total response). The function is a smooth curve; however, the shoulder peak to the right of the peak frequency of 51.5 radians per second is not well-defined due to the two places where the slope of the curve changes. Choosing the first shoulder on the right and the obvious shoulder on the left, the damping is g = 0.135.

Figure 19, e, shows the coherence spectra (coherence is a measure of the degree to which the response and force time series are linearly related). A large coherence value at a given frequency (say, greater than 0.5) may be interpreted as meaning that most of the calculated response spectra were directly caused by the force and only slightly affected by extraneous noise such as buffet or turbulence noise. Figure 19, e, shows that the coherence in the frequency range of the half-power point of the wing mode varies from 0.6 to 0.9, which is interpreted as meaning the FLEX response is well-separated from any response caused by noise. Therefore, the modal data should be valid.

Figure 19, f, shows the transfer function spectra for the wing mode. The figure shows a clean, symmetric, well-defined transfer function (gain) with the peak frequency of 8.16 Hz and half-power damping value of 0.119.

Figure 19, g, displays the same wing data as the phase angle between the response and the FLEX force. The upper figure shows a reasonably smooth curve with a discernible slope for the left frequency range of the mode. The dashed line is an estimate of the slope and yielded a damping of g = 0.146.

Averaging the frequency and damping values from all displays for each basic analysis method yields an average frequency of 8.14 Hz and an average damping of 0.132, with corresponding mean deviations of 0.043 Hz and 0.009 for the damping. These deviations are considered highly acceptable.

Figure 20, a through g, shows the data results for the horizontal tail mode, which is considered a noisy mode with a low response amplitude. The correlation function (figure 20, a) used 500 lags on a 25-second time history length sampled at 360 samples per second.

These analysis results offer interpretation problems. For example, the half-power point amplitude on the power spectra of the response (figure 20, b) and on the transfer function (figure 20, f) is below three peaks. The largest peak is obviously the mode's peak frequency, but it is not obvious whether the sides of the major "clean" peak should be extrapolated downward to the half-power point (dashed lines) to calculate the damping, or whether the entire width of all three peaks together should be considered to belong to same mode. The most conservative approach would be to use the lowest damping value of the extrapolated peak, yielding g = 0.06. Using the entire width covered by all three peaks gives g = 0.152. One aid in deciding which value to use is to compare them with values obtained from other displays of the same data. However, the other displays also offer the possibility of two different damping values. Averaging both sets of values from all four displays gives the extrapolation technique g = 0.0716 and, using the width of all three peaks, g = 0.132, with a common average frequency of 16.86 Hz. The corresponding mean deviations for the average damping values are 0.0072 and 0.027, respectively, which favors the conservative extrapolation technique.

Figure 21, a through g, shows the analysis results for three closely spaced vertical tail/empennage responses which are separated by only about 1 Hz. The transfer function of figure 21, f, adequately separated the three responses and yielded well-behaved functions. The other data displays, however, do not always clearly separate the first two peak responses and inadequately define the third peak, which had a low response amplitude. For example, the power spectral density of the response of figure 21, b, shows the two major peaks are poorly separated and therefore mutually distort their spectra shapes between them, as evidenced by their lack of spectral symmetry about their respective peak frequencies. As a standard procedure in cases such as this, the dampings are calculated by using only the half of each peak which is relatively unaffected by the other mode, and then doubling the frequency band at the half-power point by assuming the other side of the spectra is a mirror image.

Thus, the left side of the peak at 10.62 Hz (66.8 radians per second) was used and doubled for the first peak. The right side of the peak at 11.5 Hz (72.25 radians per second) was used and doubled for the second peak. The third peak at 12.73 Hz (80 radians per second) is not defined at all on figure 21, b. The quadrature spectra (figure 21, d) adequately defines the response for the first two modes but not the third, in spite of the fact that the coherence (figure 21, e) shows high values for the third peak.

Averaging the different displays for figure 21, a through g, yields for the first mode a frequency of 10.67 Hz and g = 0.058, with a mean deviation of 0.033 Hz for frequency and 0.007 for damping. The analysis for the second mode yields average values of 11.64 Hz for the frequency and g = 0.084, with corresponding mean deviations of 0.097 Hz and 0.028. The high mean deviation of the damping for this mode may warrant only the use of the transfer function. The accuracy of the third mode values are in question because only the transfer function of figure 21, a, adequately described the mode. The test data yielded values of frequency = 13.13 Hz and g = 0.068.

These results are summarized in tables I through V. They indicate that for a variety of modes the time-lag products correlation/frequency analysis procedure provided reasonable correlation and spectral functions when excited by the FLEX system. These functions provided reliable frequency and damping results.

Figures 22, 23, and 24 show the response of the wing, horizontal, and vertical tails to random excitation for a 25-second time history. The flight condition is the same as the previous comparisons which used the FLEX force excitation.

Figure 22, a, shows the autocorrelation functions in the time domain (360 lags = 1 second) for the left and right wingtips. The dominating frequencies are 3 Hz (wing first bending), 8 Hz (wing second bending, visible only for the right wing), and 27.5 Hz (wing second torsion). Figure 22, b, shows the power spectra of the autocorrelations of the left and right wingtips along with the phase angle between the two. It was expected that the phase angle plot would indicate if a particular peak was a symmetric or an antisymmetric mode. Two distinct modes appear on both wing spectra. The first peak at 6.6 Hz appears to be too low in frequency to be a wing mode, but it could be a fuselage mode. The second peak at 8.1 Hz does correlate in frequency and damping with the wing symmetric second bending mode obtained from the FLEX excited response; however, the phase plot shows a 160-degree phase angle, indicating an antisymmetric mode. However, the antisymmetric mode was measured

at a higher frequency of 8.99 Hz (55.5 radians per second) from the FLEX excited response and appears as a shoulder at 55.5 radians per second in figure 22, b. Thus, it appears that a reliable determination of symmetry from this method is impractical. Figure 22, c, displays the spectra with a narrower frequency window which eliminates the peak at 6.6 Hz. This yields a more coarse frequency resolution. However, the shoulder at 55.5 radians per second (8.83 Hz) now appears as a distinct peak and does correspond in frequency to the antisymmetric mode. Windowing caused the damping of the mode at 8.1 Hz to decrease by 50 percent compared to the nonwindowed mode.

Figure 23, a through c, shows the horizontal tail response from random excitation. The response levels of the second bending mode are so small that the spectra of figure 23, b and c, appear as noise, and no useful information can be obtained from them.

Figure 24 shows the vertical tail response from random excitation. The two distinct modes yielded frequencies and damping values (figure 24, b and c) in rough agreement with the FLEX excited results using timelag products auto-correlation. These data results using random excitation appear in tables I through V.

Figure 24 shows the autocorrelation of random response data did give some reasonable answers for peak responses with relatively low damping. However, random excitation did not adequately excite all of the important modes to sufficient amplitudes for accurate determination of the peak frequency and damping using this analysis procedure on the 25-second time sample. Definite determination of symmetric or antisymmetric response was also found to be impractical. The random excitation results may have improved if longer time data samples were analyzed or if the vehicle could have encountered higher turbulence amplitudes.

In the appendix are other variations of the analysis procedure. Included are using a Hanning filter, using the oscillator signal instead of the FLEX for cross-correlation, employing a curve fit to estimate frequency and damping, and time and frequency windowing. These variations did not yield significant improvements for the cases studied.

CONCLUDING REMARKS

The time-lag products correlation/frequency analysis procedure is described, and results from application of this procedure, including many of its variations and options, to B-1 prototype airplane flight flutter test data are presented. Subcritical frequency and damping trends obtained from analysis of response data, excited by onboard inertial shakers using sinusoidal frequency sweeps, are presented for six transonic flight conditions where buffet and turbulence effects are appreciable. Examples of the analysis procedure applied to peak responses presenting various analysis problems are discussed. The examples include modes with noisy peak responses and low response amplitudes, closely spaced modes affected by buffet and turbulence inputs, and clean, well-separated modes. The results showed that the analysis procedure adequately described the peak responses excited by the onboard shakers. This enabled reliable frequency and damping values to be obtained. The analysis procedure was also applied to random excitation responses. The results showed that reasonable frequency and damping information could be obtained by random excitation for some of the modes which were adequately excited and had a relatively low damping. However, in some cases reliable frequencies and damping of important modes could not be obtained from response to random excitation, using the data analysis procedures described in this report.

APPENDIX

Other Data Analysis Variations of the Time-lag Products
Correlation/Frequency Analysis Procedure

Hanning filter. - Figures A1, A2, and A3 show the effect of applying the
Hanning filter (or window) to the transfer functions and phase angle spectras
for the five peak responses using FLEX excitation. Inspection of the shape of
the functions and resulting frequency and damping lead to the conclusion that
the Hanning filter had a negligible effect on smoothing these particular peak
responses.

Using the oscillator signal instead of the FLEX force. - Figure A4, a, b,
and c, shows the effect of using the oscillator signal instead of the FLEX
force for all five peak responses. The advantage of using the oscillator signal
(which was used to command the FLEX wand frequency) instead of the FLEX force
time history in the cross-correlation and cross-spectra calculations is that the
oscillator signal has little noise, which could help smooth the spectra, while
the force signal does suffer from noise, such as is caused by "rattle" in the
system. The disadvantages come from the fact that the FLEX wand response
slightly lags the oscillator command due to a finite reaction time of the
hydraulic system and time lags introduced by rectification, which also changes
with frequency (figure 3). This phase lag would introduce an error in the
cross-correlation calculations and the resulting spectra displays. Another
disadvantage is that the oscillator signal amplitude slightly decreases with
increasing frequency, while the FLEX force does not follow this trend, as
shown in figure 10. This would also introduce errors in the calculations.

Figure A4, a, b, and c, shows the gain and phase spectra using the oscil-
lator signal (and Hanning filter). Comparison of figure A4, a, which uses the
oscillator, with figure 22, which uses the FLEX force, shows no significant
differences for the wing response. However, the comparison for the horizontal
tail response in figures A4, b, and 23 shows the oscillator reduces the amount
of definition of the gain peak, as evidenced by the longer extrapolation to the
half-power point required by the oscillator results. This caused a slight
increase in damping from the gain and a slight decrease in damping from the
phase. The vertical tail/empennage response comparison in figures A4, 6, and
24 exhibits the same characteristics as the horizontal tail.

Thus, the use of the oscillator instead of the FLEX force slightly reduces
the accuracy of the damping results of the timelag products method, but not to
the extent that would invalidate the result for these cases.

27

Curve fitting, time, and frequency windowing. - Figures A5 through A7 show the least squares curve fit routine applied to the time lag products method for various time and frequency windows. Various order polynomials were applied to each mode, with the best fit of the gain and phase being shown. The wing mode, shown in figure A5, using wide frequency and time windows had a curve fit which greatly underestimated the damping but matched the peak frequency. Figure A5, b, shows the same mode using a 33-percent narrower frequency window and a 50-percent narrower time window, resulting in a fairly good curve fit.

Figure A6, a and b, shows the curve fits for the horizontal tail mode. The curve fit estimated the spectra to include the entire width of all three peaks rather than to isolate the center peak. The windowed mode of figure A6, b (54-percent narrower frequency and 50-percent narrower time window) had a curve fit which tended to flatten out the peak even more and gave a greater over-estimation of the damping. The manual frequency and damping calculation for the nonwindowed and windowed conditions gave essentially the same values, but in this instance both cases had the same frequency resolution.

Figure A7, a, shows the vertical tail/empennage responses. The curve fit did not fit the spectrum due to more than one mode being present. It still fails when the mode is windowed by 50-percent narrower frequency and time windows, as in figure A7, b. The manual calculation shows that the effect of windowing has only a small effect on the frequency and damping results. Thus, this least squares curve fit is not presently developed to the point where it is a reliable tool to accurately estimate modal frequency and damping. The effect of reducing the analysis time windows by 50 percent and the frequency windows by 33 to 50 percent did not appreciably affect the frequency and damping results for the manual calculations.

The data analysis results from these analysis options appear in tables I through V.

REFERENCES

1. Blackman, R. B., and Tukey, J. W., The Measurement of Power Spectra From the View of Communications Engineering. Dover Publications, Inc., New York, 1958

2. Cole, Henry J., On-Line Failure Detection and Damping Measurement of Aerospace Structures by Random Decrement Signatures. NASA CR-2205, March 1973

3. Hanning, R. W., Numerical Methods for Scientists and Engineers. McGraw-Hill, 1962

4. Soovere, J., Turbulence Excited Frequency Domain Damping Measurement and Truncation Effects. Proceedings of NASA Symposium on Flutter Testing Techniques, NASA SP-415, October 1975

5. White, R. G., Use of Transient Excitation in the Dynamic Analysis of Structures. The Aeronautical Journal of the Royal Aeronautical Society, Volume 73, December 1969

TABLE I. - WING SYMMETRIC SECOND BENDING MODE FREQUENCY AND DAMPING
(Mach = 0.95, Altitude = 1,794 meters, q = 51.5 kN/m^2)

Force	Smoothing	Comp time (sec)	Freq resol (Hz)	Analysis Window Frequency bandwidth (Hz)	Analog record length (sec)	Coherence Min	Max	Pwr spect density of response Freq	g	Co-Quad spectra Freq	g	Gain (Transfer function) Freq	g	Phase Freq	g	Average Freq σ	g σ
								Time-lag-products correlation method									
Flex	None	63.0	0.04	2.9 - 10.5	25.0	0.60	0.90	8.08	0.1261	8.20	0.1351	8.16	0.119	-	0.146	8.14 0.043	0.132 0.009
Flex	Hanning	63.0	0.04	2.9 - 10.5	25.0	0.60	0.90	8.08	0.1261	8.20	0.1351	8.16	0.1122	-	0.1460	8.15 0.043	0.1300 0.011
Flex	Hanning + curve-fit		0.04	2.9 - 10.5	25.0	-	-	-	-	-	-	8.21	0.0497	-	-	8.21 -	0.0497 -
Osc	None	63.0	0.04	2.9 - 10.5	25.0	0.58	0.95	8.08	0.1261	8.16	0.1318	8.20	0.1068	-	0.1482	8.15 0.043	0.1282 0.012
Osc	Hanning	63.0	0.04	2.9 - 10.5	25.0	0.58	0.95	8.08	0.1261	8.16	0.1318	8.20	0.1068	-	0.1482	8.15 0.043	0.1282 0.012
Random	None	64.0	0.04	2.9 - 10.5	25.0	-	-	8.1	0.1235	-	-	-	-	-	-	8.1	0.1235
Random	Hanning	64.0	0.04	2.9 - 10.5	25.0	-	-	8.1	0.1235	-	-	-	-	-	-	8.1 -	0.1235
								Time-lag-products correlation method with time windowing									
Flex	Hanning	-	0.08	7.0 - 10.2	12.5	0.89	1.00	8.20	0.1427	8.20	0.1537	8.20	0.1417	-	0.1329	8.20 0.00	0.1428 0.0055
Flex	Hanning + curve-fit	32.8	0.08	7.0 - 10.2	12.5	0.89	1.00	-	-	-	-	8.11	0.1730	-	-	8.11 -	0.1730 -
Osc	Hanning	-	0.08	7.0 - 10.2	12.5	0.87	1.00	8.20	0.1427	8.16	0.1407	8.20	0.1438	-	0.1529	8.19 0.017	0.1448 0.018
Osc	Hanning + curve-fit	33.2	0.08	7.0 - 10.2	12.5	0.87	1.00	-	-	-	-	8.19	0.1588	-	-	8.19 -	0.1588 -
Random	Hanning	32.1	0.08	7.0 - 10.2	12.5	-	-	8.83	0.1135	-	-	-	-	-	-	8.83	0.1135

Notes:

All frequencies in Hz.

o = mean deviation.

X = questionable value, not used in average.

Sample rate = 360 samples/second.

50

TABLE II. - HORIZONTAL TAIL SYMMETRIC SECOND BENDING MODE FREQUENCY AND DAMPING
(Mach = 0.95, Altitude = 1,794 meters, q = 51.5 kN/m^2)

Force	Smoothing	Comp time sec	Freq resol Hz	Analysis Window Frequency bandwidth Hz	Analysis Window Analog record length sec	Coherence Min	Coherence Max	Pwr spect density of response Freq	Pwr spect density of response g	Co-Quad spectra Freq	Co-Quad spectra g	Gain (Transfer function) Freq	Gain (Transfer function) g	Phase Freq	Phase g	Average Freq σ	Average g σ
Time-lag-products correlation method																	
FLEX	None	63.5	0.08	10.3-20.7	25	0.63	1.00	16.9	0.0690	18.0 X	0.0714	16.8	0.0597	-	0.0860	16.9 / 0.050	0.0716 / 0.0072
FLEX	Hanning	63.8	0.08	10.3-20.7	25	0.63	1.00	16.9	0.0725	18.0 X	0.0761	16.8	0.0635	-	0.0969	16.8 / 0.050	0.0773 / 0.01
FLEX	Hanning & curve-fit	66.5	0.08	10.3-20.7	25	0.63	1.00	-	-	-	-	16.8	0.1521	-	-	16.8 / -	0.1521 / -
Osc	None	63.5	0.08	10.3-20.7	25	0.69	1.00	16.9	0.0696	16.9	0.0761	16.9	0.0802	-	0.0919	16.9 / 0	0.0794 / 0.0066
Osc	Hanning	63.8	0.08	10.3-20.7	25	0.69	1.00	16.9	0.0725	16.9	0.0826	16.9	0.0849	-	0.0951	16.9 / 0	0.0838 / 0.0062
Random	None	63.7	0.08	10.3-20.7	25	Frequency range not excited, no "g" available										
Random	Hanning	63.7	0.08	10.3-20.7	25	Frequency range not excited, no "g" available										
Time-lag-products correlation method with time windowing																	
FLEX	Hanning		0.08	14.8-20.7	12.5	0.87	1.00	17.0	0.0695	17.0	0.0715	16.8	0.0637	-	0.0886	16.9 / 0.10	0.0733 / 0.028
FLEX	Hanning & curve-fit		0.08	14.8-20.7	12.5	0.87	1.00	-	-	-	-	16.8	0.2094	-	-	16.8 / -	0.2094 / -
Osc	Hanning		0.08	14.8-20.7	12.5	0.88	1.00	17.0	0.0695	16.9	0.0852	16.8	0.0768	-	0.0940	16.9 / 0.067	0.0814 / 0.0082
Osc	Hanning & curve-fit		0.08	14.8-20.7	12.5	0.88	1.00	-	-	-	-	16.9	0.2023	-	-	16.9 / -	0.2023 / -

NOTE: All frequencies in Hz.
σ = mean deviation.

X = questionable value, not used in average.
Sample rate = 360 samples/second.

TABLE III. – VERTICAL TAIL/EMPENNAGE FIRST MODE FREQUENCY AND DAMPING
(Mach = 0.95, Altitude = 1,794 meters, q = 51.5 kN/m^2)

| | | | | Analysis window | | Coherence | | Pwr spect density of response | | Co-quad spectra | | Gain (transfer function) | | Phase | | Average | |
Force	Smoothing	Comp time sec	Freq resol Hz	Frequency bandwidth Hz	Analog record length sec	Min	Max	Freq	g	Freq	g	Freq	g	Freq	g	Freq σ	g σ
FLEX	None	63.0	0.04	9.5–12.7	25.0	0.22	0.50	10.6	0.067	10.7	0.0443	10.7	0.0610	—	0.058	10.7 .0333	0.0578 .0067
FLEX	Hanning	62.5	0.04	9.5–12.7	25.0	.21	.50	10.6	.067	10.7	.0443	10.7	.0610	—	.0832	10.7 .0333	.0639 .0112
FLEX	Hanning + curve-fit	81.78	0.04	9.5–12.7	25.0	.21	.50	————————— No curve fitted to this mode —————————									
Osc	None	63.0	0.04	9.5–12.7	25.0	.23	.52	10.6	.067	10.6	.0303	10.7	.0632	—	.0809	10.6 .033	.0604 .0151
Osc	Hanning	62.5	0.04	9.5–12.7	25.0	.22	.52	10.6	.067	10.6	.0479	10.7	.0632	—	.0535	10.6 .033	.0574 .0072
Random	Hanning	64.5	0.04	9.5–12.7	25.0	—	—	11.1	.0514	—	—	—	—	—	—	11.1 —	.0514 —
Random	None	63.4	0.04	9.5–12.7	25.0	—	—	11.1	.0514	—	—	—	—	—	—	11.1 —	.0514 —
FLEX	Hanning + curve-fit	47.9	0.08	9.2–12.7	12.5	.26	.80	10.7	.0591	10.7	.0444	10.7	.0388	—	—	10.7 0	.0472 .0077
Osc	Hanning + curve-fit	47.4	0.08	9.2–12.7	12.5	.22	.85	10.7	.0591	10.6	.0521	10.7	.0448	—	.0774	10.7 .033	.0584 .010
Random	Hanning	31.6	0.08	11.1–13.7	12.5	—	—	11.1	.0457	—	—	—	—	—	—	11.1 —	.0457 —

NOTES: All frequencies in Hz   X – questionable value, not used in average

σ = mean deviation   sample rate = 360 samples/second

TABLE IV. - VERTICAL TAIL/EMPENNAGE SECOND MODE FREQUENCY AND DAMPING
(Mach = 0.95, Altitude = 1,795 meters, q = 51.5 kN/m^2)

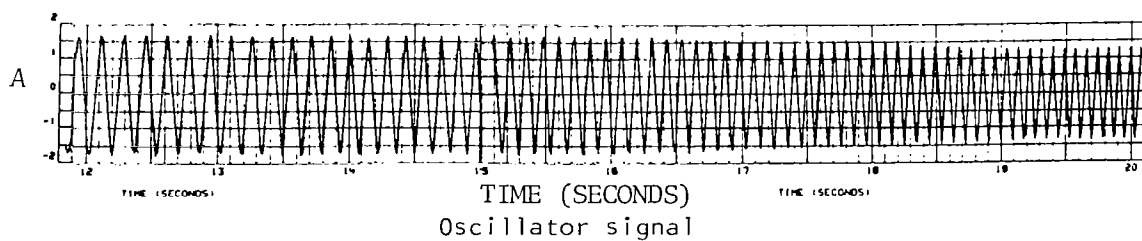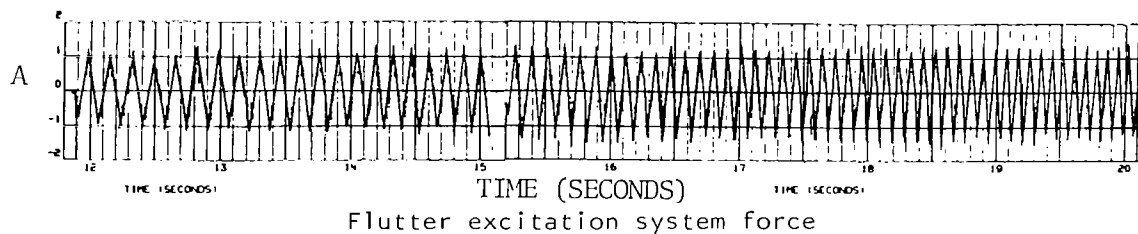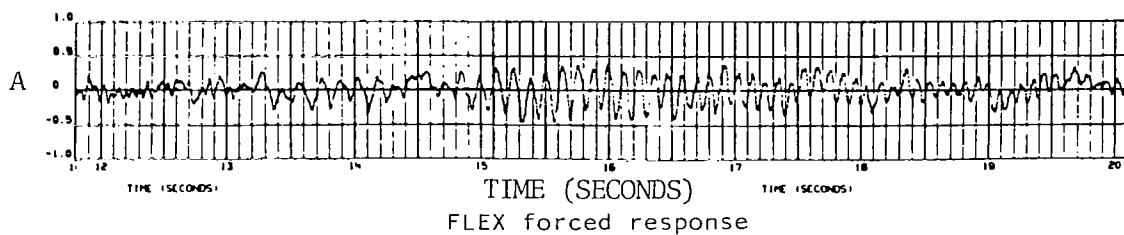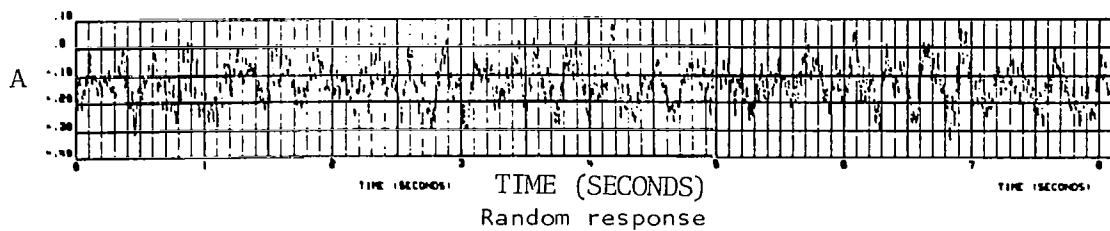|				Analysis window		Coherence		Pwr spect density of response		Co-Quad Spectra		Gain (transfer function)		Phase		Average	
Force	Smoothing	Comp time sec	Freq resol Hz	Frequency bandwidth Hz	Analog record length sec	Min	Max	Freq	g	Freq	g	Freq	g	Freq	g	Freq σ	g σ
FLEX	None	63.0	0.04	9.5–12.7	25.0	0.29	0.78	11.5	0.1176	11.7	0.033	11.7	0.079	—	0.107	11.6 .100	0.0842 .0282
FLEX	Hanning	62.5	0.04	9.5–12.7	25.0	.30	.79	11.5	.1176	11.2	.0308	11.6	.0850	—	.1154	11.4 .167	0.0872 .0293
FLEX	Hanning + curve-fit	81.78	0.04	9.5–12.7	25.0	.30	.79	—	—	—	—	11.8	0	—	—	11.8 —	0
Osc	None	63.0	0.04	9.5–12.7	25.0	.33	.56	11.5	.1204	11.5	.0342	11.7	.0912	—	.1452 X	11.6 .100	.0819 —
Osc	Hanning	62.5	0.04	9.5–12.7	25.0	.33	.66	11.5	.1176	11.5	.0345	11.7	.1325	—	.1082	11.6 .100	.0982 .0319
Random	Hanning	64.5	0.04	9.5–12.7	25.0	—	—	11.9	.0620	—	—	—	—	—	—	11.9 —	.0620 —
Random	None	63.4	0.04	9.5–12.7	25.0	—	—	11.9	.0620	—	—	—	—	—	—	11.9 —	.0620 —
FLEX	Hanning + curve-fit	48.3	0.08	11.1–13.7	12.5	.33	.87	11.8	.0711	11.7	.0341	11.7	.060	—	—	11.7 .033	.0551 .0140
Osc	Hanning + curve-fit	48.3	0.08	11.1–13.7	12.5	.34	.87	11.8	.0711	11.7	.0341	11.7	.060	—	.1507 X	11.7 .033	.0551 .0140
Random	Hanning	31.6	0.08	11.1–13.7	12.5	—	—	11.9	.0533	—	—	—	—	—	—	11.9 —	.0533 —

NOTES: All frequencies in Hz   X — questionable value, not used in average

σ = mean deviation   Sample rate = 360 samples/second

TABLE V. - VERTICAL TAIL/EMPENNAGE THIRD MODE FREQUENCY AND DAMPING
(Mach = 0.95, Altitude = 1,794 meters, q = 51.5 kN/m^2)

				Analysis window		Coherence		Pwr spect density of response		Co-quad spectra		Gain (transfer function)		Phase		Average	
Force	Smoothing	Comp time sec	Freq resol Hz	Frequency bandwidth Hz	Analog record length sec	Min	Max	Freq	g	Freq	g	Freq	g	Freq	g	Freq σ	g σ
FLEX	None	63.0	0.04	9.5–12.7	25.0	—	—	—	—	13.2	—	13.1	0.068	—	X	13.1 .200	0.068 —
FLEX	Hanning	62.5	0.04	9.5–12.7	25.0	0.30	0.90	—	—	13.2	—	13.1	.068	—	—	13.0 .200	.0748 .0067
FLEX	Hanning + curve-fit	81.78	0.04	9.5–12.7	25.0	.30	.90	— No curve fitted to this mode —									
Osc	None	63.0	0.04	9.5–12.7	25.0	.34	.89	12.7	.0815	—	—	13.1	.0728	—	—	12.9 .200	.0772 .0043
Osc	Hanning	62.5	0.04	9.5–12.7	25.0	.32	.88	12.7	.0815	13.2	.0447	13.1	.0739	—	—	13.0 .200	.0667 .0147
Random	Hanning	64.5	0.04	9.5–12.7	25.0	—	—	13.4	.0534	—	—	—	—	—	—	13.4 —	.0534 —
Random	None	63.4	0.04	9.5–12.7	25.0	—	—	13.4	.0534	—	—	—	—	—	—	13.4 —	.0534 —
FLEX	Hanning + curve-fit	48.3	0.08	11.1–13.7	12.5	.54	.93	13.1	.0584	13.1	.0306	13.1	.0448	—	—	13.1 0	.0446 .0093
Osc	Hanning + curve-fit	48.3	0.08	11.1–13.7	12.5	.54	.92	13.1	.0584	13.1	.0306	13.1	.0448	—	—	13.1 0	.0446 .0093
Random	Hanning	31.6	0.08	11.1–13.7	12.5	—	—	13.2	.0553	—	—	—	—	—	—	13.2 —	.0553 —

NOTES: All frequencies in Hz   X — questionable value, not used in average

σ = mean deviation   sample rate = 360 samples/second

Figure 1. B-1 Prototype test aircraft.
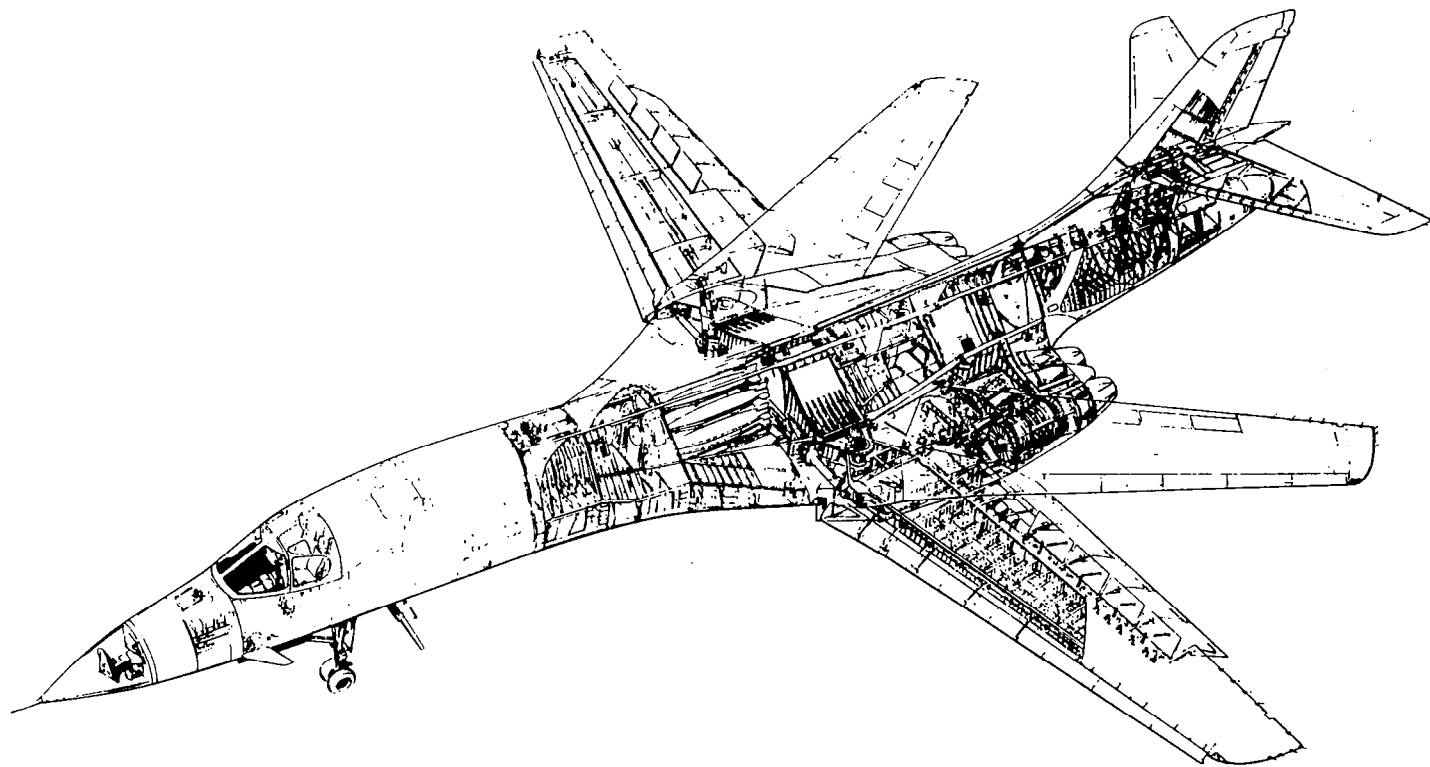
Figure 2. - Structural arrangement.

Note:

A2019-T - Telemetered channel
Response accelerometers in velocity (inches/second).
FLEX force accelerometers in g's.

A2025-T

A2345-T (FLEX)

A2344-T (FLEX)   A2024-T

A2026-T

S5249-T

S5247-T

S5245-T

A2342-T (FLEX)   A2020-T

A2023-T

A2022-T

A2030

A2040

A2033

A2034

A2735-T

A2343-T (FLEX)

M1227-T (FLEX oscillator)

A2029

A2036-T

A2041

A2038-T

A2032

A2035

A2003

A2347-T

A2004

A2039

A2219

A2217

A2028

A2006

A2020-T

A2017

A2007

A2016

A2015

A2031

A2019-T

A2341-T (FLEX)

S5160
S5161 } Actuator load strain gages

A2027

Note: ▲ Vertical accelerometers

● Lateral accelerometers

X Strain gage

Figure 3. - Location of instrumentation.
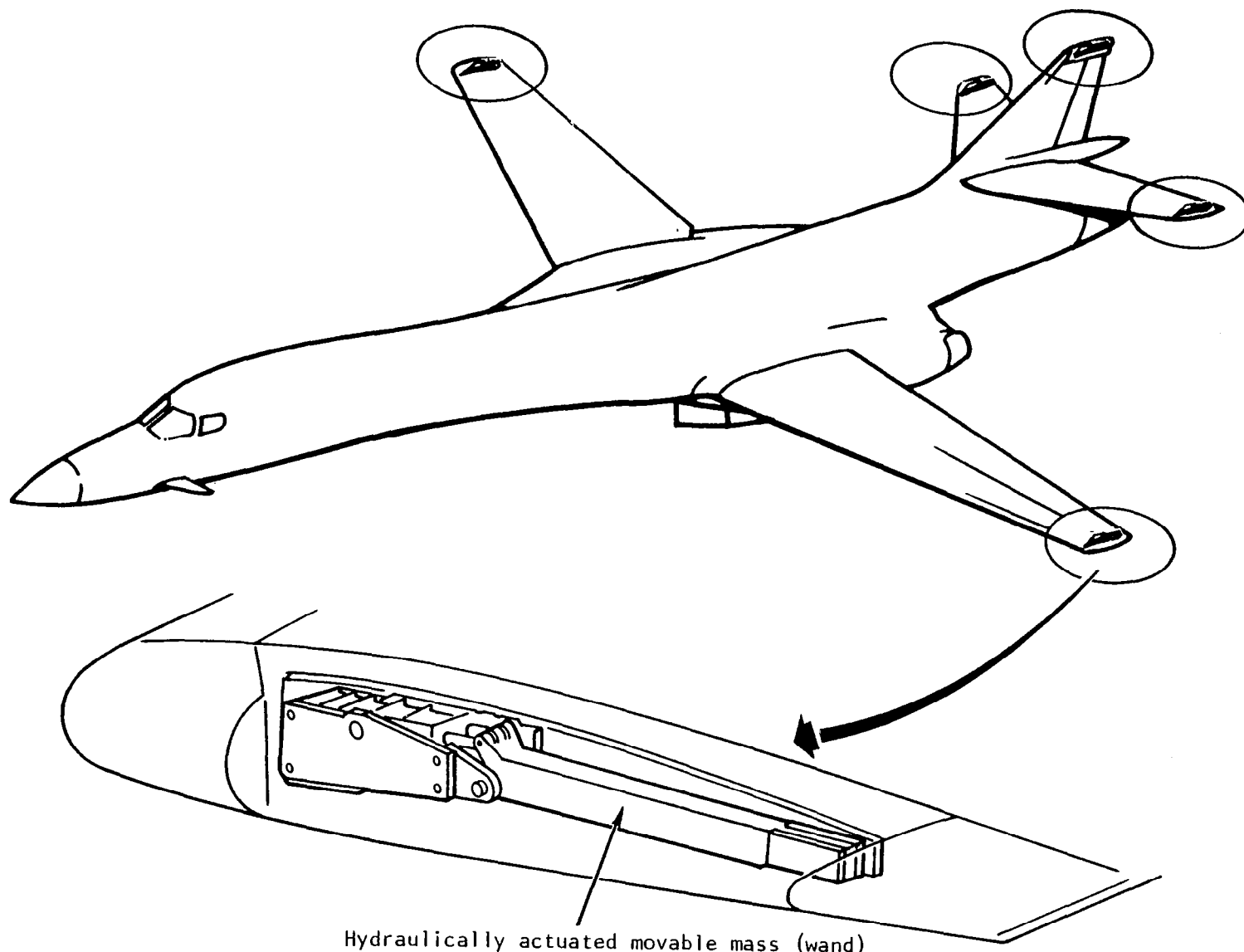
Hydraulically actuated movable mass (wand)

Figure 4a. - Flutter excitation system.
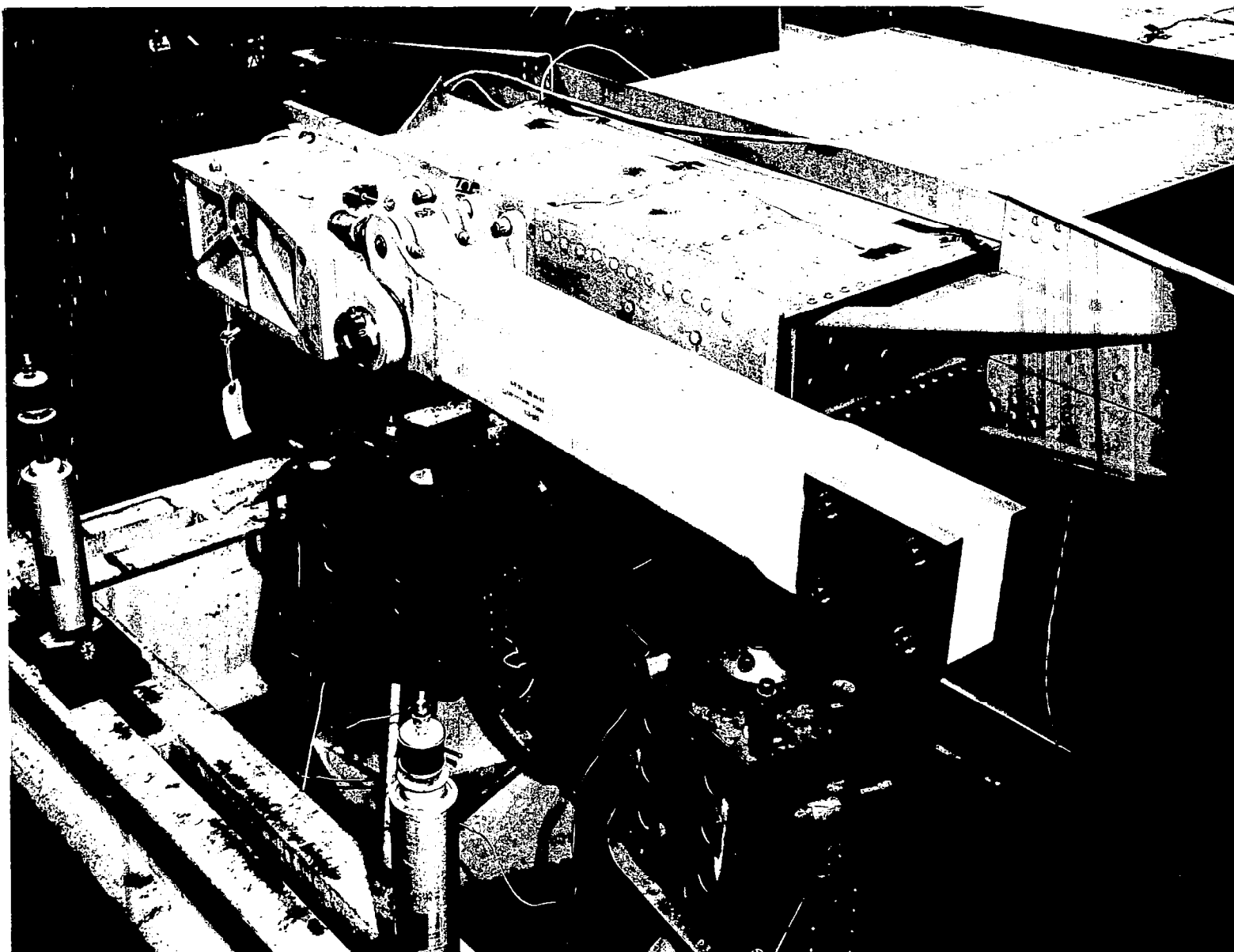
Figure 4b. FLEX exciter on test stand.
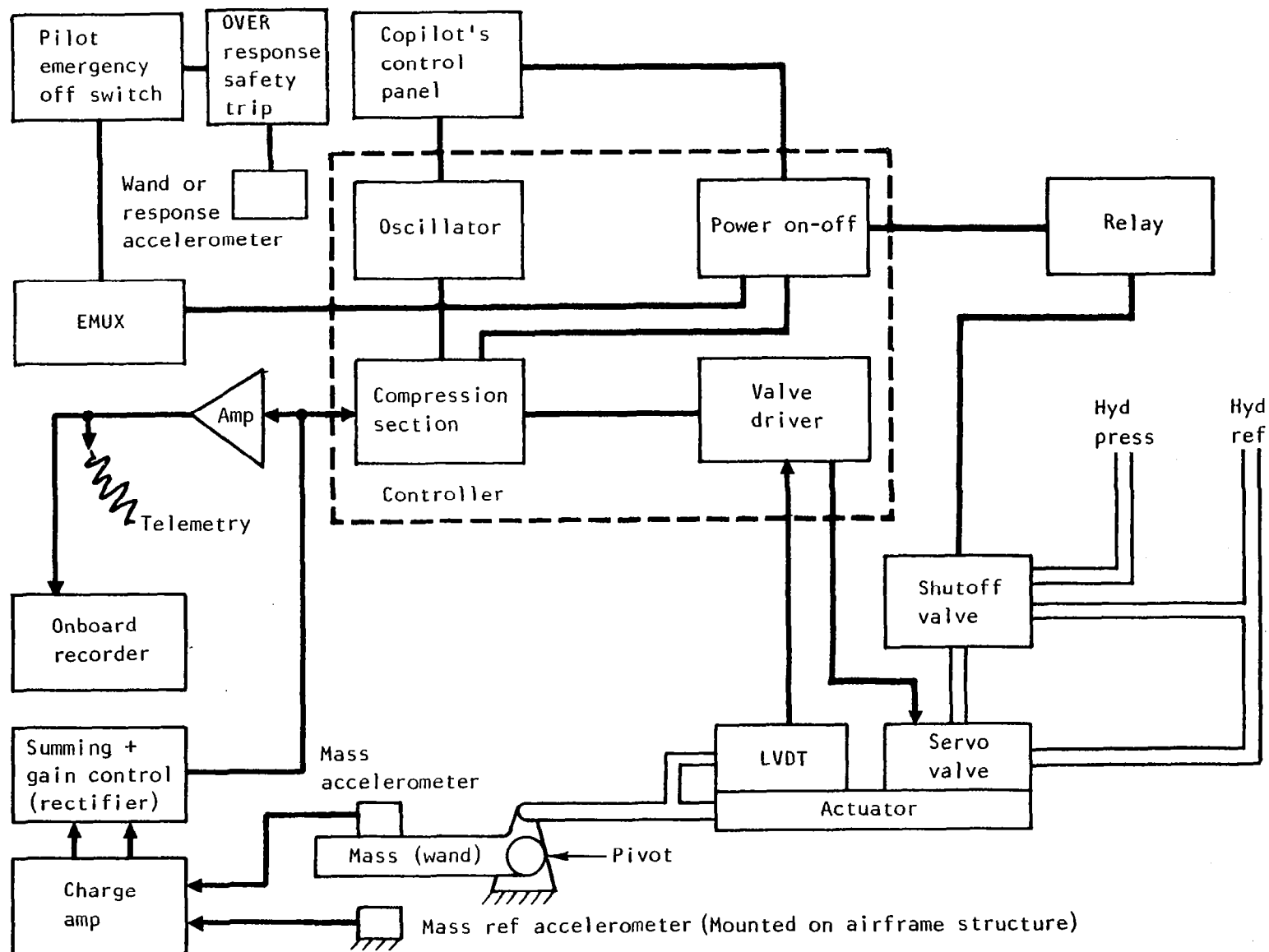
Figure 5. - Flutter excitation system control loop.
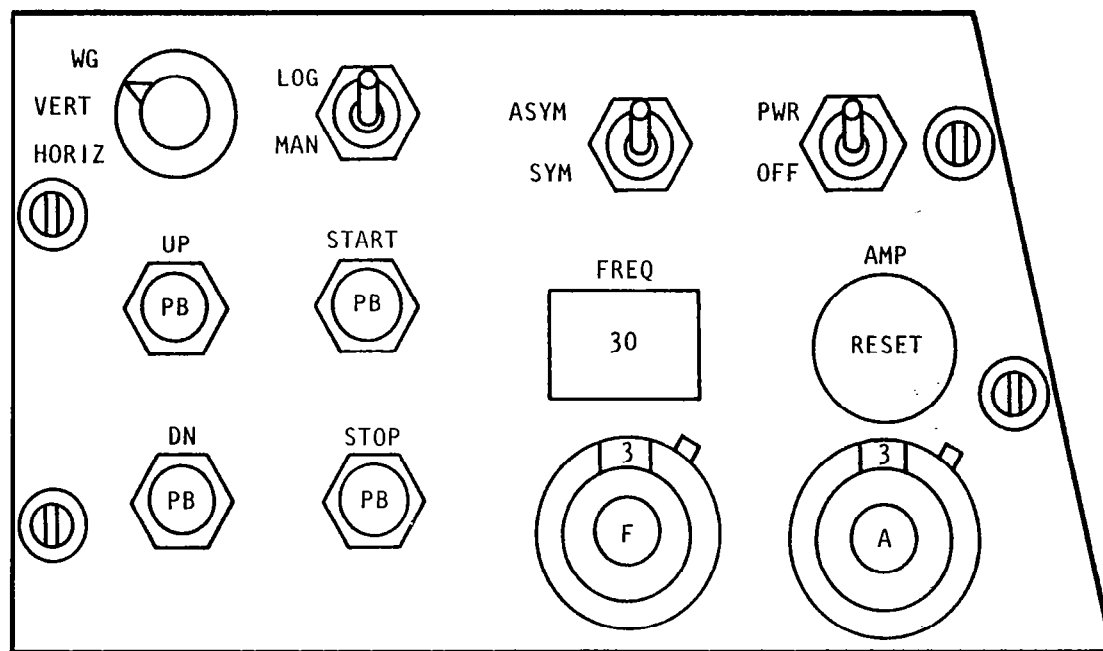
Figure 6. - Copilot's FLEX control panel.
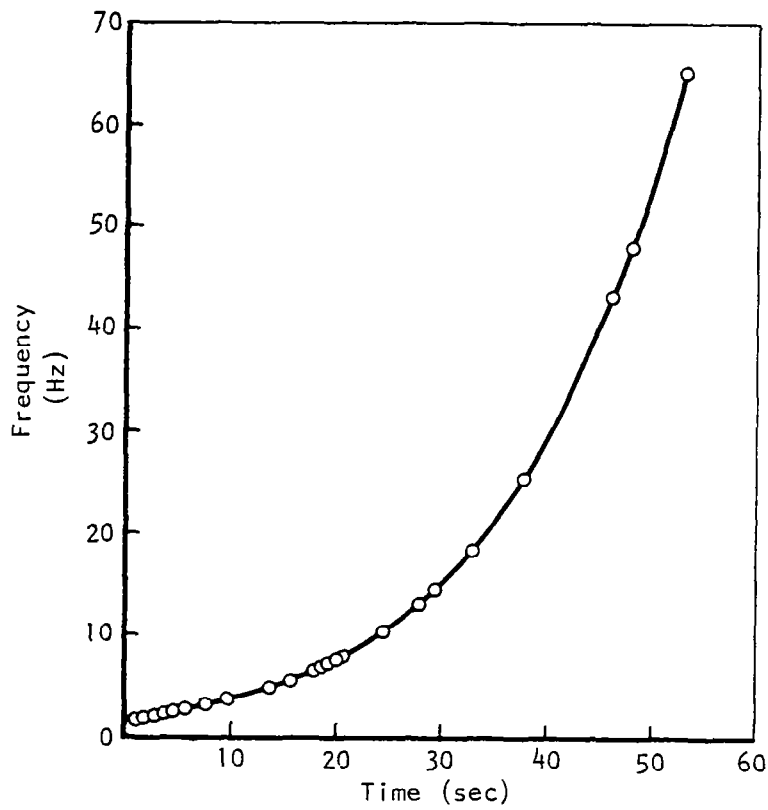
Figure7.- Flutter excitation system sweep frequency versus time.
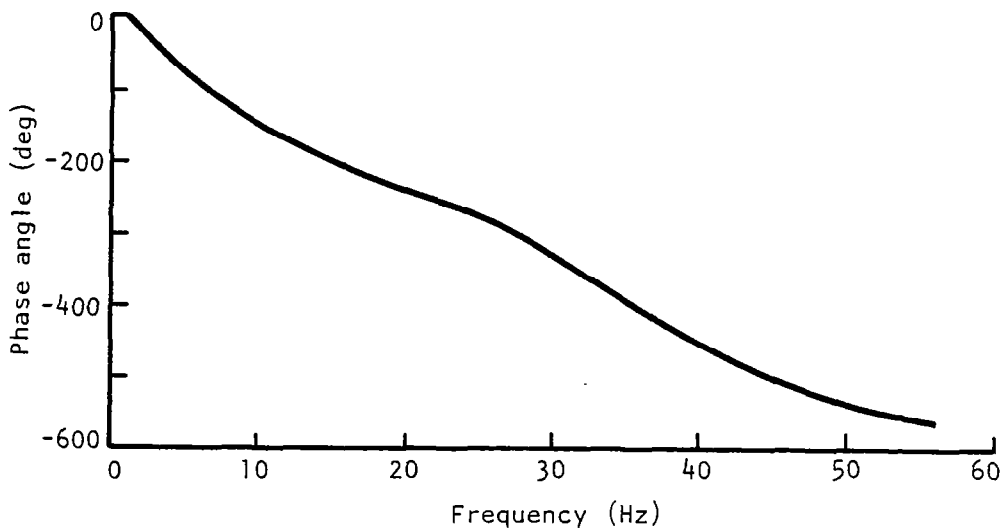
Figure 8. - Phase angle between the FLEX force and the oscillator command signal.
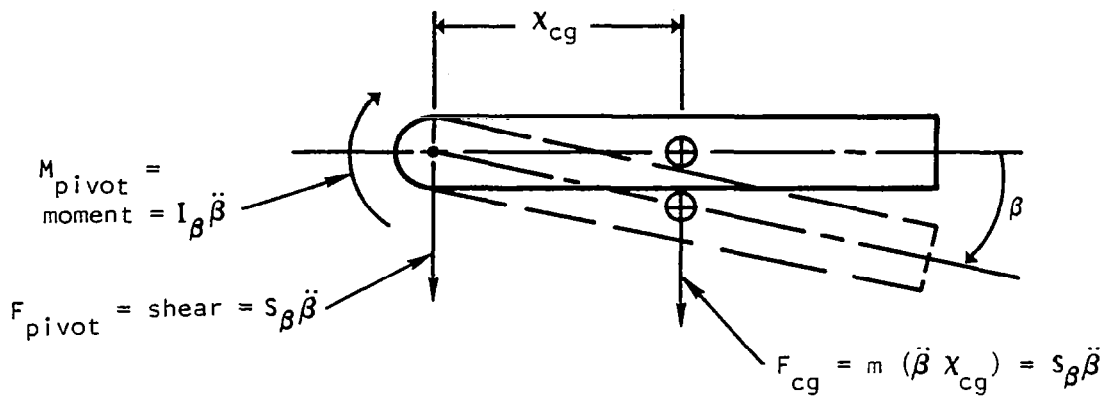
(a) Shaker force output of FLEX wand
with distributed mass

$$X_e = \frac{moment}{shear} = \frac{I_\beta \ddot{\beta}}{S_\beta \ddot{\beta}} = \frac{I_\beta}{S_\beta}$$

$$m_e = \frac{I_\beta}{X_e^2} = \frac{S_\beta}{X_e}$$
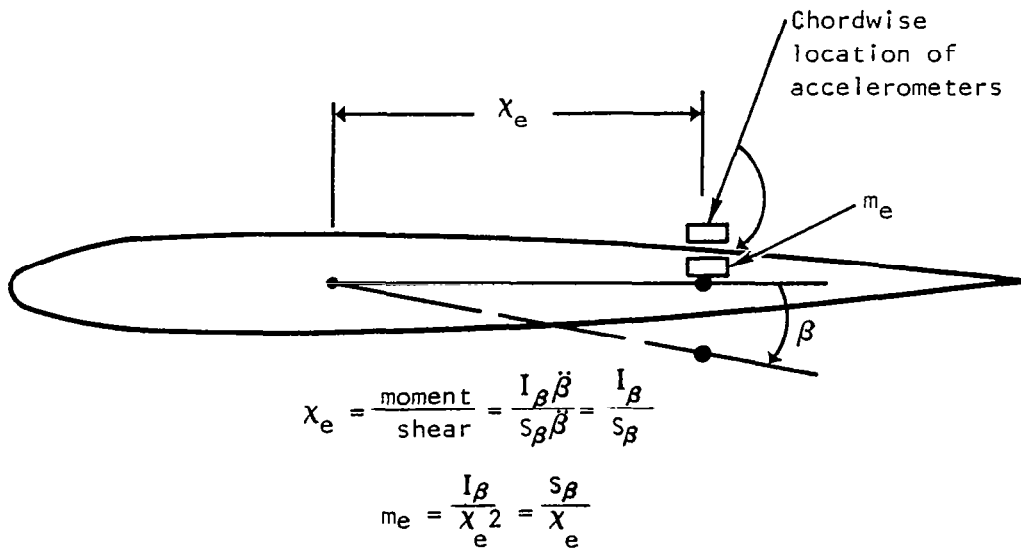
(b) Equivalent point mass

Figure 9. - Required chordwise location of the shaker accelerometers.
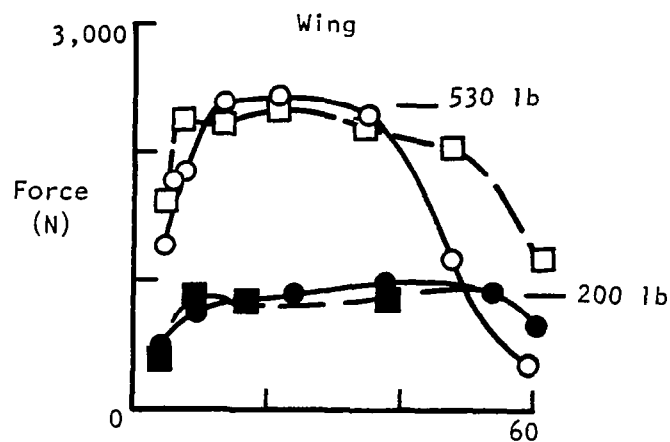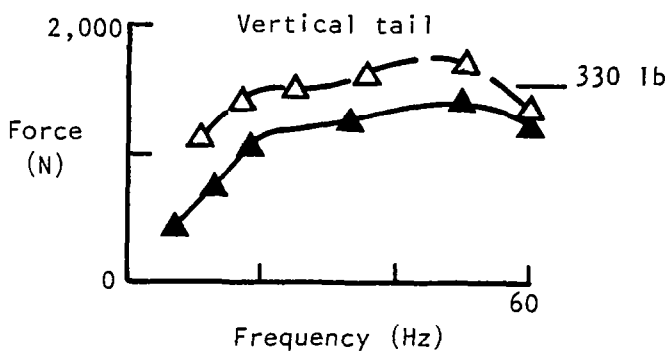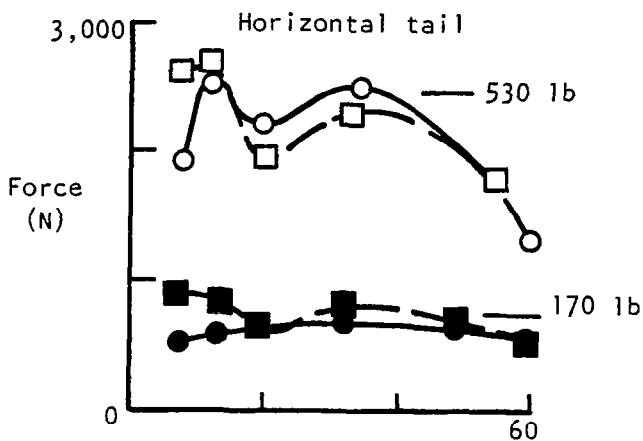
Figure 10. - Typical flutter excitation system forces input to structure at surface tips.
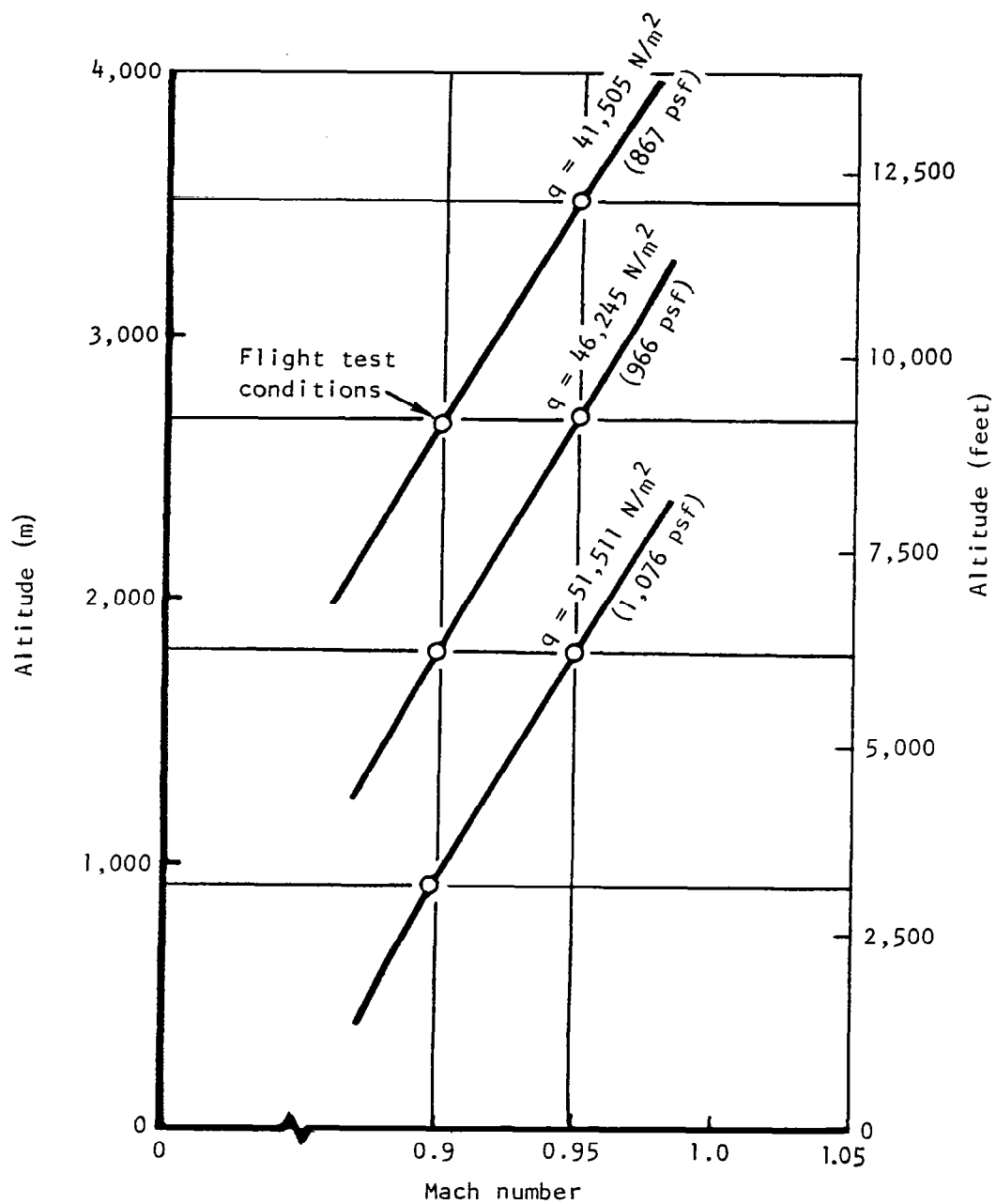
Figure 11. - Flight conditions used for data analysis along lines of constant Mach number, constant altitude, and constant dynamic pressure.

Telemetry

● Real-time monitoring

Gain

Plots

Onboard tape

Time-lag products correlation analysis on minicomputer

● Near-real-time data analysis

Time-lag products
correlation analysis
on large storage computer

Phase
Gain
Co-Quad
PSD

Plots

● Postflight data analysis
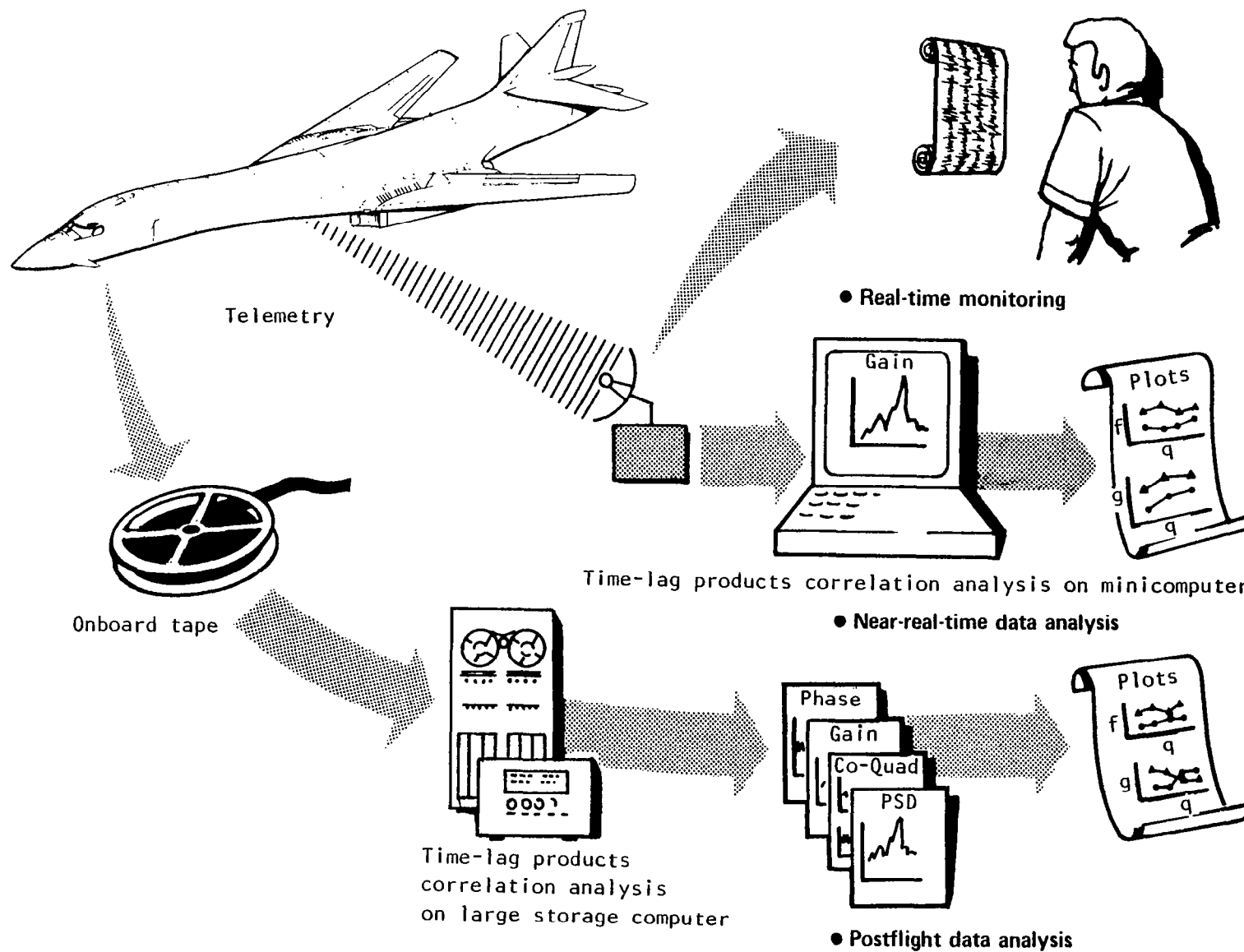
Figure 12. - Flight flutter test data analysis methodology.

(a) Auto-or cross-correlation function

$$freq = n/t$$

$$g = \frac{1}{n\pi} \ln \frac{A_0}{A_n}$$

(b) Autospectra density function

$$f = \frac{\omega_0}{2\pi} = peak\ freq$$

$$g = \frac{\omega_2 - \omega_1}{\omega_0}$$

(c) Co-and quadrature spectra

$$Co: freq = \frac{\omega_0}{2\pi}$$

$$Quad: g = \frac{\left(\frac{\omega_2}{\omega_1}\right)^2 - 1}{\left(\frac{\omega_2}{\omega_1}\right)^2 + 1}$$
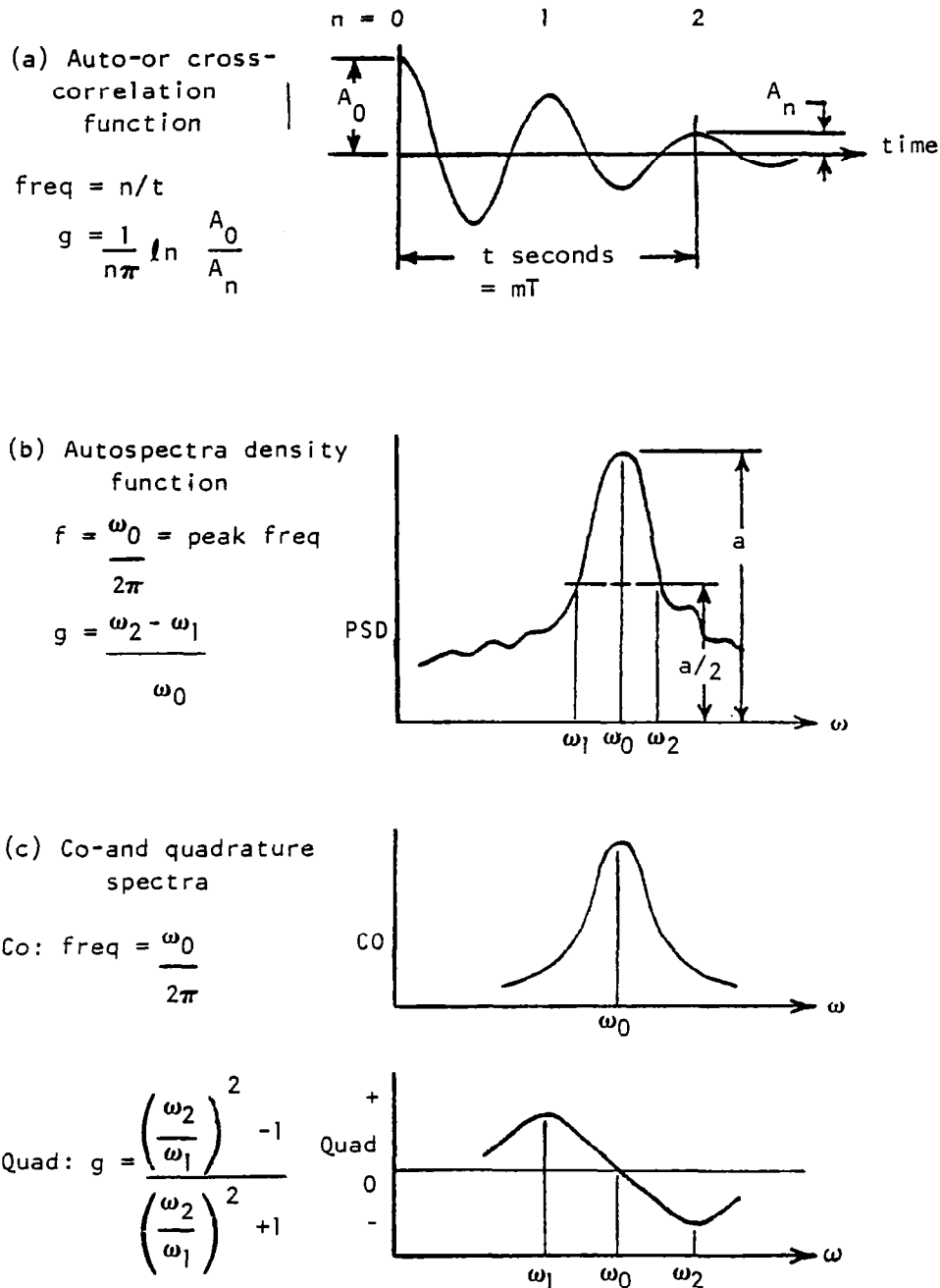
Figure 13. - Five methods of manually calculating modal frequency and/or damping from the time-lag-products correlation/frequency analysis procedure.

(d) Gain or transfer
     function

$$f_o = \frac{\omega_0}{2\pi} = \text{peak freq}$$

$$g = \frac{\omega_2 - \omega_1}{\omega_0}$$
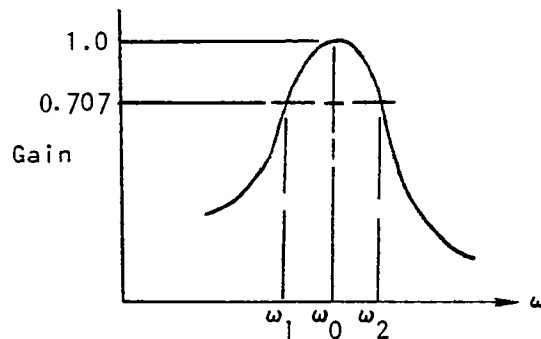
(e) Phase angle between
     force and response

$$g = \frac{2}{\frac{1}{57.3}\left(\phi_2^\circ - \phi_1^\circ\right)\left[\dfrac{\omega_2 - \omega_1}{\omega_0}\right]}$$
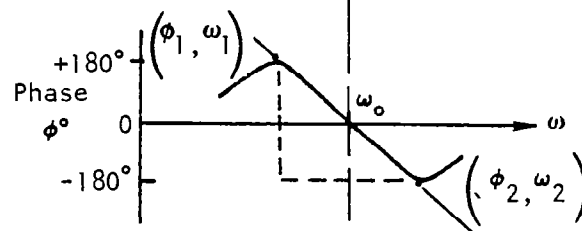
Figure 13. - Continued.
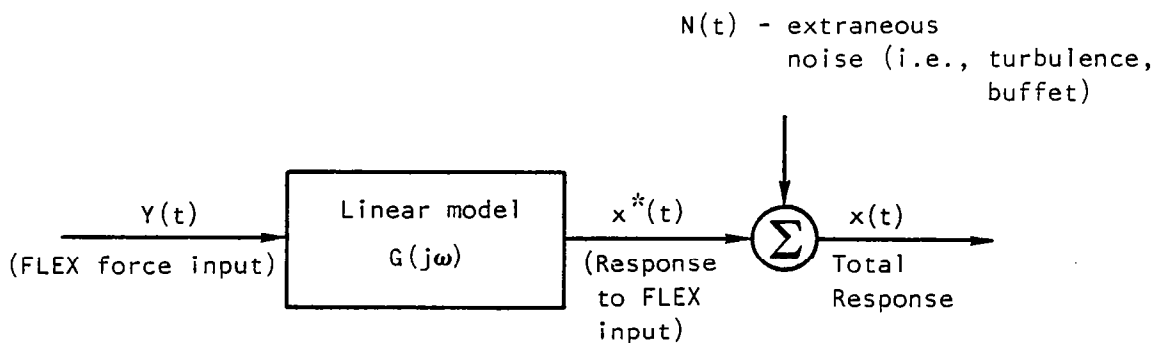
Figure 14. - General cross-spectral analysis model.
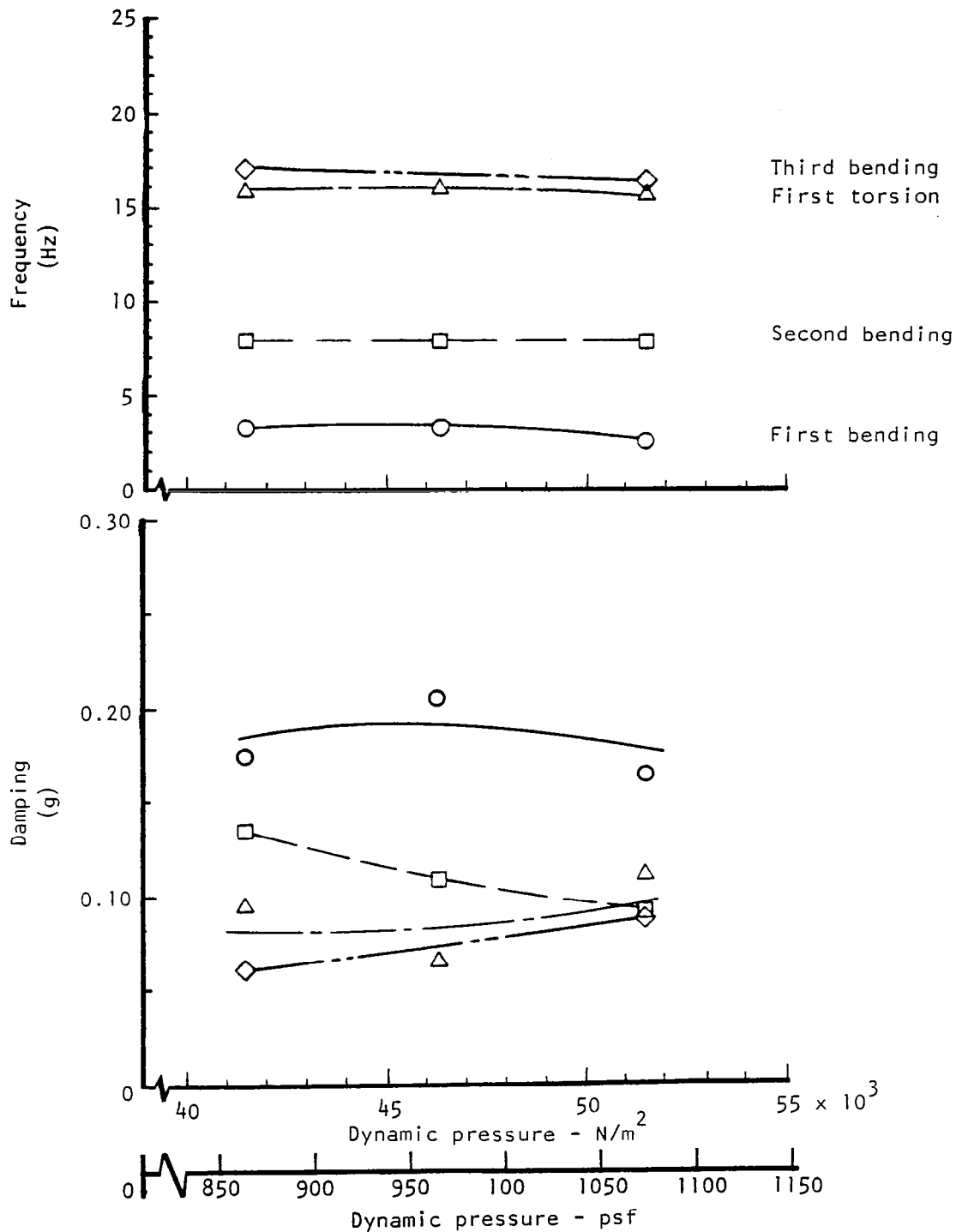
(a) Wing symmetric response at Mach = 0.90

Figure 15. - Flight flutter test data using time-lag-products
correlation method at Mach = 0.90.
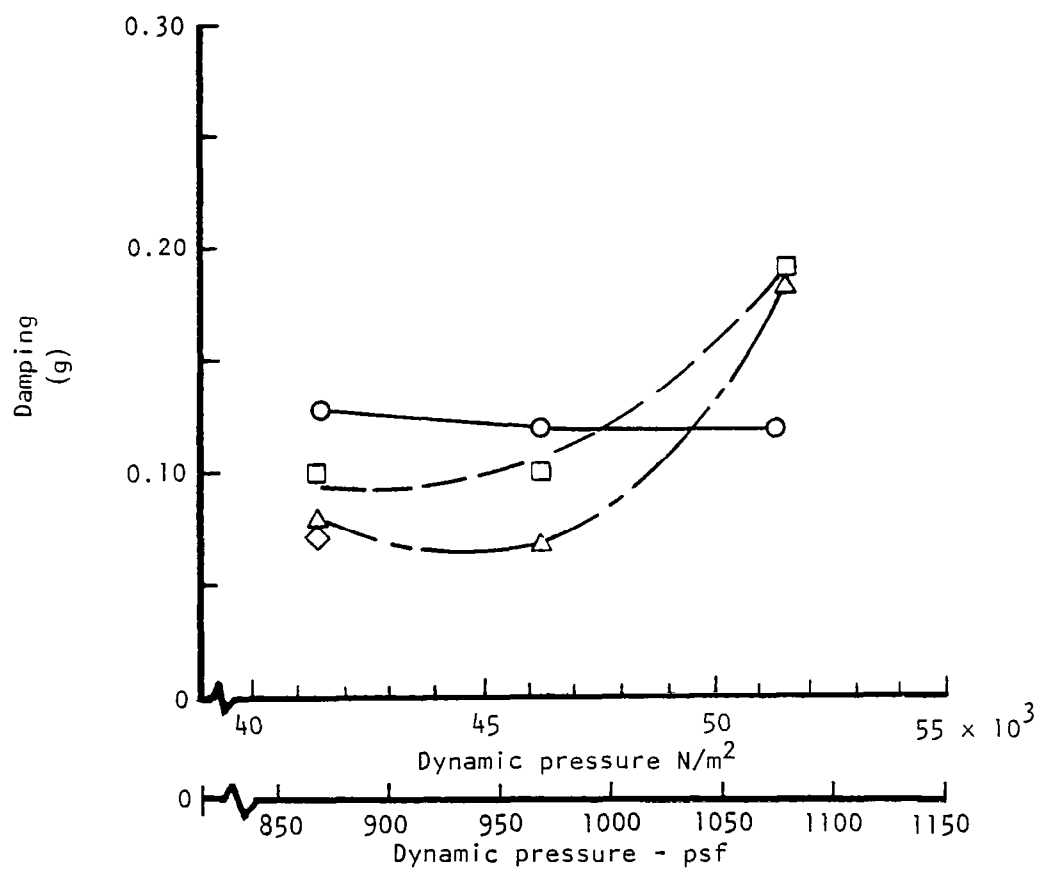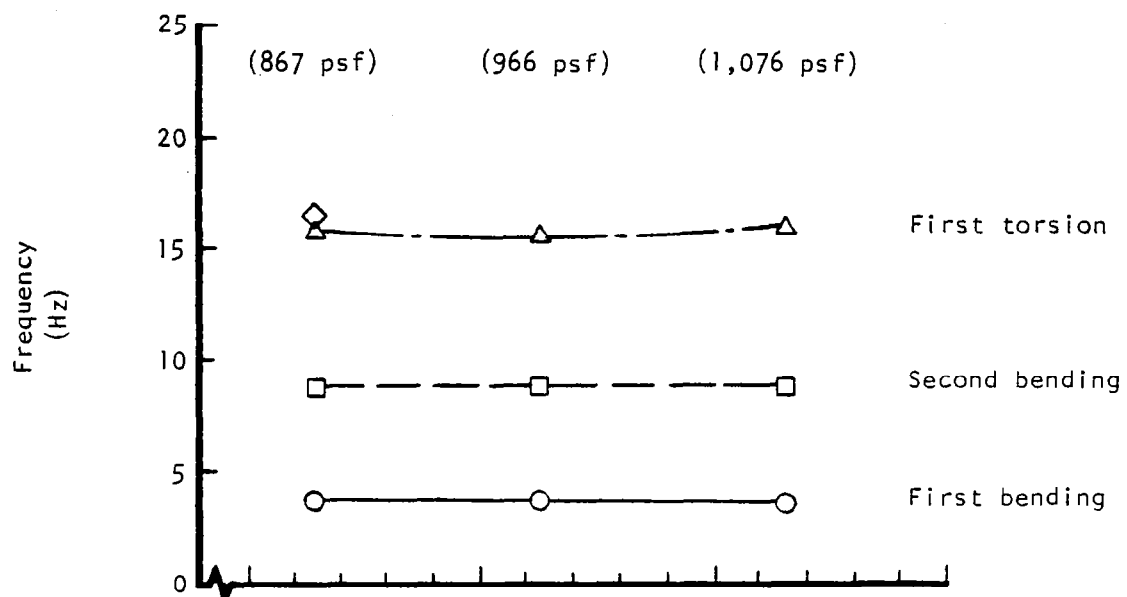
(b) Wing antisymmetric response at Mach = 0.90

Figure 15. - Continued.
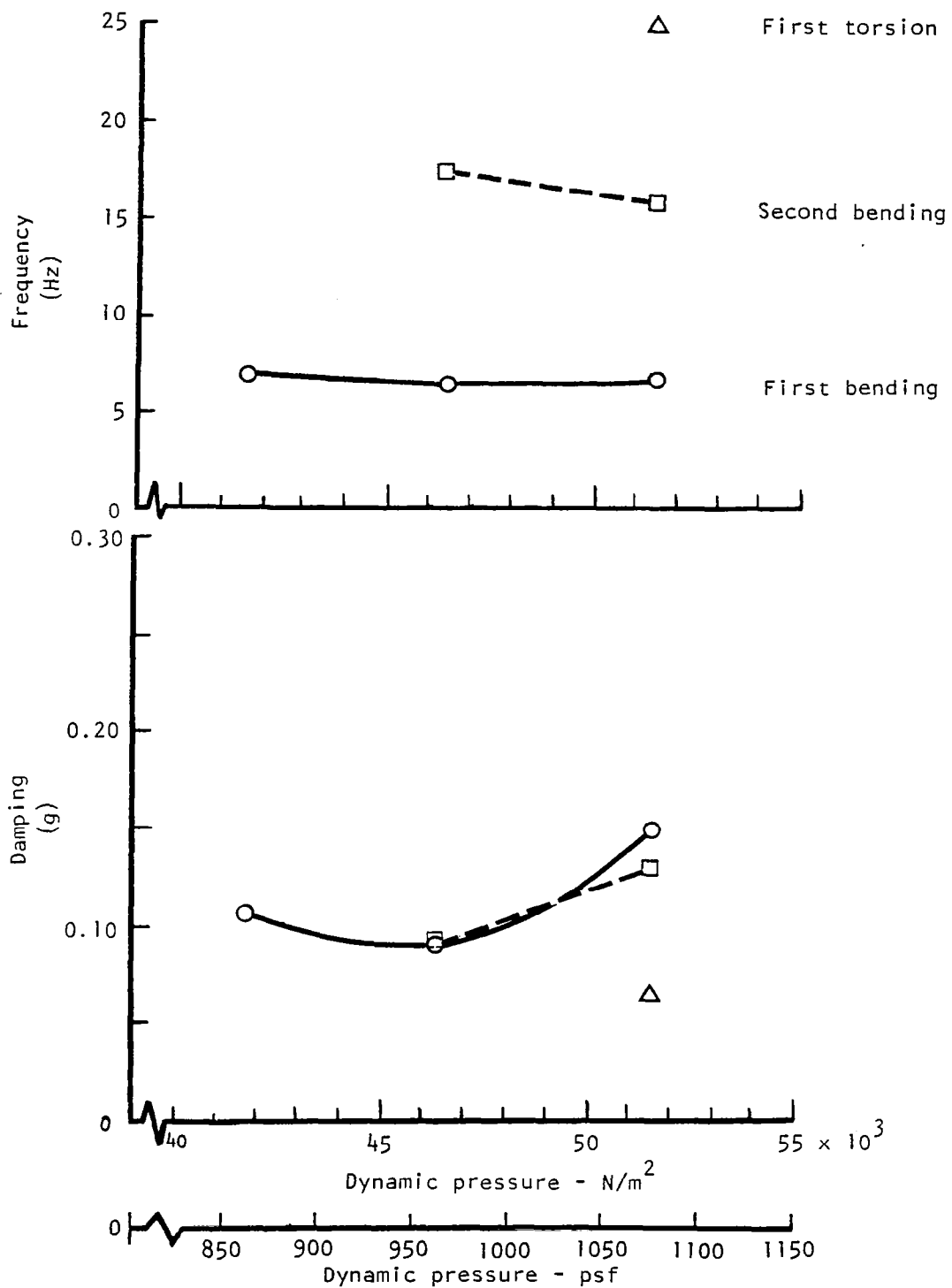
(c) Horizontal tail symmetric response at Mach = 0.90

Figure 15. - Continued.
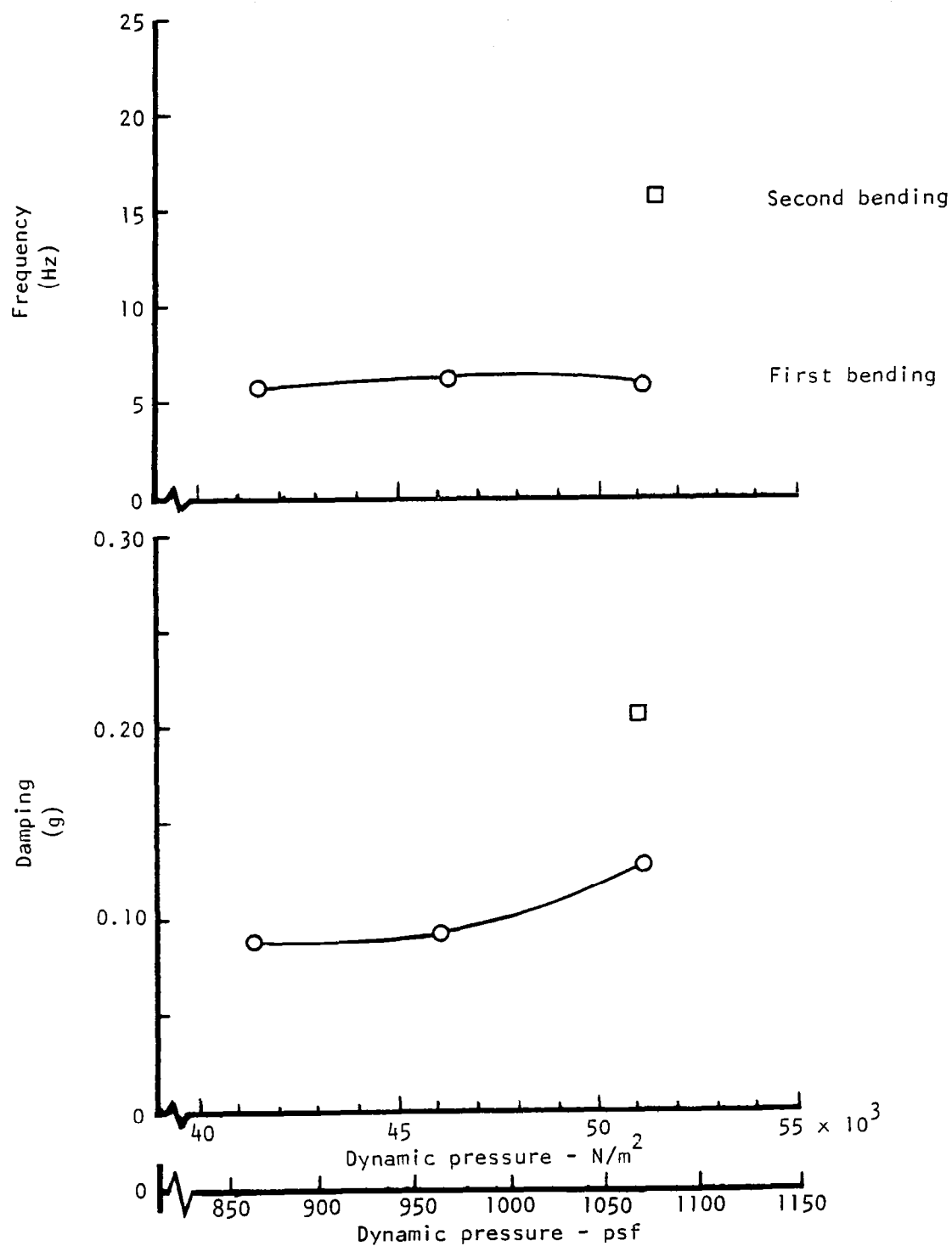
(d) Horizontal tail antisymmetric response at Mach = 0.90

Figure 15. - Continued.
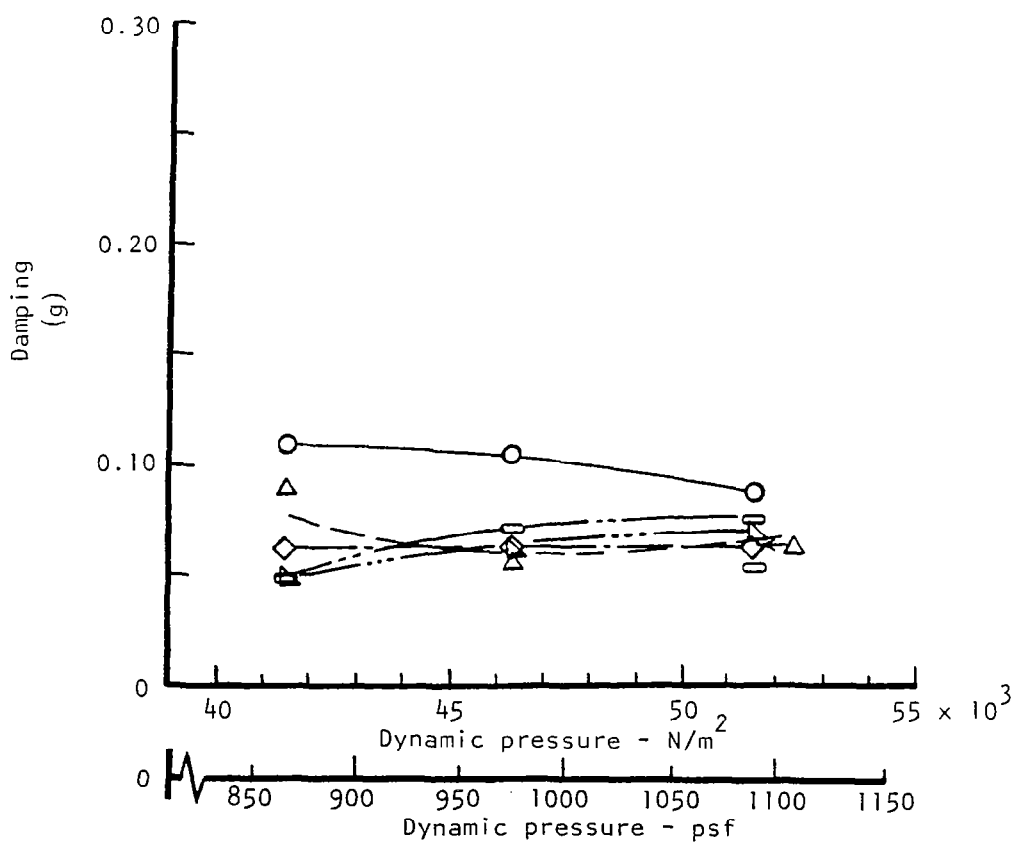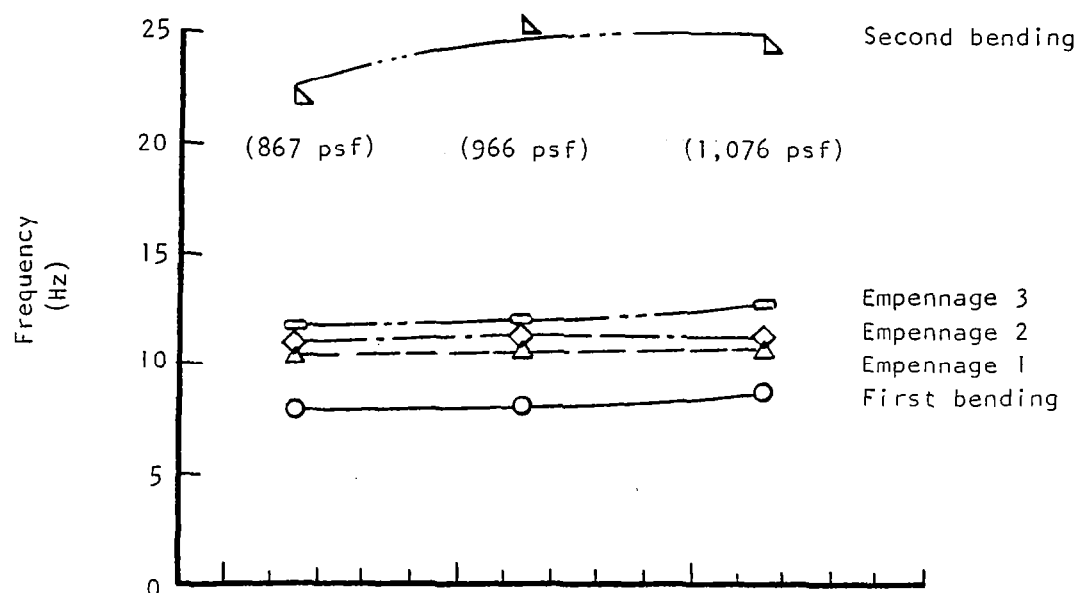
(e) Vertical tail/empennage response at Mach = 0.90

Figure 15. - Concluded
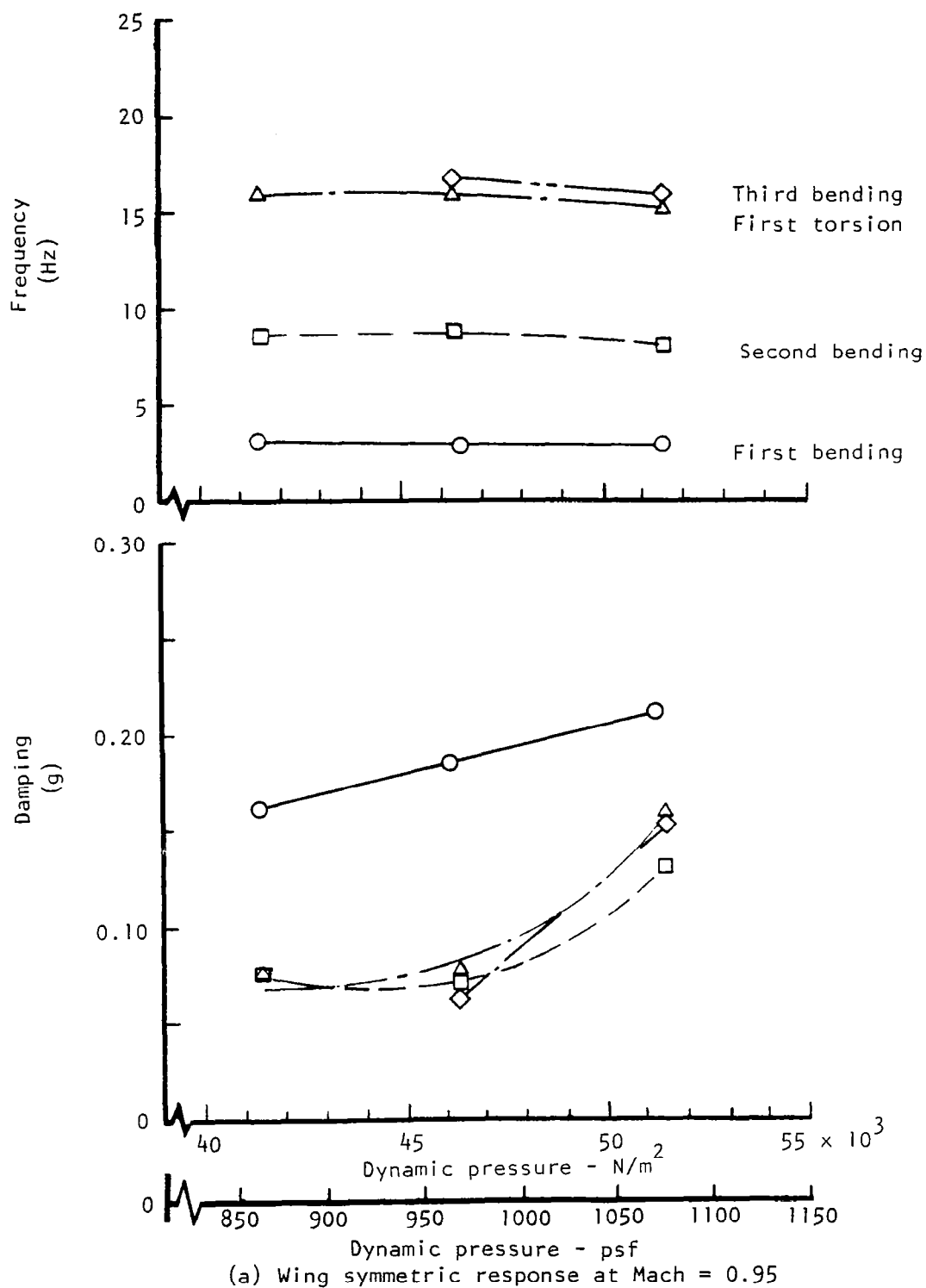
Figure 16. - Flight flutter test data using time-lag-products
correlation method at Mach = 0.95.
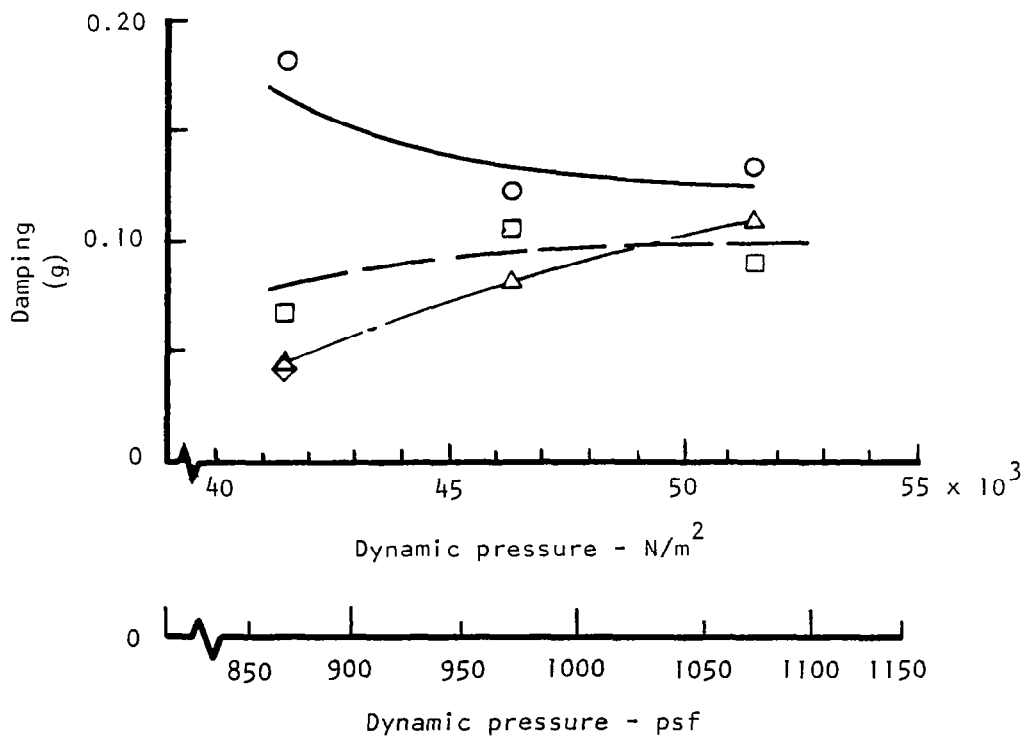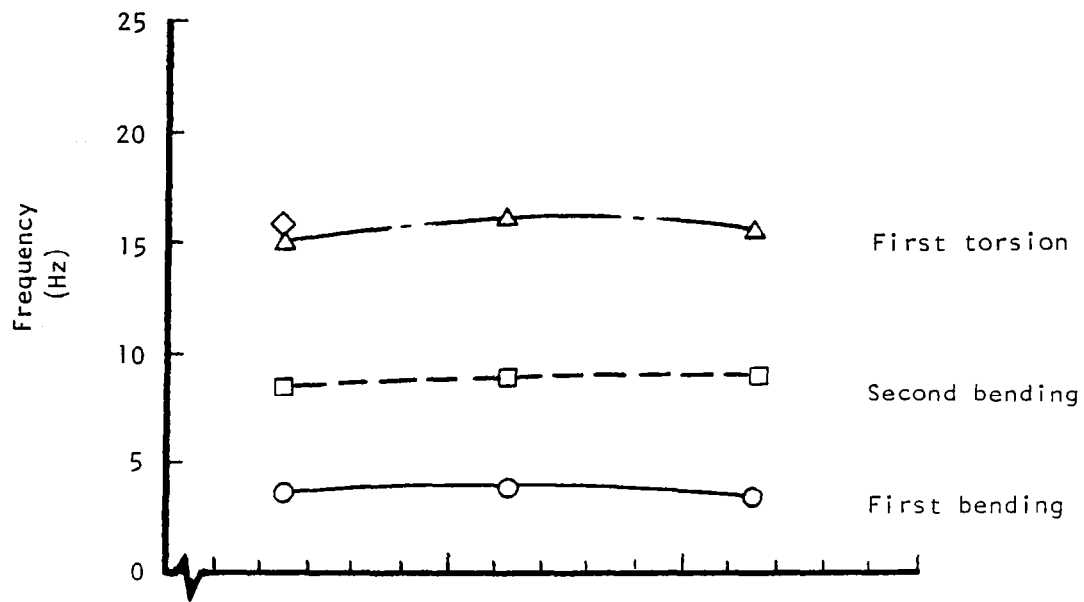
(b) Wing antisymmetric response at Mach = 0.95

Figure 16. - Continued.
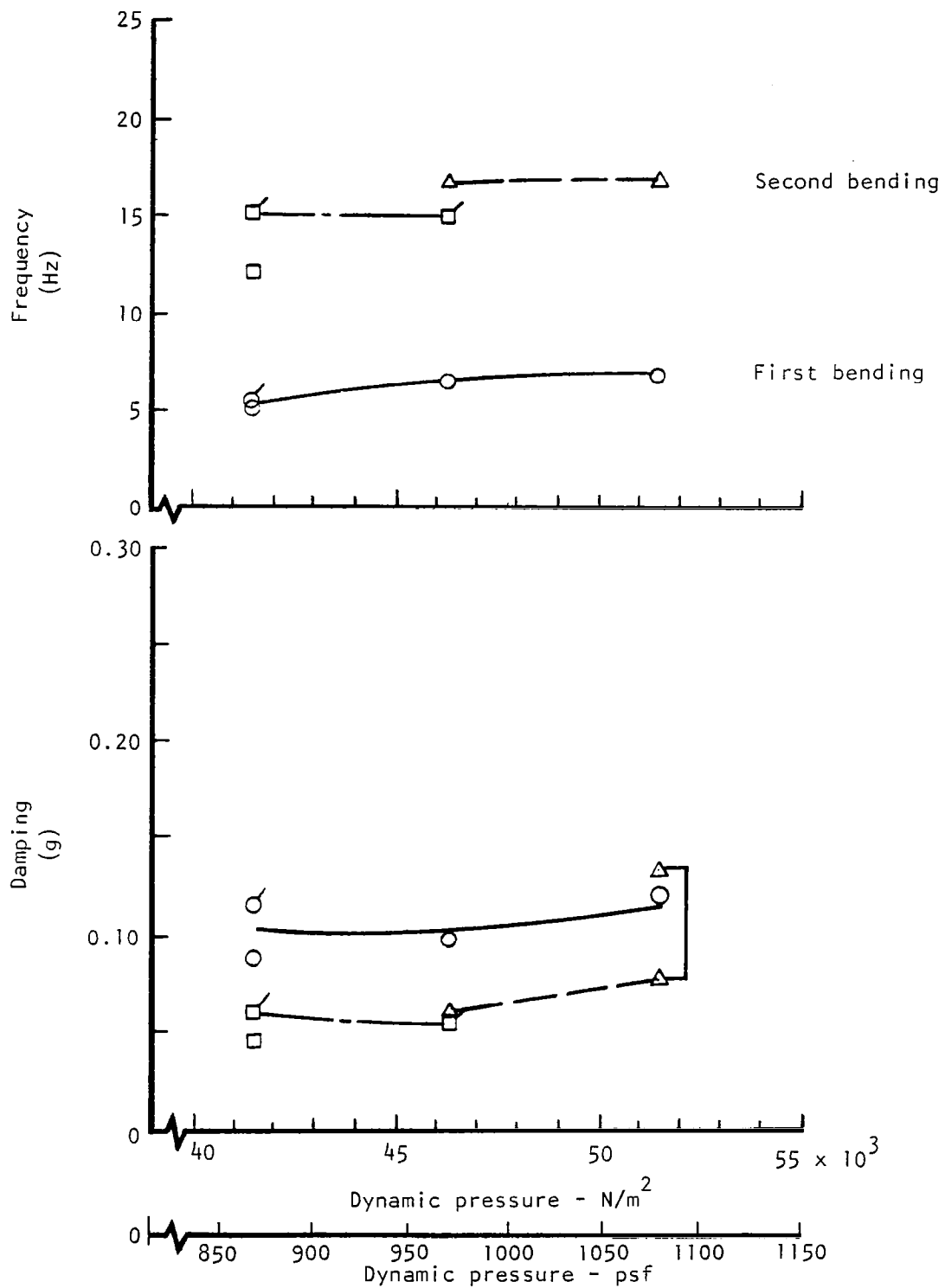
(c) Horizontal tail symmetric response at Mach = 0.95

Figure 16. - Continued.
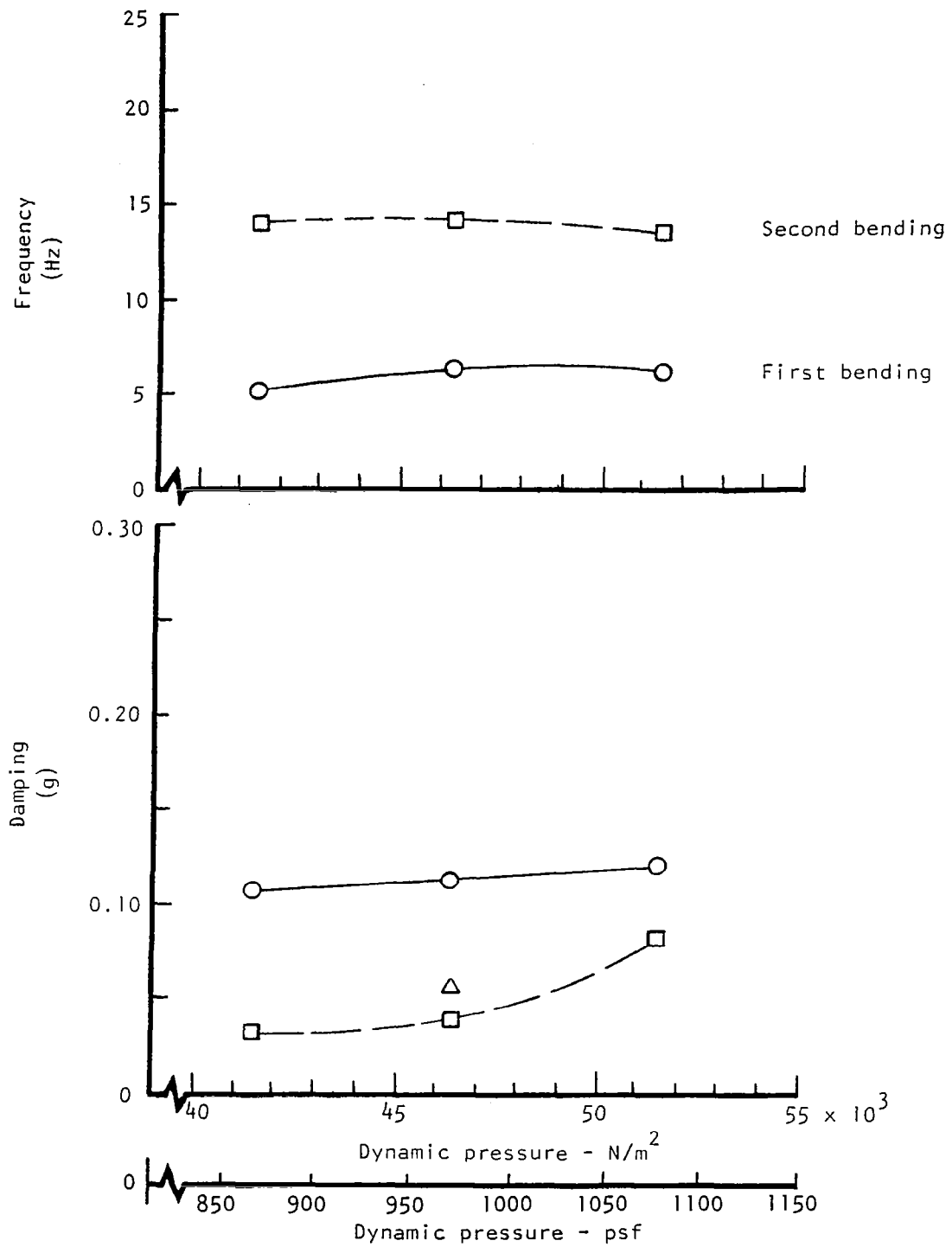
(d) Horizontal tail antisymmetric response at Mach = 0.95

Figure 16. - Continued.
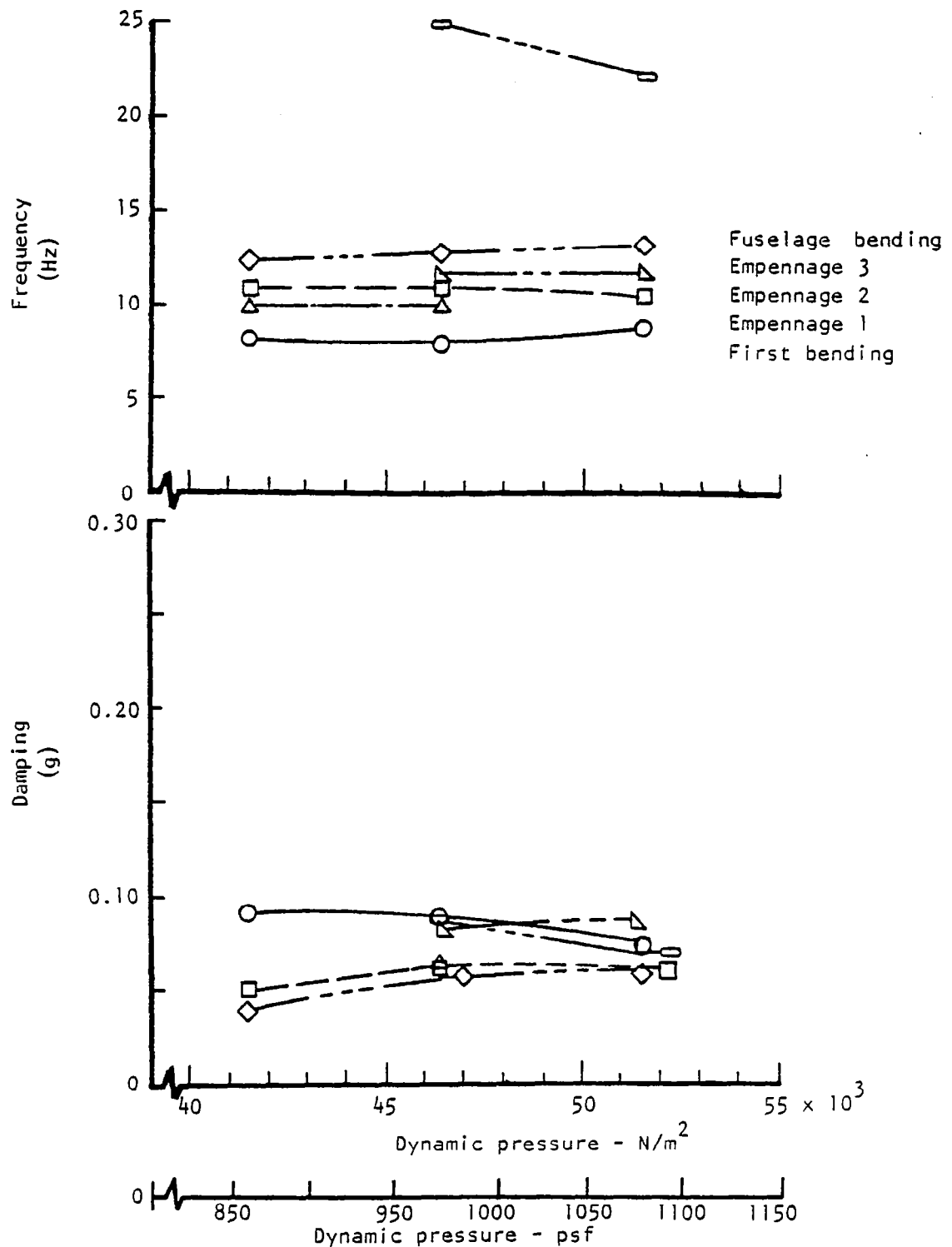
(e) Vertical tail/empennage response at Mach = 0.95

Figure 16. - Concluded.

Wing symmetric
second bending mode

Example of a "clean,"
well separated
peak response
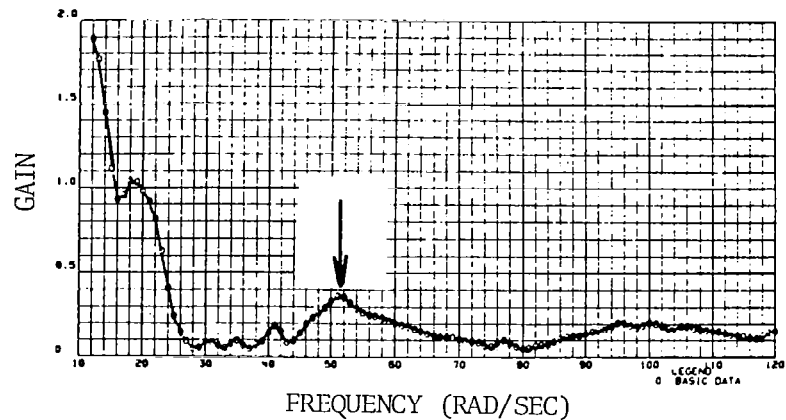
Horizontal tail
symmetric second
bending mode

Example of a noisy
peak response with
a relatively low
response amplitude
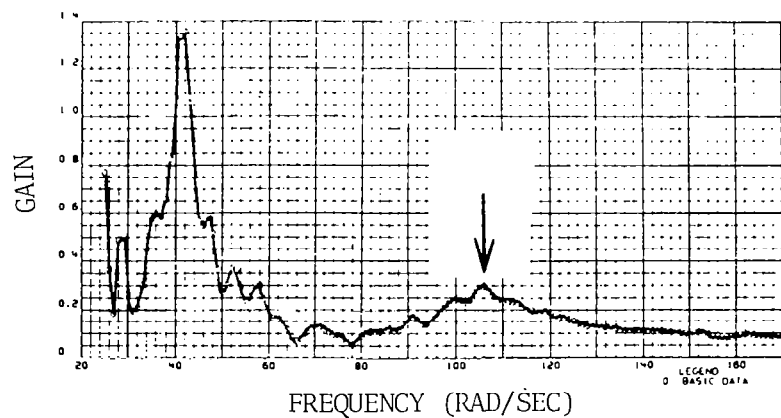
Vertical tail/empennage
modes

Example of three closely
spaced peak responses
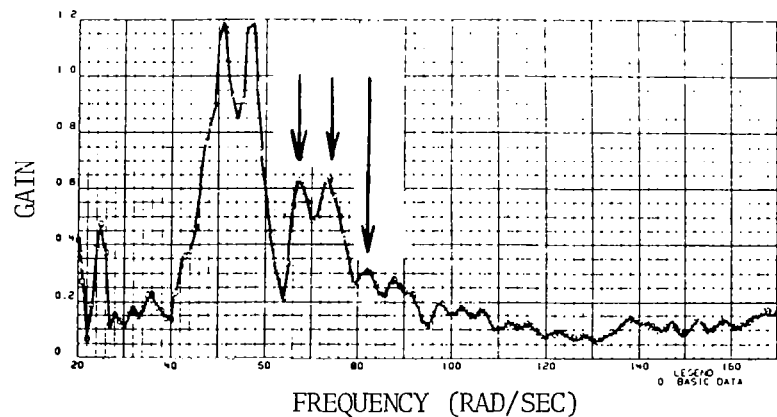
(a) FLEX excited transfer functions (GAIN)
using Time-lag-products cross-correlation
method

Figure 17. - Examples of analysis results of five peak responses
at Mach = 0.95, q = 51.5 kN/m^2.

59
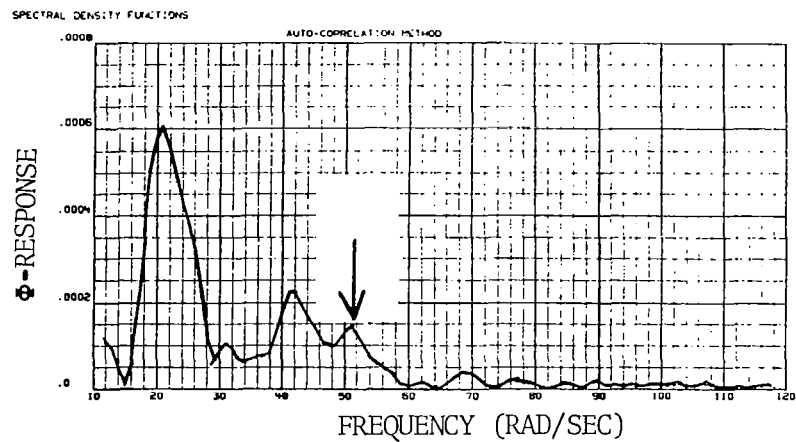
Wing mode

Horizontal tail
mode
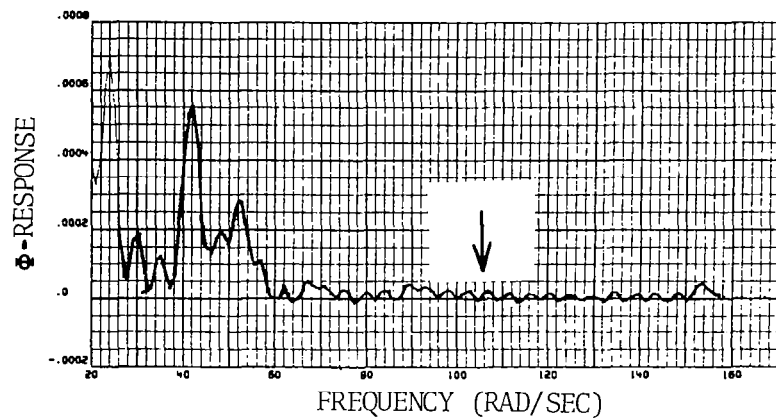
Vertical tail/
empennage modes
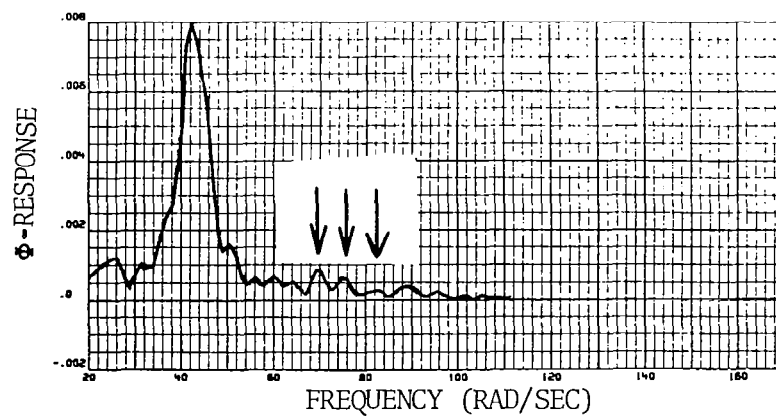
(b) Random excitation power spectral densities of responses using
     time-lag-products autocorellation method
          Figure 17. - Continued.

Random response

FLEX forced response

Flutter excitation system force

Oscillator signal

(a) Wing symmetric second bending mode,
"clean mode"

Figure 18. - Time histories of five peak responses
at 360 samples per second at Mach = 0.95, q = 51.5 kN/m^2.

TIME (SECONDS)
Random response

TIME (SECONDS)
FLEX forced response

TIME (SECONDS)
Flutter excitation system force

TIME (SECONDS)
Oscillator signal
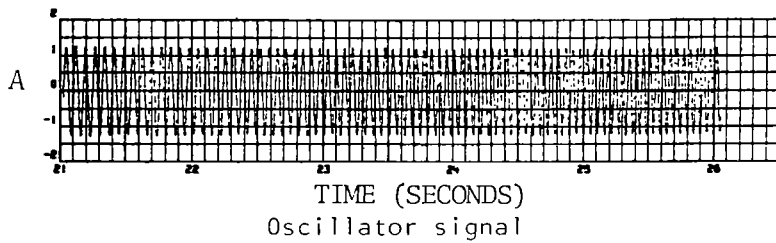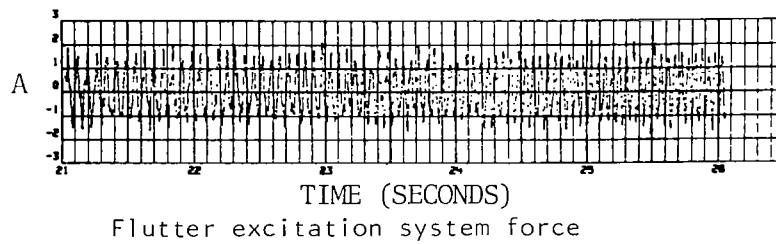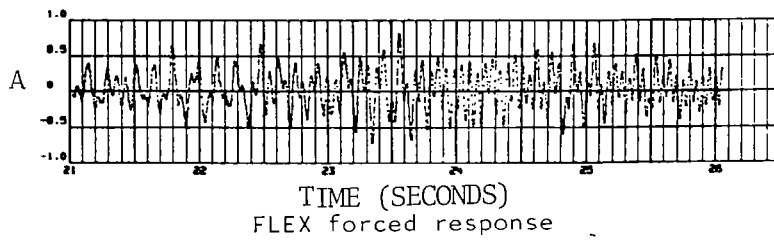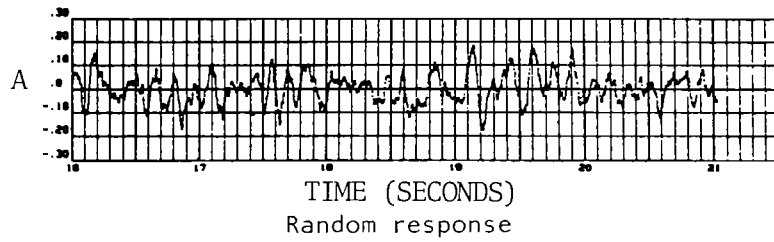
(b)   Horizontal tail symmetric second bending mode

Figure 18. - Continued.

TIME (SECONDS)

Random response

TIME (SECONDS)

FLEX forced response

TIME (SECONDS)

Flutter excitation system force

TIME (SECONDS)

Oscillator signal
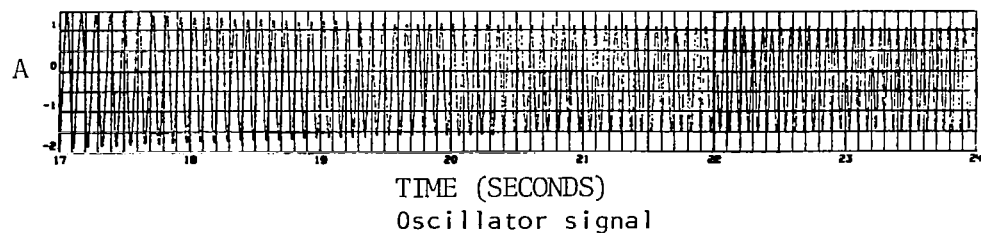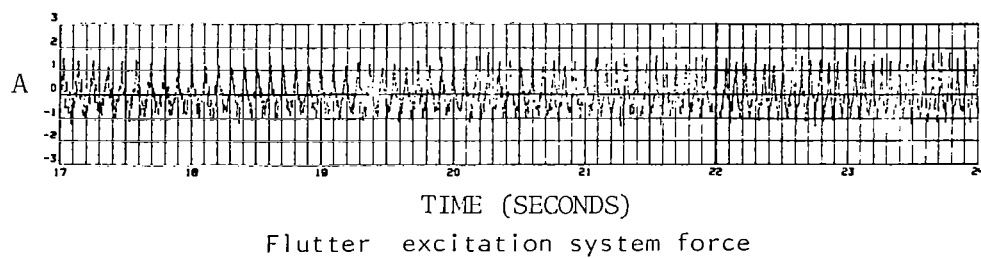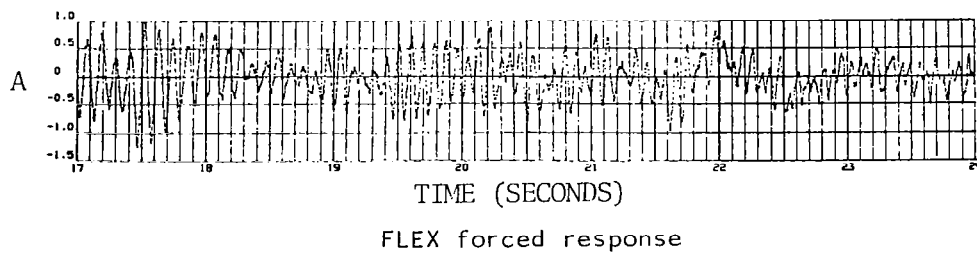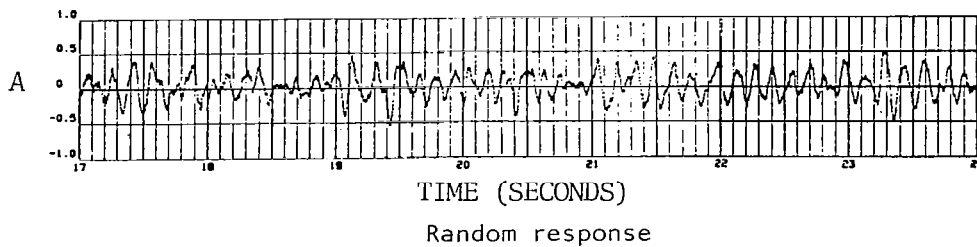
(c) Vertical tail/empennage modes

Figure 18. - Concluded.

(a) Cross-correlation
    function
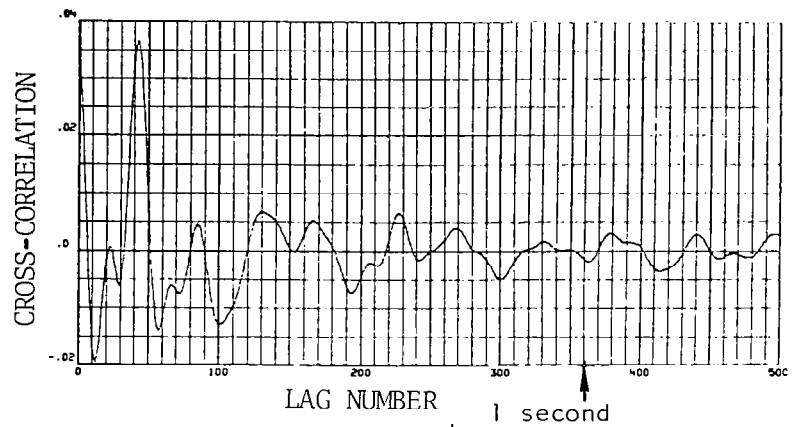
(b) Power spectra
    of response

    freq = 8.08 Hz
       g = 0.126
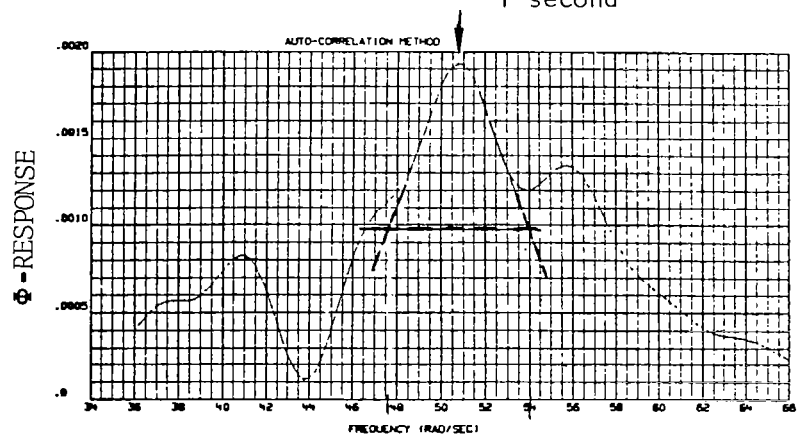
(c) CO-spectra

    Freq = 8.20 Hz
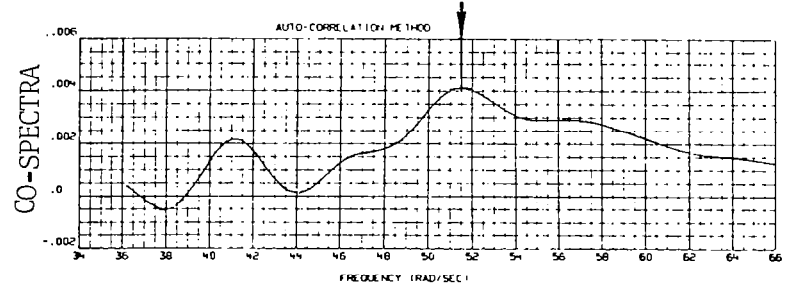
(d) Quadrature spectra

    g = 0.135
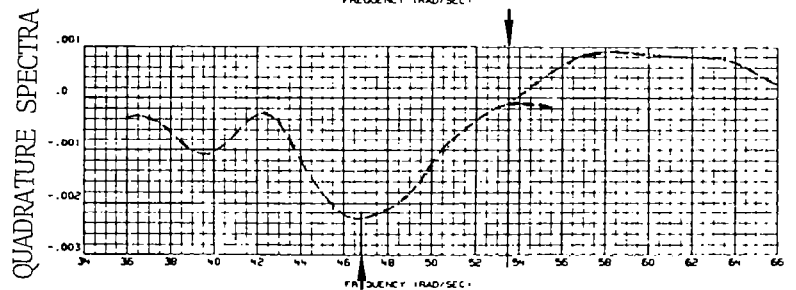
Figure 19. - Analysis results of a "clean" peak response - wing symmetric second
bending, Mach = 0.95, q = 51.5 kN/m^2.

(e) Coherence spectra
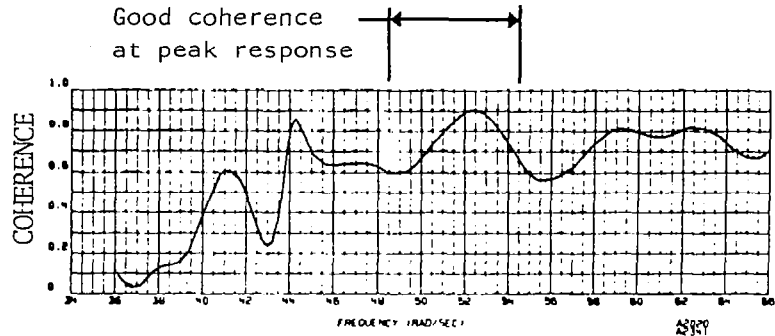
(f) Transfer function of
     response and FLEX force

     freq = 8.16 Hz
         g = 0.119
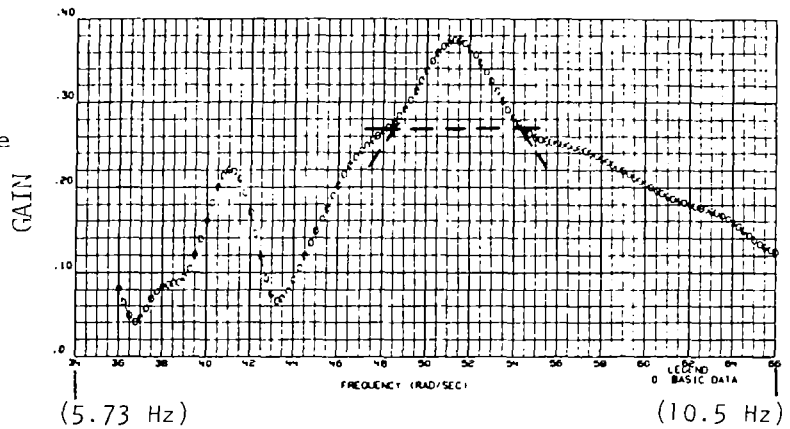
(g) Phase angle between
     response and FLEX force

     g = 0.146
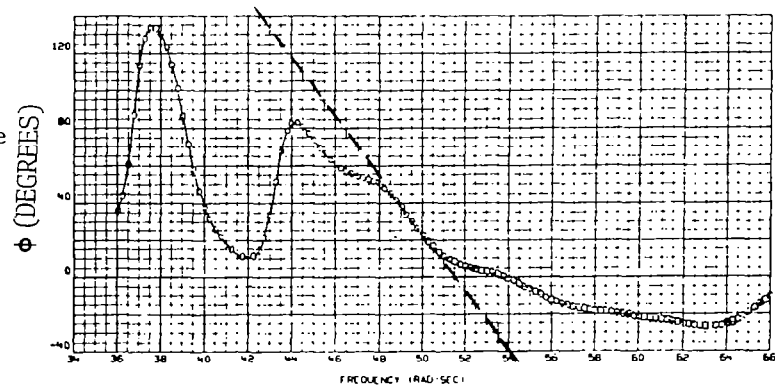
Average values: freq = 8.14, σ = 0.043
                     g = 0.132, σ = 0.009

Figure 19. – Concluded.

(a) Time-lag products
    cross-correlation
    function

CROSS-CORRELATION

LAG NUMBER

(One Second)
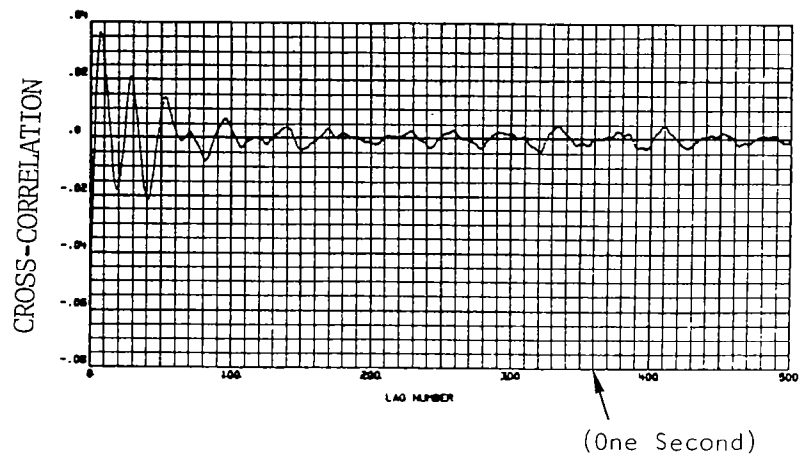
(b) Power spectra of response

    freq = 16.91 Hz
      g = 0.069
           (extrapolated)
      or = 0.183
           (entire peak)

Φ -RESPONSE

FREQUENCY (RAD/SEC)
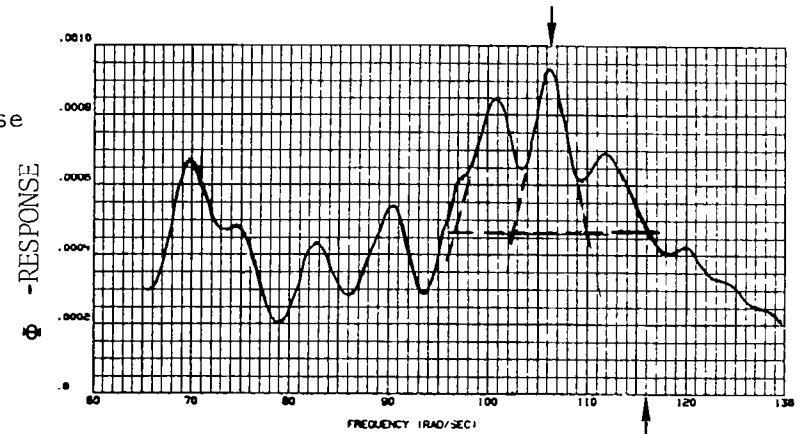
(c) Co-spectra

    freq = 16.87 Hz
           (extrapolated)
      or   18.02 Hz
           (entire peak)
        (17.45 Hz average)

CO-SPECTRA

FREQUENCY (RAD/SEC)
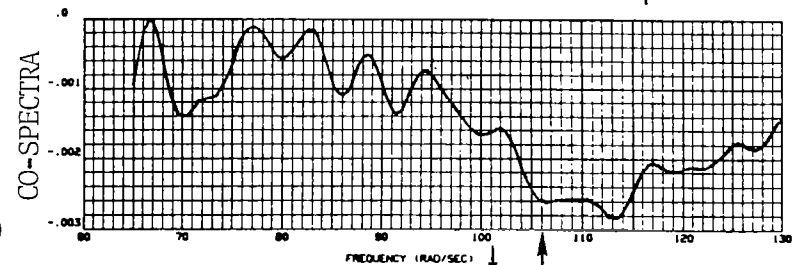
(d) Quadrature spectra

    g = 0.0714 (extrapolated)
      or 0.11 (entire peak)

QUADRATURE SPECTRA

FREQUENCY (RAD/SEC)
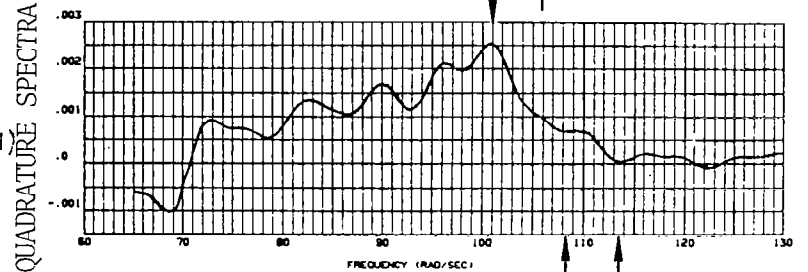
Figure 20. - Analysis results of a "noisy" mode with low response amplitude -
    horizontal tail symmetric second bending, M = 0.95, q = 51.5 kN/m^2.

66

Good coherence at peak reponse

(e) Coherence spectra

(f) Transfer function
(GAIN) or response
and FLEX force

freq = 16.79 Hz
g = 0.06
(extrapolated)
or = 0.152
(entire peak)
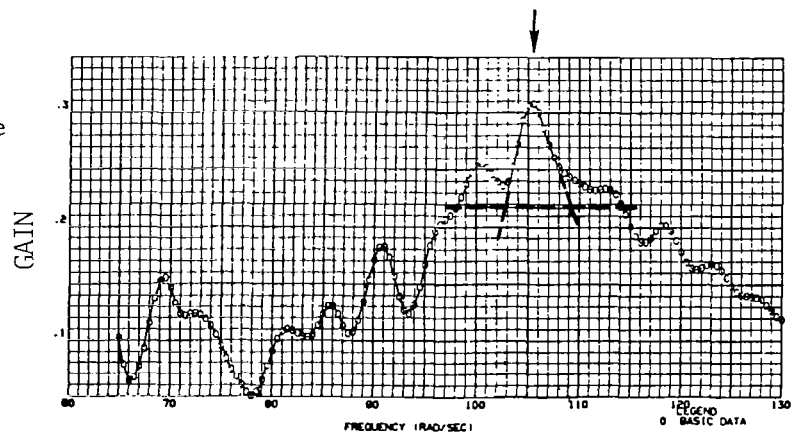
(g) Phase angle between
response and FLEX
force

g = 0.086
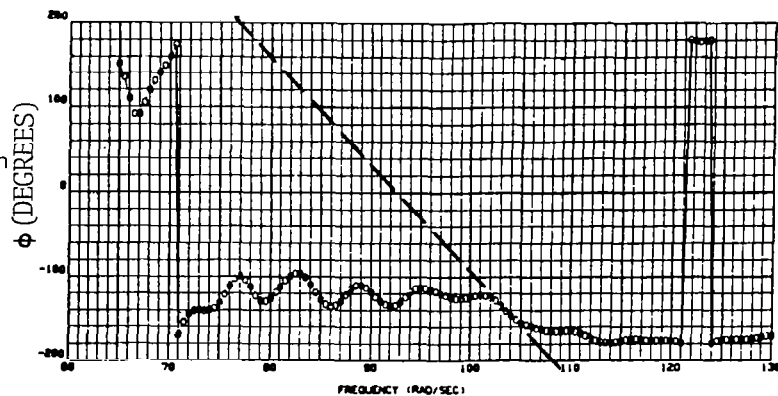
Average values	freq = 16.9,	σ = 0.050
(extrapolated)	g = 0.0716	σ = 0.0072
(entire peak)	g = 0.132	σ = 0.027

Figure 20. - Concluded

67

(a) Cross-correlation
    function

(b) Power spectra of
    response

    $freq_1$ = 10.62 Hz

    g_1 = 0.067

    $freq_2$ = 11.5 Hz

    g_2 = 0.138

    $freq_3$ = ?

    g_3 = ?
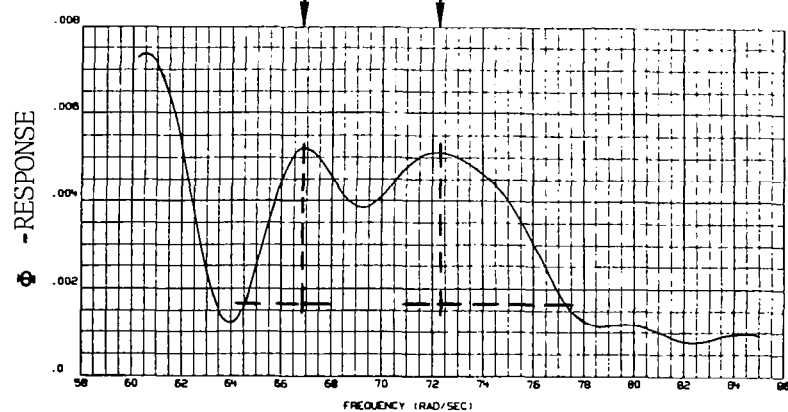
(c) Co-spectra

    $freq_1$ = 10.70 Hz

    $freq_2$ = 11.73 Hz

    $freq_3$ = 13.15 Hz

(d) Quadrature spectra

    g_1 = .044

    g_2 = .033

    g_3 = ?
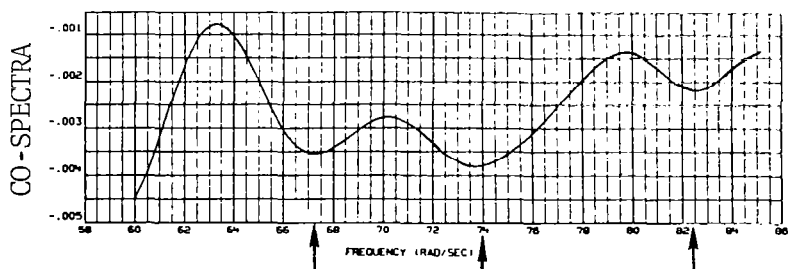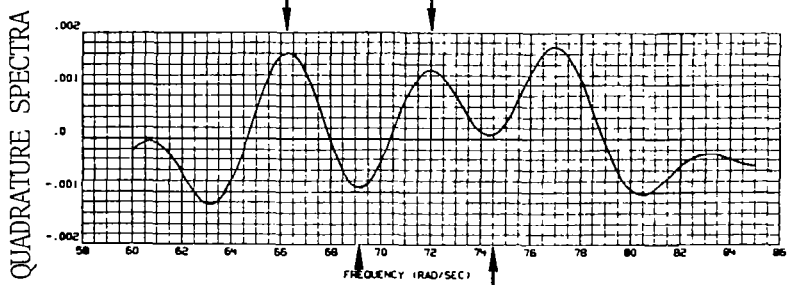
Figure 21. - Analysis results of three closely spaced modes - vertical tail/
empennage, Mach = 0.95, q = 51.5 kN/m^2.

68

(e) Coherence

FAIR TO GOOD
COHERENCE AT
PEAK RESPONSES

(f) Transfer function (GAIN)

    freq = 10.70 Hz
      g = 0.0617
    freq = 11.7 Hz
      g = 0.079
    freq = 13.13 Hz
      g = 0.068
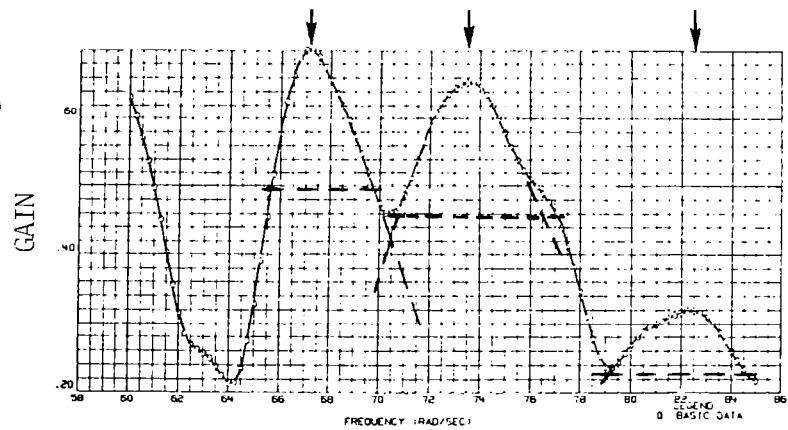
(g) Phase angle between
    reponse and FLEX force

$g_1 = 0.058$

$g_2 = 0.107$

$g_3 = ?$
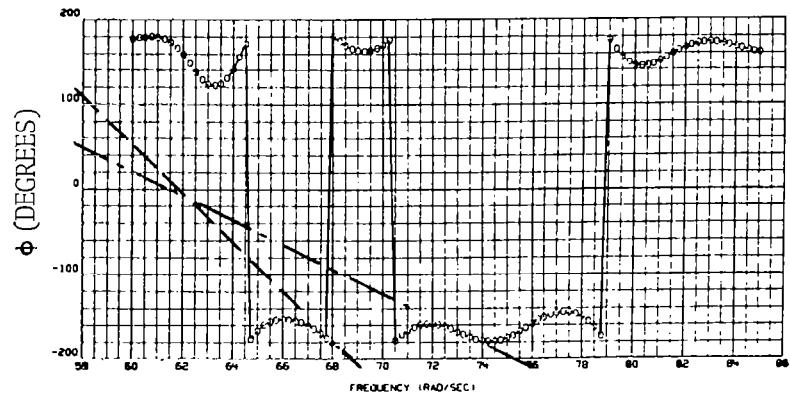
Average values:

$f_1 = 10.7$ Hz, $\sigma = 0.033$ $g_2 = 0.0842$, $\sigma = 0.0282$

$g_1 = 0.0578$, $\sigma = 0.0067$ $f_3 = 13.1$ Hz, $\sigma = 0.20$

$f_2 = 11.6$ Hz, $\sigma = 0.10$ $g_3 = 0.068$, $\sigma = -$

Figure 21. - Concluded.

Left wingtip

Right wingtip

(one second)
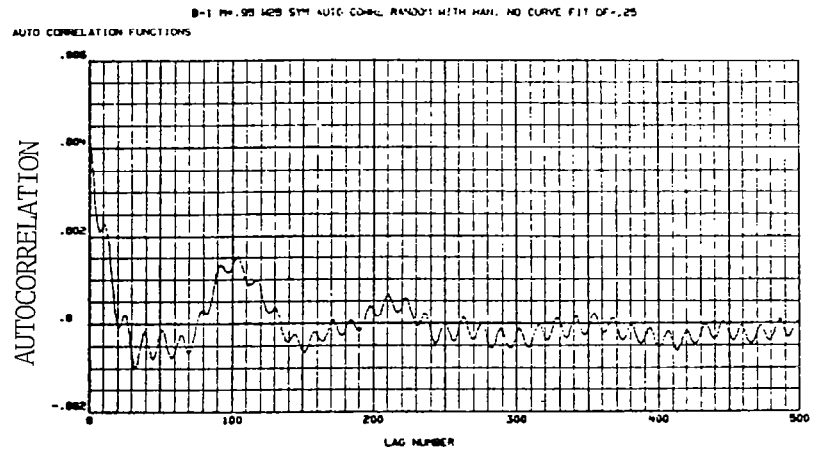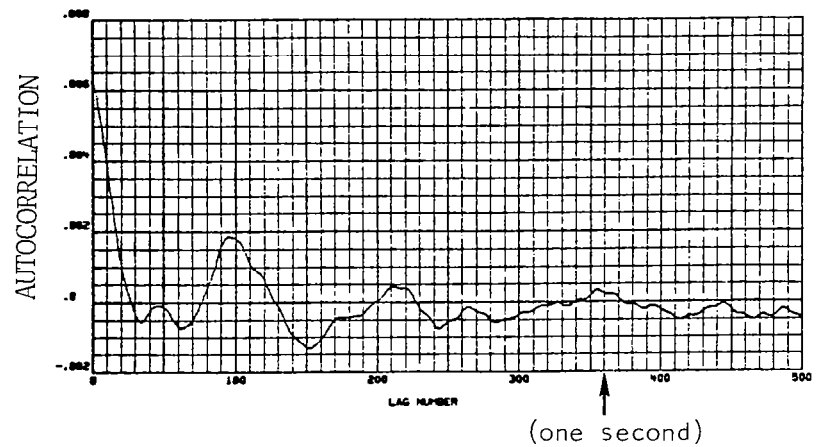
(a)   Autocorrelation functions

Figure 22. - Analysis of wing second bending response to random excitation, Mach = 0.95, q = 51.5 kN/m², for 25-second time history.

70

Left wingtip:

Freq = 6.56 Hz
g = 0.156

Freq = 8.11 Hz
g = 0.125

Right wingtip:

Freq = 6.60 Hz
g = 0.179

Freq = 8.16 Hz
g = 0.0975

Phase angle
between left and
right wingtips
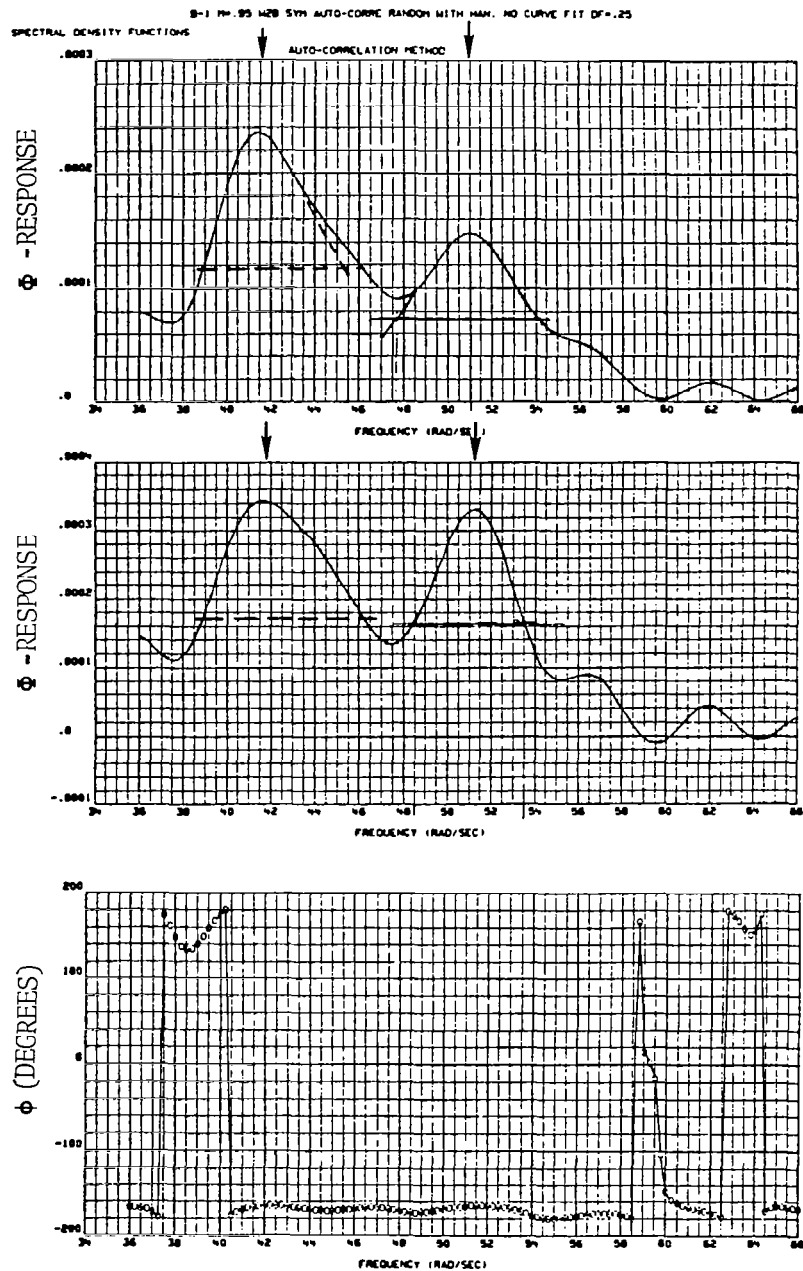
(b) Power spectra of autocorrelation of responses and phase
angle of cross-correlation for 36 to 66 rad/sec, frequency
resolution = 0.25 rad/sec.

Figure 22. - Continued.

71

Left wingtip:

Freq = 8.04 Hz
g = 0.064

Freq = 8.83 Hz
g = 0.054
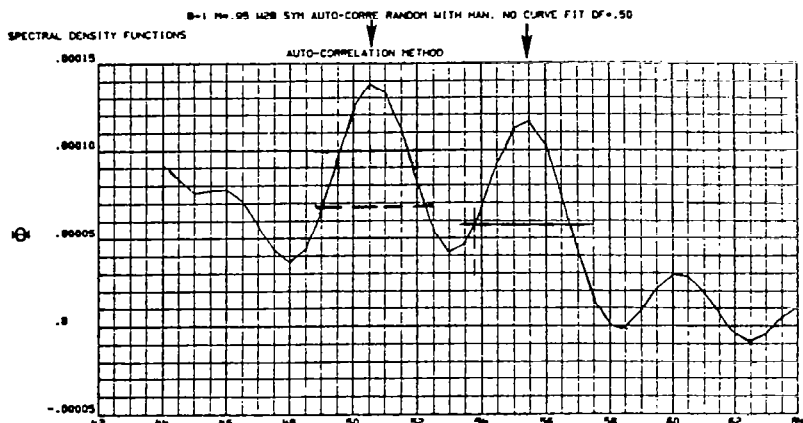
Right wingtip:

Freq = 8.08 Hz
g = 0.066

Freq = 8.83 Hz
g = 0.658
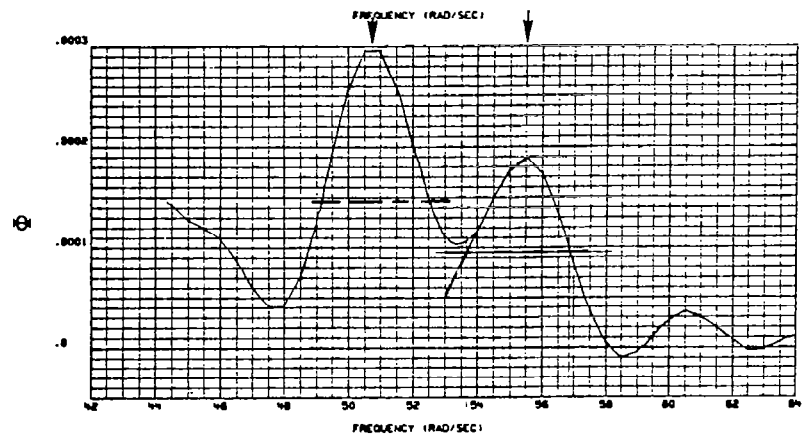
Phase angle between
left and right
wingtips
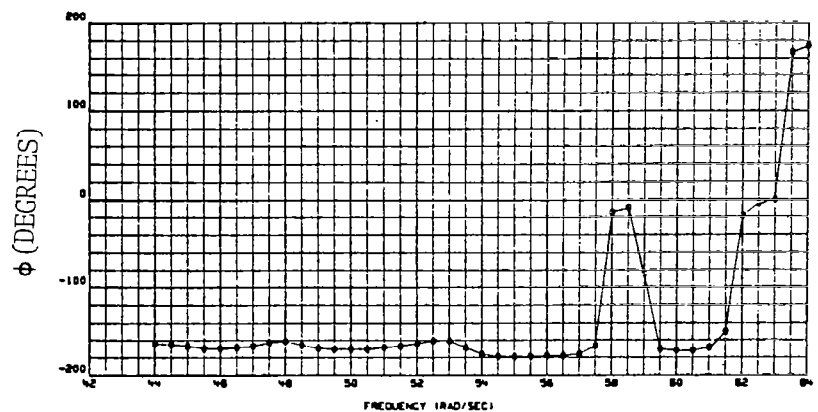
(c) Same as figure 22 (b), except 44 to 64 rad/sec window and
     frequency resolution = 0.50 rad/sec.

Figure 22. - Continued.

72

Right
horizontal
tail tip

Left
horizontal
tail tip

(one second)
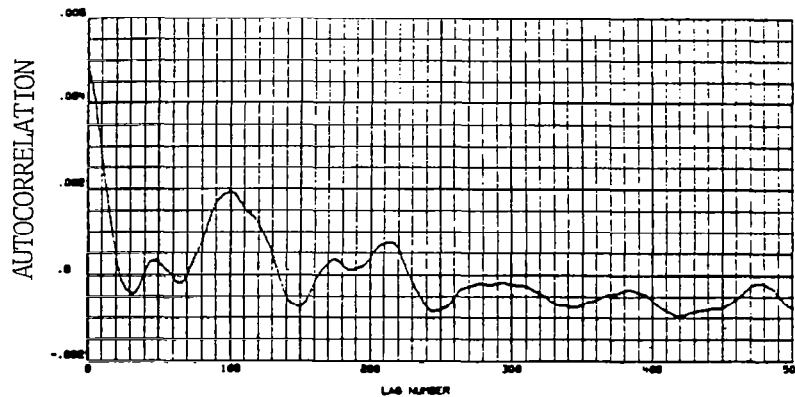
(a)   Autocorrelation functions

Figure 23. - Analysis of horizontal tail second bending response to
random excitation at Mach = 0.95, q = 51.5 kN/m^2, for 25-second
time history with Hanning filter.

73

Left horizontal
tail tip
    freq = ?
       g = ?
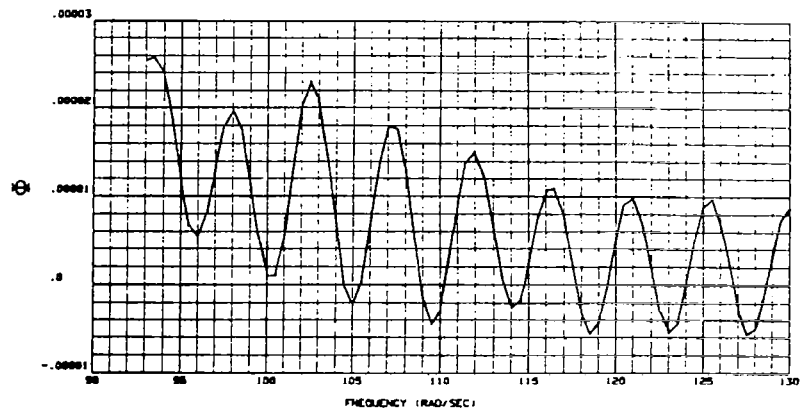
Right horizontal
tail tip
    freq = ?
       g = ?
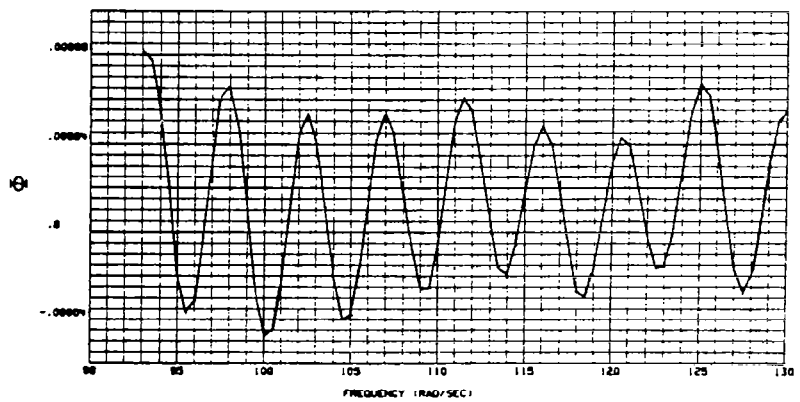
Phase angle between
left and right
horizontal tail
response
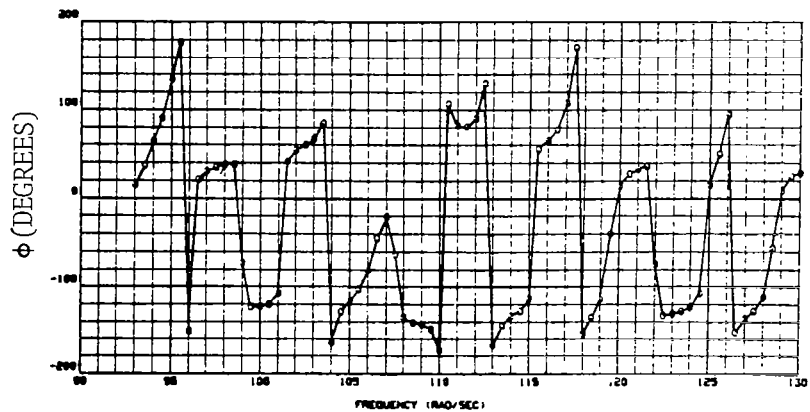
(b)   Power spectra of autocorrelations of
      responses and phase angle of cross-
      correlation for 93 to 130 rad/sec,
      frequency resolution = 0.50 rad/sec.

Figure 23. - Continued.

Vertical tail tip

AUTOCORRELATION

(one second)
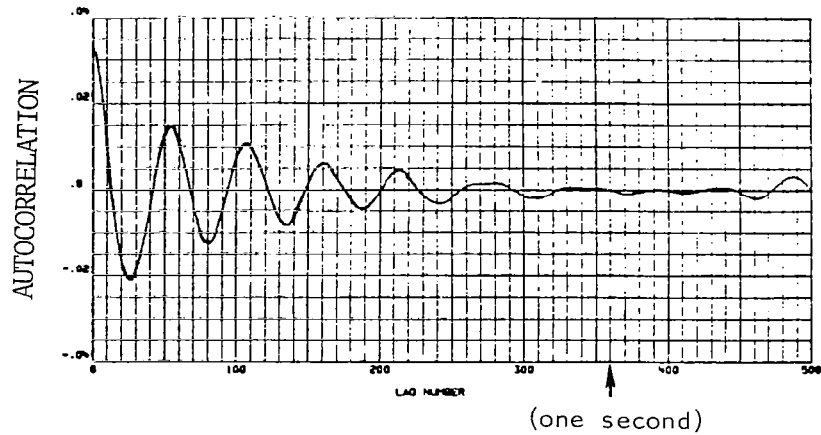
(a) Autocorrelation function

Vertical tail tip
 freq = 11.14 Hz
    g = 0.0514

 freq = 11.9 Hz
    g = 0.062
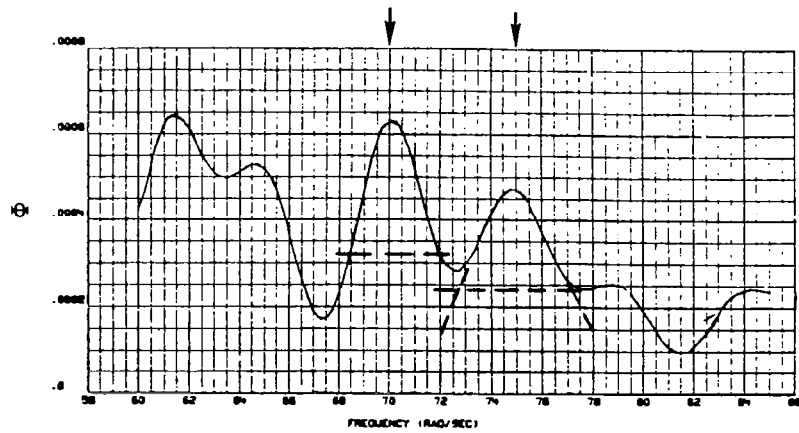
(b) Power spectra of autocorrelation of
     responses for 60 to 85 rad/sec,
     frequency resolution = 0.50 rad/sec.

Figure 24. - Analysis of vertical tail/empennage response to
     random excitation at Mach = 0.95, q = 51.5 kN/m^2,
        for 25-second time history with Hanning filter.

Vertical tail tip
 freq = 11.1 Hz
     g = 0.0457

 freq = 11.9 Hz
     g = 0.0533

 freq = 13.2 Hz
     g = 0.0533

Φ -RESPONSE
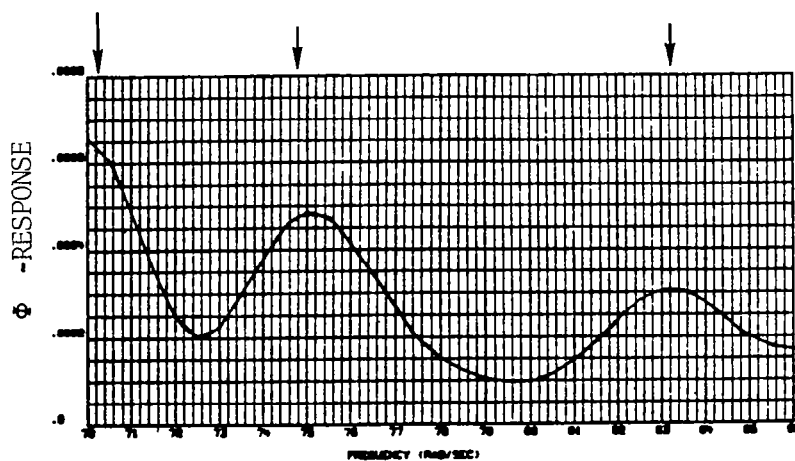
FREQUENCY (RAD/SEC)

(c) Power spectra of autocorrelation of
    responses for 70 to 86 rad/sec,
    frequency resolution = 0.50 rad/sec.

Figure 24. - Concluded.
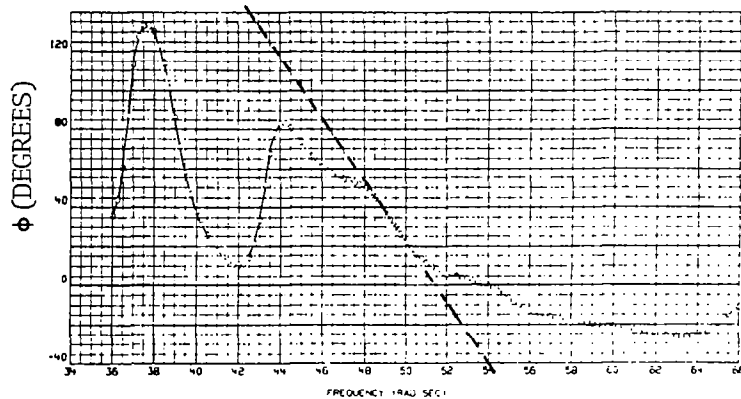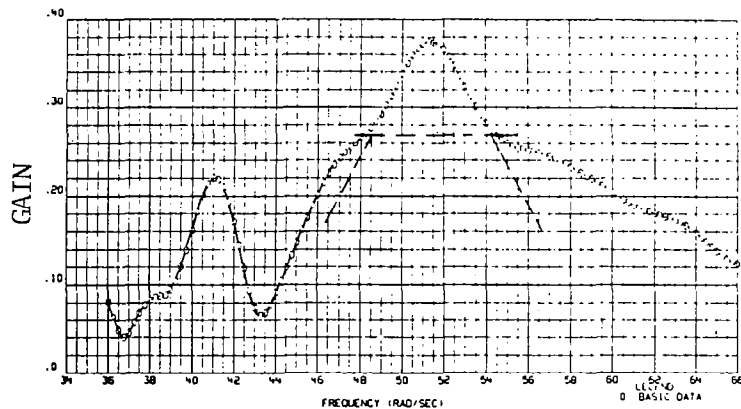
No Hanning filter
Gain: freq = 8.16 Hz, g = 0.119
Phase: g = 0.142
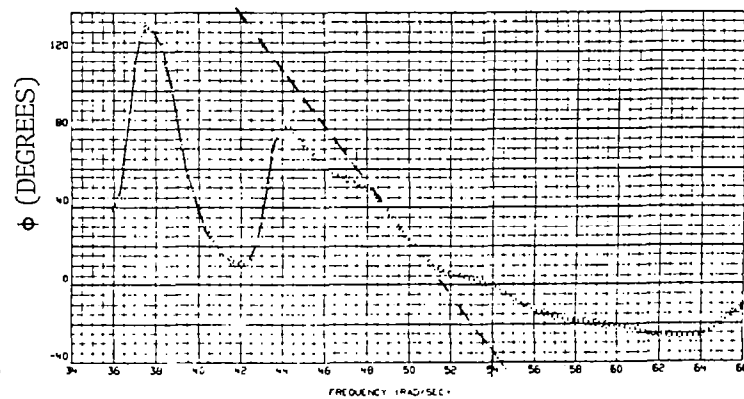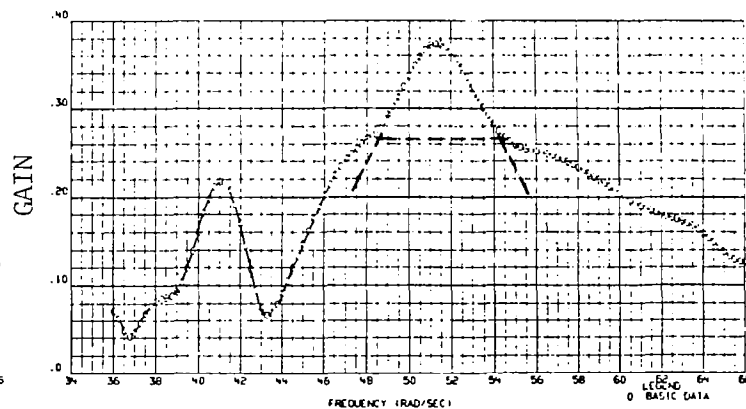
With Hanning filter
Gain: freq = 8.16 Hz, g = 0.11
Phase: g = 0.146

Figure A1. - Effect of Hanning filter on wing symmetric second bending mode gain and phase spectra at Mach 0.95, q = 51.5 kN/m^2.
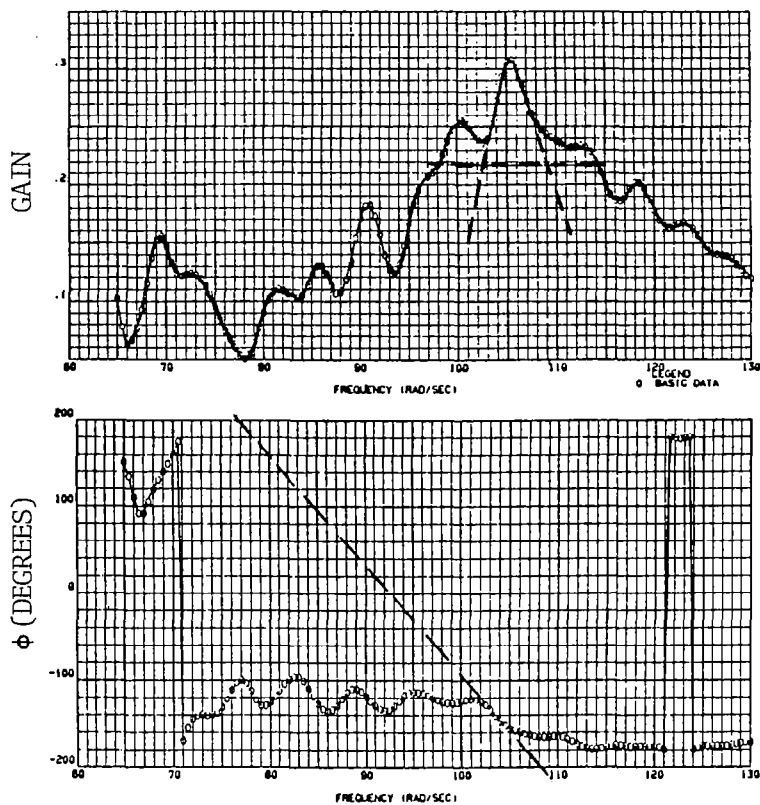
No Hanning filter
Gain: freq = 16.79 Hz, g = 0.0597 or 0.152

Phase: g = 0.086
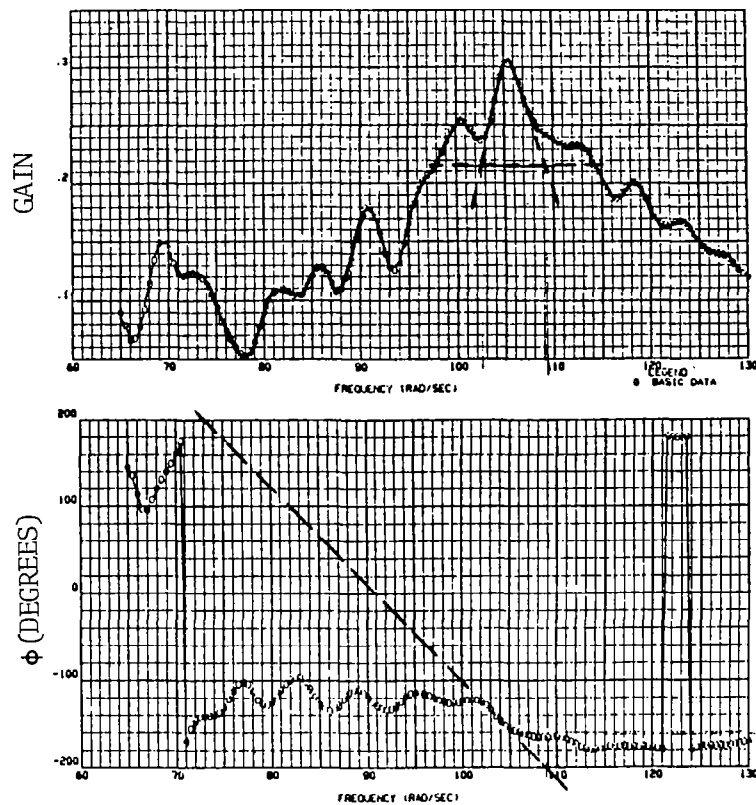
With Hanning filter
Gain: freq = 16.79 Hz, g = 0.0637 or 0.152

Phase: g = 0.097

Figure A2. - Effect of Hanning filter on horizontal tail symmetric second bending mode gain and phase spectra at Mach = 0.95, q = 51.5 kN/m^2.
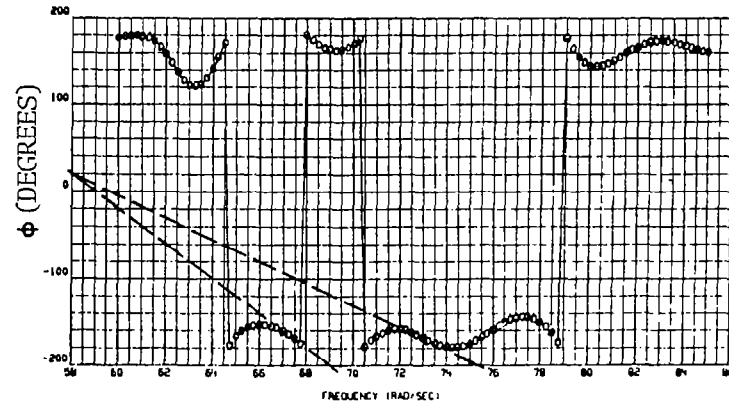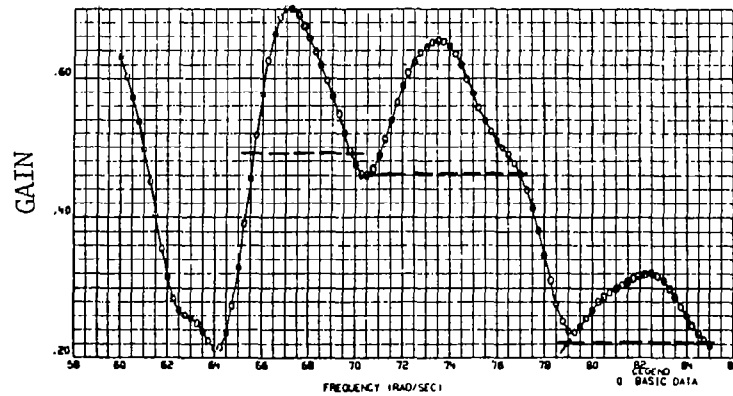
No Hanning filter

Gain: freq = 10.68 Hz, g = 0.0617; freq = 11.69 Hz,
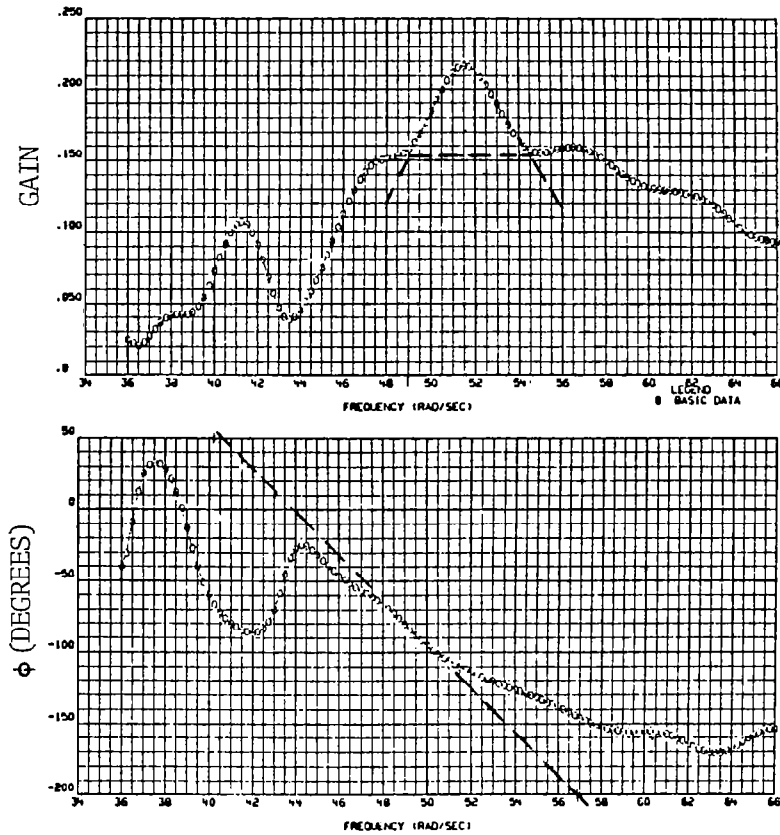   g = 0.085; freq = 13.09 Hz, g = 0.067

Phase: g = 0.0854; g = 0.154; g = ?
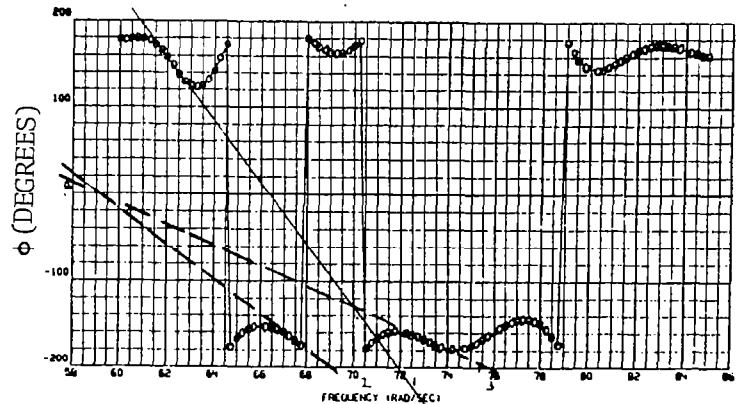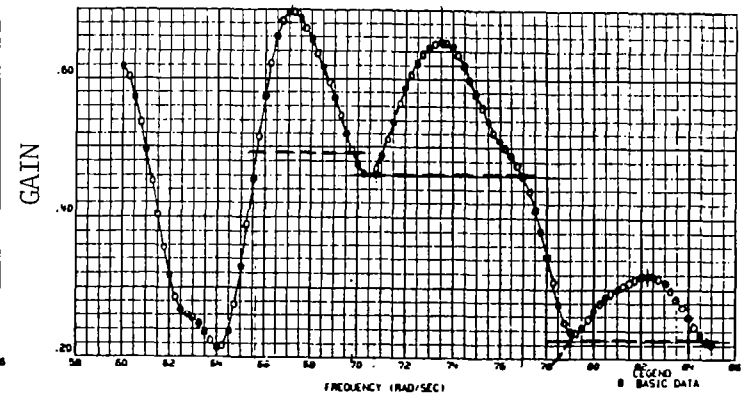
With Hanning filter

Gain: freq = 10.68 Hz, g = 0.0617; freq = 11.69 Hz,
        g = 0.085; freq = 13.09 Hz, g = 0.067

Phase: g = 0.0854; g = 0.154; g = ?

Figure A3. - Effect of Hanning filter on vertical tail/empennage modes gain
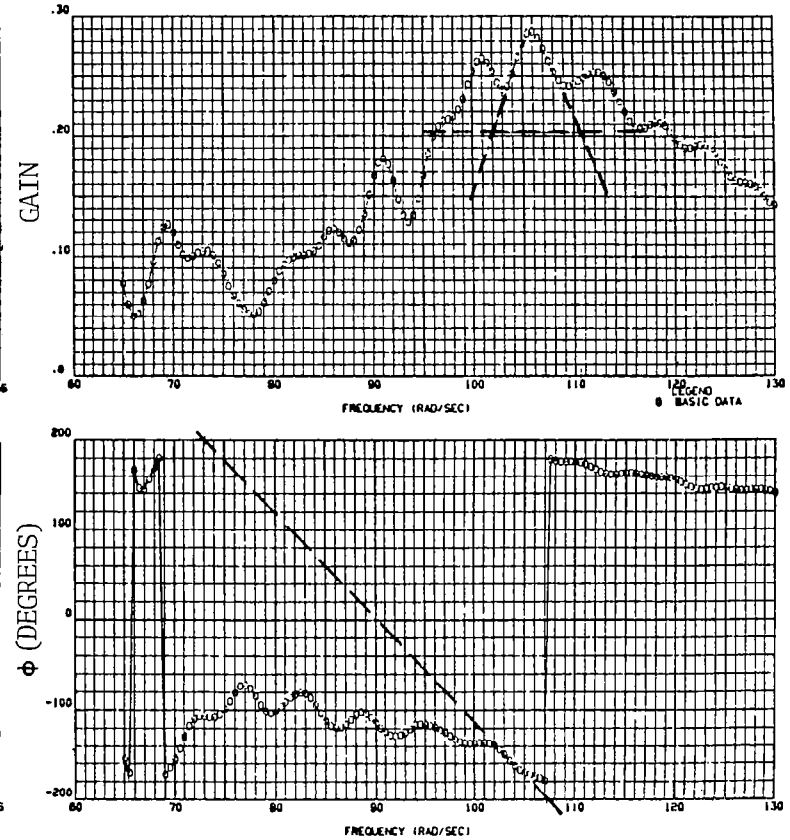and phase spectra at Mach = 0.95, q = 51.5 kN/m^2.

(a) Wing symmetric second bending

Compare with figure 22, which uses
FLEX force.
Gain: freq = 8.2 Hz, g = 0.107
Phase: g = 0.145

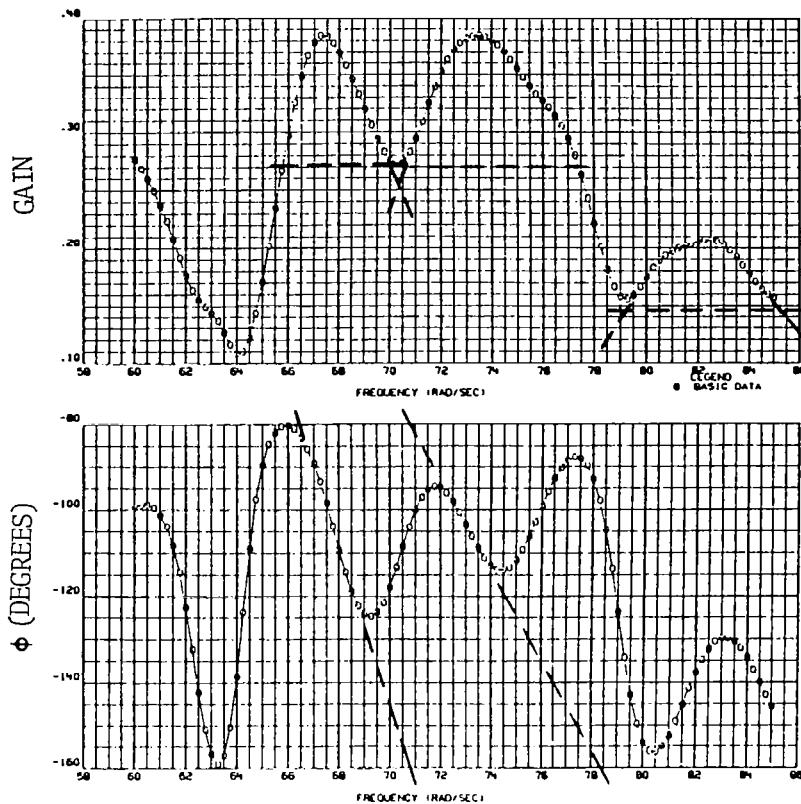(b) Horizontal tail symmetric second bending mode

Compare with figure 23, which uses
FLEX force.
Gain: freq = 16.87 Hz, g = 0.081
Phase: g = 0.093

Figure A4. - Effect of using oscillator signal instead of FLEX force on gain and
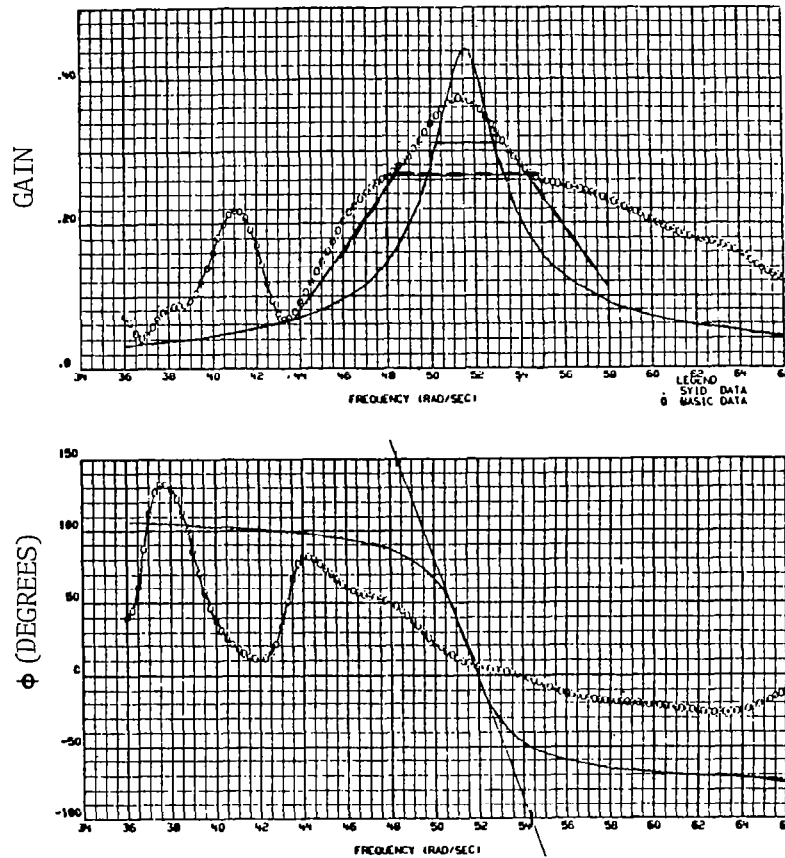phase (with Hanning filter) at Mach = 0.95, q = 51.5 kN/m^2.

(c) Vertical tail/empennage modes

Compare with figure 24,
which uses FLEX force.
Gain: freq = 10.70 Hz, g = 0.69,
        freq = 11.70 Hz, g = 0.0925,
        freq = 13.09 Hz, g = 0.073
Phase: g = 0.0905, g = 0.147, g = ?

Figure A4. - Concluded.
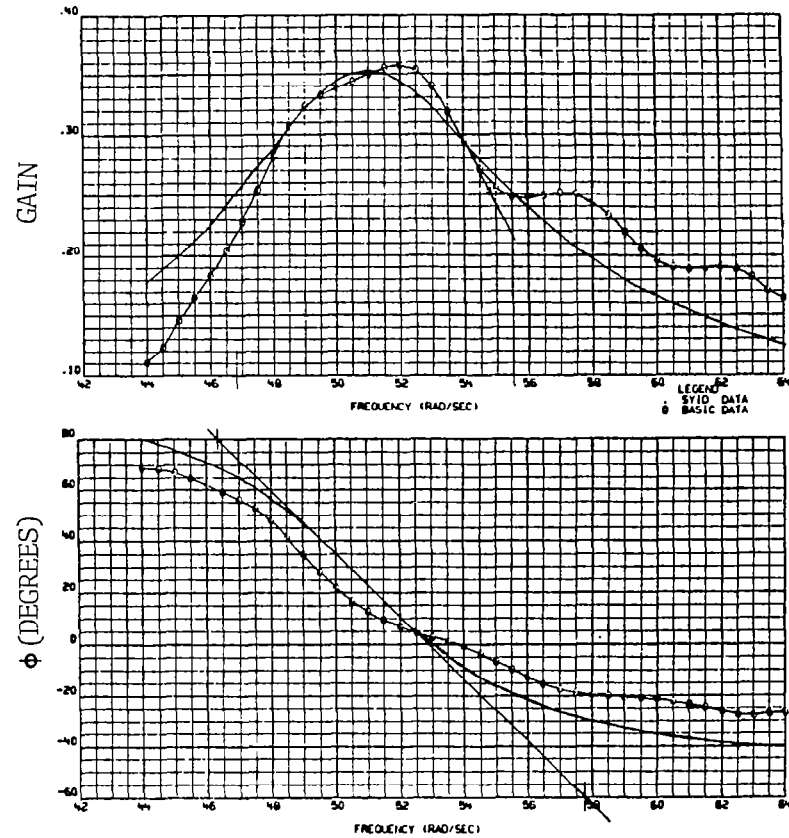
Time-lag-products cross-correlation
  Best curve-fit (order = 1/2):
    Freq = 8.21 Hz,   g = 0.050

  Manual:
    Freq = 8.16 Hz,   g = 0.119

  (a) Frequency resolution = 0.25 rad/sec (0.0397 Hz),
      frequency window = 36 to 66 rad/sec,
      time window = 25 seconds

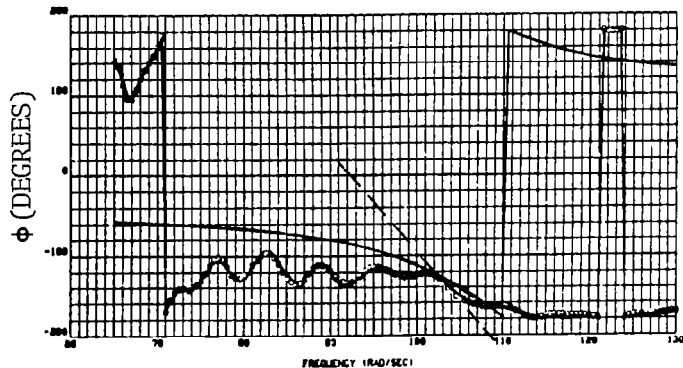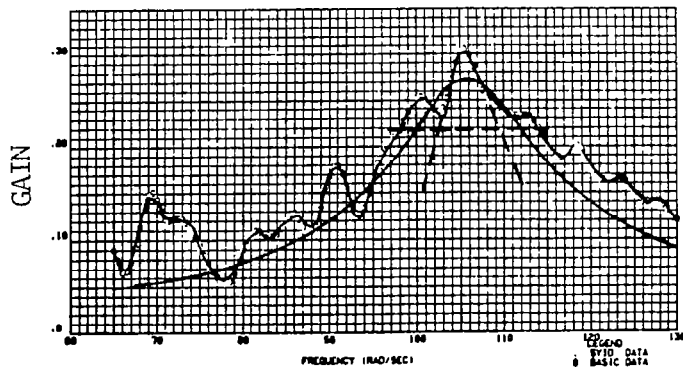Time-lag-products cross-correlation
  Best curve-fit (order = 2/3);
    Freq = 8.11 Hz,   g = 0.173

  Manual:
    Freq = 8.28 Hz,   g = 0.141

  (b) Frequency resolution = 0.50 rad/sec (0.0794 Hz),
      44-64 rad/sec frequency window,
      time window = 12.5 seconds

Figure A5. - Least squares curve fit of gain and phase for wing symmetric second bending mode at
Mach = 0.95, q = 51.5 kN/m^2, with various time and frequency windows.

Time-lag-products cross-correlation:
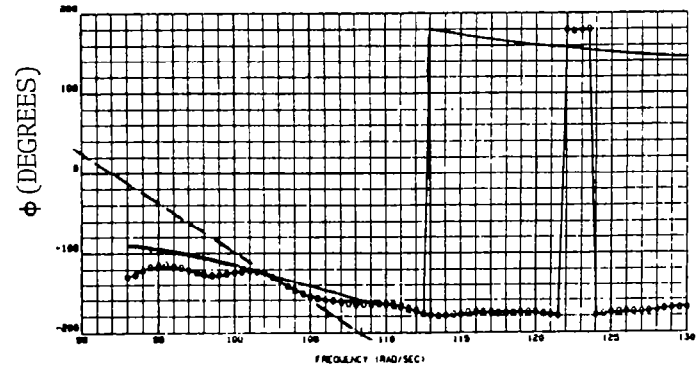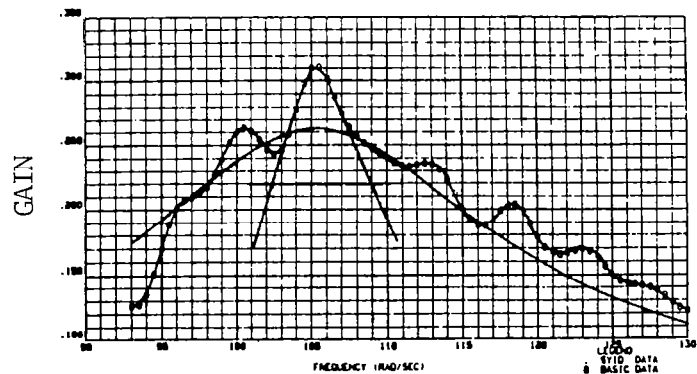   Best curve-fit (order 1/2):
      Freq = 16.87 Hz, g = 0.1521
    Manual:
      Gain: freq = 16.79 Hz,
            g = 0.0637 or
            = 0.155 (3 peaks together)
      Phase: g = 0.097

Time-lag-products cross-correlation:
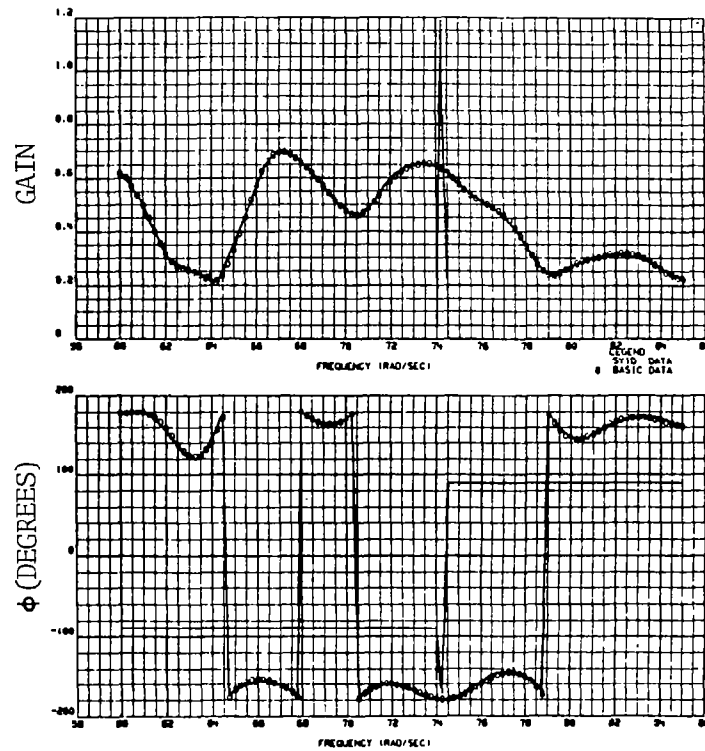   Best curve-fit (order 1/2):
      Freq = 16.8 Hz, g = 0.2094
    Manual:
      Gain:
          Freq = 16.75 Hz,
         g = 0.0637 or
           = 0.152 (3 peaks together)
    Phase: g = 0.090

(a) Frequency resolution = 0.50 rad/sec (0.0794 Hz), (b) Frequency resolution = 0.50 rad/sec (0.0794 Hz),
    time window = 25 seconds, frequency   frequency window = 93 to 130 rad/sec,
    window = 65 to 130 rad/sec   time window = 12.5 seconds

Figure A6. - Least squares curve fit of gain and phase for horizontal tail symmetric second
bending mode at Mach = 0.95, q = 51.5 kN/m^2, with various time and frequency windows with Hanning.

Time-lag-products cross-correlation:
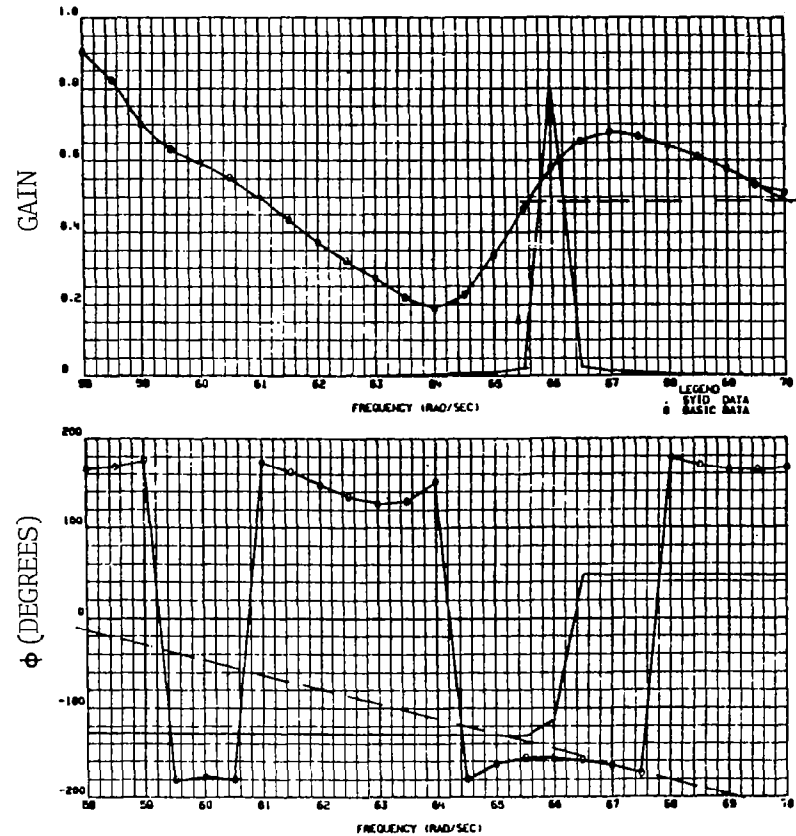   Best curve-fit (order 2/3):
        Freq = 11.82 Hz, g = 0
    Manual:
        Gain: freq = 10.64 Hz, g - 0.0617,
                freq = 11.69 Hz, g - 0.085,
                freq = 13.09 Hz, g = 0.067
        Phase: g = 0.0854, g = 0.134, g = ?

Time-lag-products cross-correlation:
    Best curve-fit (order 2/2):
        Freq = 10.50 Hz, g = 0
    Manual:
        Gain: freq = 10.66 Hz, g = 0.063
        Phase: g = 0.103

(a) Frequency resolution = 0.50 rad/sec (0.0794 Hz), (b) Frequency resolution = 0.50 rad/sec (0.0794 Hz),
    frequency window = 60 to 85 rad/sec   frequency window = 58 to 70 rad/sec
    time window = 25 seconds   time window = 12.5 seconds

Figure A7. - Least squares curve fit of gain and phase for vertical tail/empennage modes at
    Mach = 0.95, q = 51.5 kN/m^2, with various time and frequency windows with Hanning.

1. Report No. NASA CR-3152	2. Government Accession No.	3. Recipient's Catalog No.
4. Title and Subtitle DETERMINATION OF SUBCRITICAL FREQUENCY AND DAMPING FROM B-1 FLIGHT FLUTTER TEST DATA		5. Report Date June 1979
		6. Performing Organization Code
7. Author(s) S. K. Dobbs and C. H. Hodson		8. Performing Organization Report No.
		10. Work Unit No.
9. Performing Organization Name and Address Rockwell International Corporation Los Angeles Aircraft Division Los Angeles, CA 90009		
		11. Contract or Grant No. NAS4-2278
		13. Type of Report and Period Covered Contractor Report
12. Sponsoring Agency Name and Address National Aeronautics and Space Administration Washington, DC 20546		
		14. Sponsoring Agency Code

16. Abstract

The application of the time-lag products correlation/frequency analysis procedure to determine subcritical frequency and damping from structural response measurements made during flight flutter test of the B-1 prototype airplane is described. A detailed description of the analysis procedure is presented, and the test airplane and flight test procedures are described. Summary frequency and damping results are presented for six transonic flight conditions. Illustrative results obtained by applying various options and variations of the analysis method are presented for one flight condition.

17. Key Words (Suggested by Author(s)) Flutter Subcritical Response Flight Test B-1 Airplane	18. Distribution Statement Unclassified – Unlimited Subject Category 39

19. Security Classif. (of this report) Unclassified	20. Security Classif. (of this page) Unclassified	21. No. of Pages 84	22. Price* $6.00

* For sale by the National Technical Information Service, Springfield, Virginia 22161